

DEVELOPMENT OF SMART FUNCTIONAL SURFACES FOR BIOSENSOR
APPLICATIONS

Except where reference is made to the work of others, the work described in this dissertation is my own or was done in collaboration with my advisory committee. This dissertation does not include proprietary, restricted or classified information.

Shankar Ganesh Sokkalinga Balasubramanian

Certificate of Approval

Jeffrey Fergus
Associate Professor
Materials Engineering

Aleksandr Simonian, Chair
Professor
Materials Engineering

Vitaly Vodyanoy
Professor
Anatomy, Physiology and
Pharmacology

Dong-Joo Kim
Assistant Professor
Materials Engineering

George T. Flowers
Interim Dean
Graduate School

DEVELOPMENT OF SMART FUNCTIONAL SURFACES FOR BIOSENSOR
APPLICATIONS

Shankar Ganesh Sokkalinga Balasubramanian

A Dissertation

Submitted to

the Graduate Faculty of

Auburn University

in Partial Fulfillment of the

Requirements for the

Degree of

Doctor of Philosophy

Auburn, Alabama
August 9, 2008

DEVELOPMENT OF SMART FUNCTIONAL SURFACES FOR BIOSENSOR
APPLICATIONS

Shankar Ganesh Sokkalinga Balasubramanian

Permission is granted to Auburn University to make copies of this dissertation at its discretion, upon request of individuals or institutions and at their expense. The author reserves all publication rights.

Signature of Author

Date of Graduation

VITA

Shankar Ganesh Sokkalinga Balasubramanian, son of Mrs. Chandra Balasubramanian and Mr. G. Balasubramanian was born on June 15th, 1981 in Nedungunam, Tamil Nadu, India. After his high school, he was selected nationally one among the 35 students to join Central Electrochemical Research Institute (CECRI), a premier national laboratory of India dedicated for electrochemical science and technology. He got involved with many scientists in CECRI to work as an assistant which inculcated in him a keen interest in research. CECRI played an important role in nurturing his basic & applied skills and motivated him to pursue graduate research in biosensor. After graduating with a Bachelor of Technology degree in Chemical & Electrochemical Engineering at CECRI, he joined Professor Simonian at Auburn for PhD in Materials Engineering to investigate the application of advanced materials for biosensors and biomaterials development. He was fortunate to have wonderful mentor and colleagues here at Auburn and enjoyed every bit of stay here.

DISSERTATION ABSTRACT
DEVELOPMENT OF SMART FUNCTIONAL SURFACES FOR BIOSENSOR
APPLICATIONS

Shankar Ganesh Sokkalinga Balasubramanian

Doctor of Philosophy, August 9, 2008
(B. Tech., Central Electrochemical Research Institute,
Madurai Kamaraj University, 2002)

171 Typed Pages

Directed by Aleksandr Simonian

Biosensing platforms and antimicrobial coatings were developed to combat problems associated with infectious diseases. Particularly, a lytic bacteriophage based surface plasmon resonance (SPR) biosensor was developed to detect food borne pathogen *Staphylococcus aureus* (*S.aureus*) in real-time with high specificity. Lytic bacteriophages are naturally developed molecular probes that infect bacteria. They are environmentally stable and inexpensive to produce compared to commercially available antibodies.

The sensitivity of SPR biosensors were further improved specifically by poly-L-lysine grafted polyethylene glycol (PLL-g-PEG) polymer. This polymer reduces non-specific adsorption of *S.aureus* on SPR gold surface by ~97%. When used as a blocking buffer in affinity sensing of model antigen, β -galactosidase by filamentous bacteriophage, this polymer improved the detection sensitivity by 2 to 3 orders of magnitude.

A facile approach was developed for sensor surface regeneration by controlling the immobilization and removal of antibodies from SPR gold surface. This was facilitated by the electro-reductive nature of alkanethiols. By combining SPR with electrochemical methods, the molecular assembly/disassembly processes were monitored in real-time with great control.

Finally, single-walled carbon nanotube (SWNT) biocomposites were prepared using DNA and lysozyme (LSZ) to develop mechanically strong antimicrobial coatings. Coulombic interactions between DNA and LSZ were exploited to fabricate multilayer antimicrobial coatings using a technique called layer-by-layer assembly. This produced large scale biomimetic coatings with significant antimicrobial activity, high Young's modulus and controlled morphology which combines the individual attributes of SWNTs and natural materials.

ACKNOWLEDGEMENTS

In the first place, I would like to express my deepest and sincere gratitude to my mentor Dr. Aleksandr L. Simonian for providing his unflagging support, guidance, motivation along with indefatigable patience during the course of this research.

I am grateful to my committee members, Dr. Fergus, Dr. Vodyanoy and Dr. Kim for their invaluable advice and discussions during this research work. My special thanks to Dr. Kim for agreeing to be the part of my committee at the last moment even during his busy schedule. My sincere appreciation to Dr. Shannon for his insightful discussions and also serving as an external reader. This work wouldn't be possible without the financial support from NSF and AUDFS. I am also grateful to Dr. V. Davis, Dr. Omar, Dr. Z. Y. Cheng, Dr. Petrenko and Dr. Prorok for their collaboration.

I am always thankful to Mr. Roy Howard, Ms. Shirley Lyles, Mr. LeVar Odum and Ms. Sandra Williams for all their help. I wouldn't have enjoyed the stay here at Auburn without the constant support from my colleagues Leamon, Sista, Sheetal, Madhumati, Tony, Valber, Dhriti, Prakash, Rigved and Greg.

My friends made this stay at Auburn an enjoyable one. Though I am not able to name everyone here, I would like to specifically convey my gratitude to Anand, Vivek, Karthik, Pradeep, Raghu, Naren, Ram, Vijay, Kavita, Kausar and Shanthi. Finally, I would like to dedicate this work to my parents, brothers, Subasri and dear friend Siva Shankar baba. I love you guys.

The following patent, peer-reviewed publications and conference presentations were a product of this dissertation:

Patent:

- Davis, V., Simonian, A. L., Nepal, D., *Balasubramanian, S*, “Preparation of Precisely Controlled Thin Film Nanocomposites of Carbon Nanotubes and Biomaterials”– U.S. Provisional Patent Application No. 61/000,938, filed on 30 October 2007

Peer-reviewed publications:

- Dhriti Nepal#, *Shankar Balasubramanian*#, Aleksandr Simonian, and Virginia Davis, “Mechanically Strong Antibacterial Thin Film Based on Single-Walled Carbon Nanotubes Armored with Biopolymers”, *Nano Letters ASAP article*, May 2008 (# equal contribution)
- *Shankar Balasubramanian*, Iryna B. Sorokulova, Vitaly J. Vodyanoy, and Aleksandr L. Simonian, “Lytic Phage as a Specific and Selective Probe For Detection of Staphylococcus Aureus—A Surface Plasmon Resonance Spectroscopic Study”, *Biosensors and Bioelectronics*, 2007, 22, 948-955
- *Shankar Balasubramanian*, Alexander Revzin, Aleksandr Simonian, “Electrochemical Desorption of Proteins from Gold Electrode Surface”, *Electroanalysis*, 2006, 18, 1885-1892 (Invited article)
- Vishwaprakash Nanduri, *Shankar Balasubramanian*, Srinivas Sista, Vitaly J. Vodyanoy, and Aleksandr L. Simonian, “Highly Sensitive Phage-based Biosensor for the Detection of β -galactosidase”, *Analytica Chimica Acta*, 2007, 589, 166-172
- H. Luckarift, *Shankar Balasubramanian*, S. Paliwal, G. Johnson and A. Simonian, “Enzyme-Encapsulated Silica Monolayers For Rapid Functionalization of a Gold Surface”, *Colloids and Surfaces B: Biointerfaces*, 2007, 58, 28-33 (Invited article)
- Dong Wei, Omar Oyarzabal, Tung-Shi Huang, *Shankar Balasubramanian*, Srinivas Sista, Aleksandr Simonian, “Development of Surface Plasmon Resonance Biosensor For The Identification of *Campylobacter jejuni*”, *Journal of Microbiological Methods*, 2007, 69, 78-85

Conference Presentations:

- Covalent Immobilization of Organophosphorus Hydrolase on Carbon Nanotubes for Biosensor Applications, accepted for oral presentation at *12th International Meeting on Chemical Sensors, Jul. 13-16, 2008, Columbus, OH*
- Electrochemical characteristics of SWNT-biopolymer nanocomposites, accepted for *213th meeting of The Electrochemical Society, May 18-23, 2008, Phoenix, AR*
- Mechanically Robust Antibacterial Thin Films Composed of Single-Walled Carbon Nanotubes and Biopolymers, *2008 AIChE Spring National Meeting, Apr. 6-10, New Orleans, LA*
- Production and characterization of protein and DNA based single wall carbon nanocomposites by layer-by-layer assembly, *MRS Fall Meeting, Nov. 26-30, 2007, Boston, MA*
- Gold surface modified with enzyme-encapsulated silica monolayers for biosensor application, *The 58th Southeast Regional Meeting of the American Chemical Society, Nov. 1-4, 2006, Augusta, GA*
- Electrochemical modulation of biological interfaces, *209th meeting of The Electrochemical Society, May 7-12, 2006, Denver, CO*
- SPR based biosensor using lytic phage as a specific and selective probe for *staphylococcus aureus* detection, *57th Pittsburgh Conference on Analytical Chemistry and Applied Spectroscopy, Mar. 12-17, 2006, Orlando, FL*
- Specific & selective detection of *staphylococcus aureus* by lytic phage using SPR biosensor, *57th Southeast / 61st Southwest Joint Regional Meeting of the American Chemical Society, Nov. 1-4, 2005, Memphis, TN*
- Prevention of non-specific binding as a way to increase sensitivity of SPR-based sensors, *206th meeting of The Electrochemical Society, October 3-8, 2004, Honolulu, HI*

Style manual or journal used: Sensors and Actuators B

Computer Software used: Microsoft Word 2003, Microsoft PowerPoint 2003, Origin Pro

7.5, Endnote X, and ImageJ

TABLE OF CONTENTS

LIST OF TABLES	xiv
LIST OF FIGURES	xv
1. INTRODUCTION	1
1.1. References.....	6
2. LITERATURE REVIEW	10
2.1. Problem.....	10
2.2. Staphylococcus aureus (<i>S.aureus</i>)	12
2.3. Pathogenesis of <i>S.aureus</i> diseases.....	13
2.4. Biosensors.....	17
2.5. Recognition elements.....	18
2.5.1. Enzyme sensors.....	18
2.5.2. Affinity sensors.....	19
2.6. Bacteriophage as an alternative probe for biosensors.....	22
2.7. Transducers.....	24
2.8. Commercial kits for <i>S.aureus</i> detection.....	25
2.9. <i>S.aureus</i> biosensors.....	27
2.10. Antimicrobial reactive coatings/surfaces.....	28
2.10.1. Nanomaterials for antimicrobial applications.....	29
2.10.2. Bio-inorganic hybrid materials for antimicrobial applications.....	30

2.11. Thesis organization	32
2.12. References	33
3. SURFACE PLASMON RESONANCE – PRINCIPLE AND EXPERIMENTAL	
SETUP	42
3.1. Optical biosensors	42
3.2. Direct detection based on guided wave	42
3.3. Biomolecules and refractive index.....	43
3.4. Surface plasmon.....	44
3.4.1. Surface plasmon polariton (SPPs) at metal/dielectric interfaces	44
3.4.2. Dispersion relations of SPP	48
3.4.3. Prism coupler	49
3.5. SPREETA™ - A commercial SPR sensor.....	51
3.5.1. Protocol for sensor setup.....	53
3.6. References.....	54
4. LYTIC PHAGE PROBE ON SPR BIOSENSOR FOR DETECTION OF	
<i>STAPHYLOCOCCUS AUREUS</i>	55
4.1. Introduction.....	55
4.2. Materials and methods	58
4.2.1. Bacterium.....	58
4.2.2. Bacteriophage and propagation.....	58
4.2.3. Reagents.....	59
4.2.4. Phage immobilization	59
4.2.5. Detection of bacteria	60

4.2.6. Binding kinetics	62
4.2.7. Detection specificity and selectivity	63
4.3. Results and discussions.....	63
4.3.1. Phage immobilization	63
4.3.2. Bacterial detection	65
4.3.3. Specificity and selectivity of the sensor response.....	69
4.4. Conclusions.....	71
4.5. References.....	72
5. BIOSENSOR SENSITIVITY IMPROVED BY PREVENTING NON-SPECIFIC ADSORPTION USING PLL-G-PEG BLOCKERS.....	77
5.1. Introduction.....	77
5.2. Materials and methods	80
5.2.1. Reagents.....	80
5.2.2. Phage.....	80
5.2.3. Bacterium.....	80
5.2.4. Synthesis of PLL-g-PEG.....	81
5.2.5. FTIR.....	81
5.2.6. Surface plasmon resonance.....	81
5.2.7. BSA-Casein blocking	82
5.2.8. PLL-g-PEG blocking	83
5.2.9. Bacterial resistant studies.....	83
5.3. Results and discussions.....	83
5.3.1. FTIR characterization of PLL-g-PEG.....	83

5.3.2. Antifouling property	87
5.3.3. Phage based bioaffinity sensing.....	87
5.4. Conclusions.....	92
5.5. References.....	93
6. ELECTROCHEMICAL DESORPTION OF PROTEINS FROM GOLD	
ELECTRODE SURFACE	96
6.1. Introduction.....	96
6.2. Materials and methods	98
6.2.1. Chemicals.....	98
6.2.2. Surface preparation and characterization.....	98
6.2.3. Combined electrochemical-SPR setup.....	99
6.2.4. Adsorption and desorption of proteins from SPR sensor surface	101
6.3. Results and discussions.....	103
6.3.1. Formation of SAM on gold.....	103
6.3.2. Immobilization of proteins on sensing surface	104
6.3.3. Reductive desorption of immobilized proteins through SAM.....	109
6.4. Conclusions.....	114
6.5. References.....	115
7. MECHANICALLY STRONG ANTIBACTERIAL COATING: SINGLE-WALLED	
CARBON NANOTUBES ARMORED WITH BIOPOLYMERS	118
7.1. Introduction.....	118
7.2. Materials and methods	118
7.2.1. Coating formation	119

7.2.2. Coating characterization	120
7.2.3. Antimicrobial activity – Turbidimetric assay	121
7.3. Results and discussions.....	122
7.4. Conclusions.....	137
7.5. References.....	138
8. OVERALL CONCLUSIONS.....	142
9. FUTURE RECOMMENDATIONS	145
9.1. Long-range surface plasmon resonance (LRSPR) biosensors	145
9.2. Devising a surface that destroy bacteria on contact.....	147
9.3. References.....	149

LIST OF TABLES

Table 2.1. Extracellular virulence factors produced by <i>S.aureus</i>	13
Table 2.2. Approximate water activities (aw) of selected bacterial pathogens associated with food illness.....	16
Table 4.1. Surface coverage for different phage immobilization times.....	68
Table 5.1. FTIR vibrational mode assignments for PLL-g-PEG	86
Table 5.2. Effect of blockers on phage- β -galactosidase detection.....	94
Table 6.1. Thickness and surface coverage calculation.....	108
Table 7.1. Comparison of enzymatic activity of lysozyme in solution and in layer-by-layer coating.....	125

LIST OF FIGURES

Fig. 2-1. Number of foodborne related outbreaks and cases reported in 10 year period from 1993 to 2002.....	11
Fig. 2-1. Breakdown of Foodborne outbreaks by its source from 1993 to 2002	11
Fig. 2-2. Schematic representation of a biosensor	17
Fig. 2-4. Biological threat agents and detection schemes.....	20
Fig. 2-5. Principle of <i>S.aureus</i> detection using commercial agglutination test kits.....	27
Fig. 3-1. Definition of planar waveguide geometry. The waves propagate along the x-direction in the Cartesian coordinate system	46
Fig. 3-2. Schematic representation of charges and surface plasmon fields propagation. The exponential dependence of E_z is shown in the right	48
Fig. 3-3. Comparison of dispersion relation between light and SPP	50
Fig. 3-4. Prism coupling to SPPs using two configurations	50
Fig. 3-5. Schematic of SPREETA™ sensor used in the study	52
Fig. 4-1. Experimental setup. A SPREETA™ sensor is docked with fluidics part to set up a flow using peristaltic pump. A polypropylene flow cell (FC) containing two independent flow channels with gasket installed on the face of SPREETA™ sensor. Silicone tubing of 0.64mm ID was inserted to the two inlet and two outlet ports. The sensor is first initialized with air and water and the references are saved for future use. The data from the sensor is fed through the control box to the computer	61
Fig. 4-2. Sensor response for different time length of phage immobilization. The net change in RI for particular immobilization is calculated by subtracting the subsequent PBS baselines. The phage surface coverage was calculated using the formula 1	65
Fig. 4-3. Optical microscope image of the sensor surface after exposure to the suspension of <i>S. aureus</i> at 10^7 cfu/ml. A – sensing channel; B – reference channel.....	66

Fig. 4-4. Dose-response curve for *S. aureus* detection by lytic phage. The net response curves were plotted after adjusting for non-specific binding and bulk RI change from control channel. The detection limit of 1×10^4 cfu/ml was calculated as the lowest *S. aureus* concentration producing distinguishable net response (signal/noise ≥ 3). Mean values (n=3) of ΔRU vs. aureus concentration is plotted. Bars are SD. Points are experimental data while curve is sigmoidal fit ($\chi^2 = 0.59$, $R^2 = 0.988$).....67

Fig. 4-5. Hill Plot of binding isotherm. Hill coefficient was found to be 0.46. Dissociation constant for phage-bacteria complex was found to be 0.66×10^5 cfu/ml. Points are experimental data while line is linear least-square fit (R = 0.99, slope = 0.46 ± 0.03)68

Fig. 4-6. The response curve for the inhibition assay showing the specificity of *S. aureus* detection by lytic phage. Different concentration of phage were pre-incubated with a known concentration of *S. aureus* for 1 hr to block the receptor sites for binding, and the solutions were flown through the sensor. As a free phage concentration increases, the more binding sites on the bacterial surface are blocked and less number of bacteria is able to bind on the sensor surface. Squares are experimental data, and bars are SD (n=3). The smooth curve is sigmoidal fit of experimental data ($\chi^2 = 0.216$, $R^2 = 0.99$).....70

Fig. 4-7. Selectivity of *S. aureus* detection by lytic phage was demonstrated by cross-examining with non-specific *Salmonella typhimurium*. The figure shows the response obtained with alternative application of incrementally increasing concentrations of *Salmonella typhimurium*. Even for the high concentrations *Salmonella typhimurium* failed to produce any significant signal and the response returns to the baseline after washing with PBS buffer.71

Fig. 5-1. FTIR spectrum showing the vibrational modes of PLL-g-PEG polymer84

Fig. 5-2. Kinetics of PLL-g-PEG adsorption to MUA modified and unmodified gold surface85

Fig. 5-3. Schematic of PLL-g-PEG adsorption to a).11-MUA modified and b).unmodified surface86

Fig. 5-4. Comparison of *S.aureus* adsorption to PLL-g-PEG, BSA-Casein blocked and unblocked gold surfaces.....86

Fig. 5-5. Real time responses obtained for phage immobilization on SPR sensor. A - PBS, B – Working (1G40) & Control phage (F8-5), C - BSA and D – PBS-Tween 20 (0.5% v/v).88

Fig. 5-6. Real-time response for β -gal detection by the selected phage immobilized on the sensor surface. Wild type F8-5 was used as a control phage to show the responses

due to non-specific binding of enzyme to the sensor surface. The signal on this fig was normalized to the baseline indicated by arrows in fig. 5-589

Fig. 5-7. Comparison of response curve for phage based β -gal detection using PLL-g-PEG and BSA-Casein as blockers.....90

Fig. 5-8. Hill Plot of binding isotherm. The parameters obtained from Hill plot are listed in Table 5-291

Fig. 6-1. Combined electrochemical SPR (ESPR) setup. A homemade electrochemical-SPR cell (ESPR cell) was used for all ESPR experiments. SPREETA sensor containing gold electrode was used as working electrode (WE), while Ag/AgCl and Pt foil were used as reference electrode and auxiliary electrode respectively. For two-electrode process, the Ag/AgCl reference electrode (RE) was removed and potential was applied against Pt counter electrode (CE). The RE and CE leads from the potentiostat were both connected to the Pt electrode in order to use potentiostat as power source.....100

Fig. 6-2. Schematic of a sequence of surface modification steps employed in the study102

Fig. 6-3. Ellipsometric thickness measurements for gold surface modified with anti-OPH immobilized on MUA SAM104

Fig. 6-4.a. Protein immobilization and reductive desorption using SPR. The sequences of the steps are as follows: 1) modification with 1 mM MUA; 2) washing with ethanol and PBS; 3) activation of surface carboxylates using 0.4 M EDC/0.1 M NHS mixture; 4) washing with PBS; 5) covalent immobilization of BSA (1mg/mL) to the activated SAM surface; 6) PBS wash and; 7) reductive desorption of the immobilized molecules at -1200 mV vs. Pt electrode in PBS using two-electrode setup and 8) confirmation of reductive desorption by applying -1200 mV. Insert figure shows the steps 3 to 8.....106

Fig. 6-4. b. Two cycles demonstrating adsorption and desorption of BSA from the electrode surface.107

Fig. 6-5. Anti-OPH antibody immobilization and reductive desorption using SPR. The sequences of the steps are follows: 1) modification with 1 mM MUA, 2) activation of surface carboxylates using 0.4 M EDC/0.1 M NHS mixture, 3) covalent immobilization of anti-OPH (0.1 mg/mL) to the activated SAM surface, 4) quenching with 50 mM Tris buffer, 5) injection of OPH (35 nM), and 6) Reductive desorption of the immobilized molecules at -1200 mV vs. Pt electrode in PBS using Two electrode setup. Insert figure represents the steps from 2 to 6109

Fig. 6-6. Cyclic voltammogram of 0.1 M HClO ₄ from combined ESPR setup. a) Cyclic voltammogram collected using ESPR device; b) DRI vs. E, i.e., potential-dependent change in SPR response.....	111
Fig. 6-7. Cyclic voltammogram of commercial BAS electrode modified with SAM and antibody. All the CV's were performed in 5mM FCN solution prepared in 10 mM PBS, pH 7.4. a) Bare gold electrode; b) gold electrode modified with 1mM MUA for 20 h; c) gold electrode modified with antibody (1 h) after SAM activation with EDC/NHS mixture; d) after reductive desorption using two-electrode system at -1200 mV vs. Pt electrode; and e) after reductive desorption using two-electrode system at -1400 mV vs. Pt electrode.....	113
Fig. 7-1. (a) Turbidimetric assay of LSZ and LSZ-SWNT conjugate in solution against <i>M. lysodeikticus</i> . (b) Rate of <i>M. lysodeikticus</i> lysis reaction (Regression line is fit to the linear portion of experimental data points in (a) using first-order kinetics).....	124
Fig. 7-2. (a) UV-vis-Near IR absorbance spectra of LBL assembly of LSZ-SWNT/ DNA-SWNT (concentration of SWNT in dispersion ~25mg/L). The inset magnifies the van Hove transitions of metallic and semiconducting SWNT. (b) Comparison of UV-vis accumulation curves for absorbance at 510nm and ellipsometry thickness measurement of the LBL assembly. c) AFM image of DNA-SWNT dried dispersion. d) Schematic diagram of LBL assembly of LSZ-SWNT and DNA-SWNT	126
Fig. 7-3. SEM images of LBL assembly of LSZ-SWNT/DNA-SWNT of the (a) 8 th layer and (b) 68 th layer. (c) Raman spectra of the assembly (8th layer) showing D-band to G-band recorded at various angles between the polarization of laser excitation and SWNT alignment direction using 514nm laser d) Raman mapping collected at 10 x10 μm area (8th layer) showing D-band and G-band. The scale bars in (a) and (b) represent 200 nm.....	128
Fig. 7-4. Raman spectra of LSZ-SWNT/DNA-SWNT (at 8th layer) (prepared by random air directions) showing D-band to G-band recorded at various angles between the polarization of laser excitation and SWNT alignment direction using 514nm laser.....	129
Fig. 7-5. UV-Vis-Near IR absorbance spectra of LBL assembly of LSZ-SWNT/ DNA-SWNT obtained from dispersion of SWNT at higher concentration (~45 mg/L). (a) without NaCl, (b) with addition of NaCl (10 mM). The insets in (a) and (b) magnifies the van Hove transitions of metallic and semiconducting SWNTs.....	130
Fig. 7-6. a). Comparison of ellipsometry thickness measurement of the LBL assembly b). Surface plasmon resonance of in-situ thin film deposition showing the surface coverage	131

Fig. 7-7. Nanoindentation tests on a 68 layer coating (LSZ-SWNT/DNA-SWNT) ₆₈ (a) Load-displacement curve from which b). Young's modulus and c). Hardness were obtained.....	133
Fig. 7-8. (a) Effect of different layers of LBL coating against <i>M. lysodeikticus</i> in turbidimetric assay. (b) Rate of <i>M. lysodeikticus</i> lysis reaction (Regression line is fit to the linear portion of experimental data in (a) using first-order rate kinetics). SEM image of samples incubated with <i>Staphylococcus aureus</i> at 37°C for 24hrs of (c) a clean silicon wafer (control) and (d) LBL assembly at 11th layer (top surface LSZ-SWNT) arrows indicating damaged cells). The scale bars in (c) and (d) represent 1µm.....	134
Fig. 7-9. The activity of 21 layer LBL coating on the first and sixtieth day by turbidimetric assay.....	136
Fig. 9-1. Proposed design of long range SPR (LRSPR) system for bacterial detection in comparison with conventional SPR.....	146
Fig. 9-2. Phage induced lysis of <i>S.aureus</i> a). on gold coated sensor surface and b). in solution.....	148

1. INTRODUCTION

The 2007 world health report by World Health Organization (WHO) [1] explicitly reveals the challenges the humanity is facing in the form of infectious diseases which threatening the public health security more than ever. The ecological balance between microorganisms and environment is ever changing because of the advancement in every facet of the human life, such as economic development, travel and trade. Thanks to globalization and lower manufacturing cost in developing countries, the recent trend in global production, processing and distribution of food products increased dramatically over the last decade. This illuminates the need for safer global food supply. US alone imports approximately 15% of its overall food supply from 150 countries including ~60% of fresh fruits & vegetable and ~75% of seafood related products. Among the imported foods, products likely to get contaminated such as ready-to-eat products, fresh produce and sea food accounts for greater proportion. This imposes a greater responsibility on the federal organizations in securing the safety of the food products reaching American homes daily.

The very fact that natural foods come from soil, water, plants and animals that are rich in bacterial flora assures the existence of bacteria in the food products unless protective measures are implemented. While some organisms can cause food to spoil others can wreak havoc by creating an outbreak. Recent multiple *E. Coli* outbreaks in 2006 & 2007 [2-4] have made federal safety organizations in US and around the world to

create more awareness and concern about food safety among public. Even with the a sustained effort from safety organizations, foodborne illness are grossly underreported in US and continues to impose socio-economical problems by affecting general and at-risk populations (older adults, young children, pregnant woman and their unborn children, organ transplant recipients and others with immunocompromised conditions). According to United States Department of Agriculture (USDA) estimates, the economic burden imposed by the foodborne illnesses due to lost in productivity and cost of medical treatment may be as much as \$83 billion. This is a direct result of 76 million illnesses, 325,000 hospitalizations and 5,000 deaths caused by these pathogens [5].

In spite of all the advances in the treatment methods, infectious diseases caused by these pathogens remain the primary cause of death worldwide and also one of the leading causes of death in the US. The diseases caused by these microorganisms can be deadly, contagious and sometimes zoonotic (for e.g. SARS). This poses a greater threat to global security without an act of bioterrorism or biological warfare, because these organisms are well equipped to adapt to new ecological conditions and can multiply within hours. These harmful pathogens can infect us in many different ways. Disease can be transmitted from an infected person to an uninfected person by one of the following means:

1. droplet contact: coughing/sneezing during cold or flu
2. direct contact: physical contact between infected and uninfected person/animal, e.g. HIV

3. indirect contact: transmission of disease causing organism from contaminated inanimate object, fomite (such as tabletop, door knobs, faucet handle etc.) to a person/animal
4. airborne transmission: aerosol of disease causing germs suspended in air, e.g. SARS, TB
5. common vehicle or fecal-oral transmission: from contaminated food or water sources, e.g. *E.Coli* O517:H7 contamination
6. vector-borne: through insects such as mosquitoes, e.g. West Nile Virus

Another disturbing trend is noticed with so-called nosocomial infection (hospital-acquired), where a patient contract an infection during the stay in the hospital independent of his medical condition when admitted to the hospital. The overuse of antibiotics in hospitals and in household following the discovery of penicillin by Sir Alexander Fleming created deadly strains of antibiotic-resistant microbes. Some of the pathogens have developed resistance against all penicillin's including methicillin and other newly developed antibiotics like vancomycin [6]. Center for Disease Control (CDC) estimates as much as 90,000 die a year because of the antibiotic-resistant strains incurring \$11billion related expenses. Mycobacterium tuberculosis and methicillin resistant *Staphylococcus aureus* (MRSA) are the two most common pathogens associated with these infections. For more than half a century, MRSA related infections pose a serious health threat to the public safety. The mortality rate is higher for blood related (bacteremia) and catheter related infections of MRSA [7]. Once exclusively associated with hospitals, these bacteria are now common in community associated *S. aureus* infections (known as staph infection) [8].

It is clear that personal hygiene plays a pivot role in public safety as well as in preventing contamination of food products and controlling dissemination of diseases. In addition to the personal hygiene, measures are needed to eliminate the source of the disease from spreading to wider population. Thus eradication of the disease at the source should be the chief strategy to reduce the socio-economical impact associated with these infections. This strategy requires better tools/materials for in-depth understanding of pathogens interaction to the environment than those currently available. Some of the strategies may include application of novel materials in identification of pathogens [9, 10], prevention of bacterial colonization using non-fouling materials [11] and application of materials such as lytic enzymes, peptides and bacteriophage to eliminate the threat at the source [12].

Often overlooked in US, the application of bacteriophage to combat antibiotic-resistant bacteria as well as in detection and identification of biowarfare agents is growing rapidly [13-15]. Bacteriophages are viruses, harmless to humans but capable of infecting and replicating within bacteria. They can be either virulent (lytic) or temperate (lysogenic) [16]. Their resistance to environmental stresses combined with extreme specificity towards the host bacterium makes them an excellent molecular probe for the detection of pathogenic bacteria. Several applications based on engineered filamentous phage for pathogen detection has been proposed and demonstrated [17-19].

With this in mind, there is an obvious need for the development of analytical devices to detect these pathogens not only for the safety but also for the prevention of disease spread. Recent revolutionary progress made in advanced instrumentation and in nanostructured materials holds promise in delivering dramatic improvement in

identifying the source and nature of contamination and ways to combat it. The modern technologies such as chemical and biosensors changed the way these pathogens are identified. These analytical devices offer several advantages such as real-time monitoring combined with rapidity and portability for field use. A review of literature shows that plethora of detection schemes are available for next-generation of pathogen detection. Surface plasmon resonance (SPR) biosensors based on optical transduction scheme are particularly attractive for the construction of biosensors as they offer, “label-free” and “near real-time” detection of analytes of interest. Coupled with high sensitivity, this technique has been widely employed for the detection of various bacteria [20-22], toxins [23, 24], and viruses [25].

Accordingly, the main objective of this work is the development of SPR based functional surfaces for biosensing applications. Chapter 2 describes the necessary literature work followed by experimental setup of SPR method in Chapter 3. Chapter 4 explores the prospects of lytic bacteriophage as a biosensor recognition probe for detection of *S.aureus* with emphasis of specificity and selectivity. Chapter 5 describes the application of poly-L-lysine-g-poly(ethylene glycol) (PLL-g-PEG) polymer for prevention of non-specific binding and hence, improving the sensitivity of SPR biosensor. When used as a blocking agent, this polymer improved the detection of model target enzyme β -galactosidase using affinity-selected filamentous phage by 2 to 3 orders of magnitude. Chapter 6 introduces a facile method to modulate biological interfaces using the electro-responsive nature of alkanethiol monolayers for biosensor & biomedical applications. Finally, Chapter 7 describes the development of novel antimicrobial coatings based on DNA and Lysozyme functionalized single-walled carbon nanotubes

(SWNT). Here various challenges associated in transforming excellent properties of SWNT to macroscopic systems were investigated. One of them is the tendency of SWNT to get aggregated. To solve this, a biomimetic approach is suggested where biomolecules such as DNA and lysozyme were used to disperse single-walled CNT (SWNT) as individuals. Also, the strong columbic interactions between DNA and lysozyme were exploited through layer-by-layer approach to develop mechanically strong novel antimicrobial coatings.

1.1. References

1. Chen, M., C. Heymann, T. Prentice, and L.T. Reinders, *The World Health Report 2007 - A safer future: global public health security in the 21st century*. 2007, World Health Organization.
2. *Update on Multi-State Outbreak of E. coli O157:H7 Infections From Fresh Spinach, October 6, 2006*. [cited 2008 January 15]; Available from: <http://www.cdc.gov/foodborne/ecolispinach/100606.htm>.
3. *FDA Investigating E. Coli O157 Infections Associated with Taco Bell Restaurants in Northeast*. 2006 [cited 2008 January 15]; Available from: <http://www.fda.gov/bbs/topics/NEWS/2006/NEW01517.html>.
4. *Multistate Outbreak of E. coli O157 Infections Linked to Topp's Brand Ground Beef Patties*. 2007 [cited 2008 January 15]; Available from: <http://www.cdc.gov/ecoli/2007/october/100207.html>.
5. Mead, P.S., L. Slutsker, V. Dietz, L.F. McCaig, J.S. Bresee, C. Shapiro, P.M. Griffin, and R.V. Tauxe, *Food-related illness and death in the United States*. *Emerging Infectious Diseases*, 1999. **5**(5): p. 607-625.

6. Lewis, R., *The Rise of Antibiotic-Resistant Infections*, in *FDA Consumer*. 1995.
7. Archer, G.L. and M.W. Climo, *Staphylococcus aureus Bacteremia -- Consider the Source*. 2001. p. 55-56.
8. Hota, B., *Contamination, Disinfection, and Cross-Colonization: Are Hospital Surfaces Reservoirs for Nosocomial Infection?* *Clinical Infectious Diseases*, 2004. **39**(8): p. 1182-1189.
9. Chambers, J.P., B.P. Arulanandam, L.L. Matta, A. Weis, and J.J. Valdes, *Biosensor recognition elements*. *Current Issues in Molecular Biology*, 2008. **10**: p. 1-12.
10. Zourob, M., E. Souna, and A.P.F. Turner, *Principles of Bacterial Detection: Biosensors, Recognition Receptors and Microsystems*. 2008: Springer. 1040.
11. Qian, X.P., S.J. Metallo, I.S. Choi, H.K. Wu, M.N. Liang, and G.M. Whitesides, *Arrays of self-assembled monolayers for studying inhibition of bacterial adhesion*. *Analytical Chemistry*, 2002. **74**(8): p. 1805-1810.
12. Tiller, J.C., C.J. Liao, K. Lewis, and A.M. Klibanov, *Designing surfaces that kill bacteria on contact*. *Proceedings of the National Academy of Sciences of the United States of America*, 2001. **98**(11): p. 5981-5985.
13. Goldman, E.R., M.P. Pazirandeh, J.M. Mauro, K.D. King, J.C. Frey, and G.P. Anderson, *Phage-displayed peptides as biosensor reagents*. *Journal Of Molecular Recognition*, 2000. **13**(6): p. 382-387.
14. Petrenko, V.A. and V.J. Vodyanoy, *Phage display for detection of biological threat agents*. *Journal of Microbiological Methods*, 2003. **53**(2): p. 253.

15. Thacker, P.D., *Set a Microbe to Kill a Microbe: Drug Resistance Renews Interest in Phage Therapy*. The Journal of the American Medical Association, 2003. **290**(24): p. 3183-3185.
16. Kutter, E. and A. Sulakvelidze, *Bacteriophages - Biology and Applications*. 2004: CRC Press.
17. Goodridge, L., J.R. Chen, and M. Griffiths, *Development and characterization of a fluorescent-bacteriophage assay for detection of Escherichia coli O157 : H7*. Applied and Environmental Microbiology, 1999. **65**(4): p. 1397-1404.
18. Mosier-Boss, P.A., S.H. Lieberman, J.M. Andrews, F.L. Rohwer, L.E. Wegley, and M. Breitbart, *Use of fluorescently labeled phage in the detection and identification of bacterial species*. Applied Spectroscopy, 2003. **57**(9): p. 1138-1144.
19. Petrenko, V.A. and I.B. Sorokulova, *Detection of biological threats. A challenge for directed molecular evolution*. Journal of Microbiological Methods, 2004. **58**(2): p. 147-168.
20. Bokken, G.C.A.M., R.J. Corbee, F. van Knapen, and A.A. Bergwerff, *Immunochemical detection of Salmonella group B, D and E using an optical surface plasmon resonance biosensor*. FEMS Microbiology Letters, 2003. **222**(1): p. 75.
21. Koubova, V., E. Brynda, L. Karasova, J. Skvor, J. Homola, J. Dostalek, P. Tobiska, and J. Rosicky, *Detection of foodborne pathogens using surface plasmon resonance biosensors*. Sensors and Actuators B: Chemical, 2001. **74**(1-3): p. 100.

22. Leonard, P., S. Hearty, J. Quinn, and R. O'Kennedy, *A generic approach for the detection of whole Listeria monocytogenes cells in contaminated samples using surface plasmon resonance*. *Biosensors and Bioelectronics*, 2004. **19**(10): p. 1331.
23. Medina, M.B., *A biosensor method for a competitive immunoassay detection of staphylococcal enterotoxin B (SEB) in milk*. *Journal Of Rapid Methods And Automation In Microbiology*, 2005. **13**(1): p. 37-55.
24. Naimushin, A.N., S.D. Soelberg, D.K. Nguyen, L. Dunlap, D. Bartholomew, J. Elkind, J. Melendez, and C.E. Furlong, *Detection of Staphylococcus aureus enterotoxin B at femtomolar levels with a miniature integrated two-channel surface plasmon resonance (SPR) sensor*. *Biosensors and Bioelectronics*, 2002. **17**(6-7): p. 573.
25. Boltovets, P.M., B.A. Snopok, V.R. Boyko, T.P. Shevchenko, N.S. Dyachenko, and Y.M. Shirshov, *Detection of plant viruses using a surface plasmon resonance via complexing with specific antibodies*. *Journal of Virological Methods*, 2004. **121**(1): p. 101.

2. LITERATURE REVIEW

2.1. Problem

The spectrum of foodborne illness is constantly changing and evolving. While tuberculosis, cholera and typhoid fever were the common foodborne diseases century ago, the scope of illness expanded to emergence of drug-resistant and new pathogens in the new millennia. Illness caused by the pathogens may be of different origin; it can be bacterial, viral, parasitic and chemical or combination of any of the above contaminants along with toxins produced by the microorganisms. Center for Disease Control (CDC) & Food and Drug Administration (FDA) defines a foodborne disease outbreak (FBDO) as “the occurrence of two or more cases of a similar illness resulting from the ingestion of a common food” [1, 2]. Fig.2-1 shows the total number of foodborne related outbreaks and cases accounted over a 10 year period from 1993 to 2002. As noticed in the figure 1, about 56 to 73 % of outbreaks have unknown etiology. Several factors may contribute to the source of unknown etiology due to their: small size, long/short incubation period, geographic dispersion, inability to identify the pathogen involved and no medical attention due to mild illness [3, 4]. A sudden increase in outbreaks was noticed after 1997 due to enhanced outbreak surveillance along with improved reporting methods such as electronic reporting method by state, local & territorial health departments.

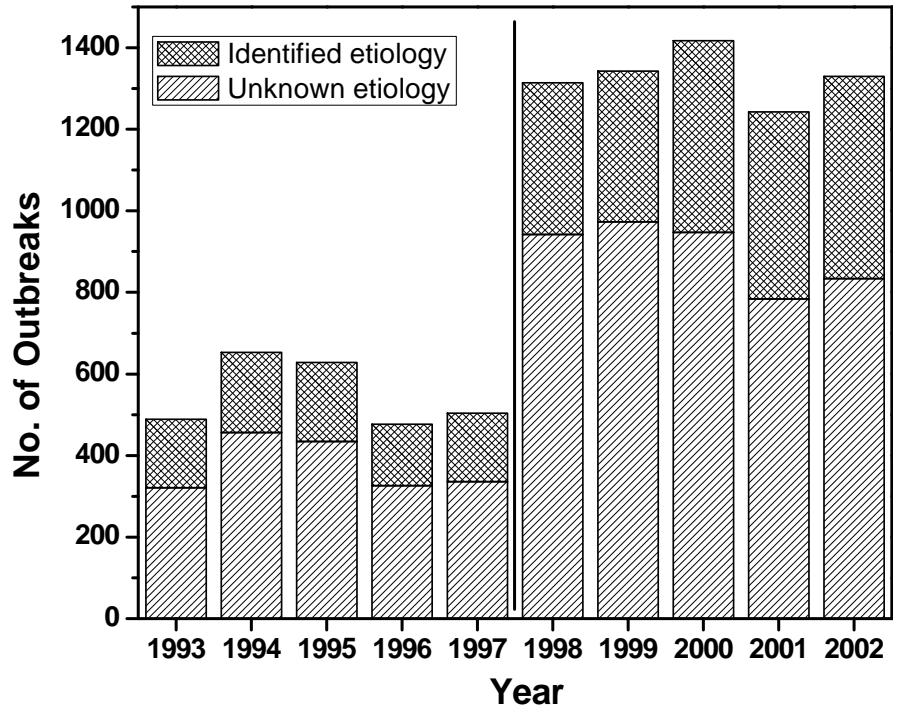


Fig. 2-1 Number of foodborne related outbreaks and cases reported in 10 year period from 1993 to 2002 [3, 4]

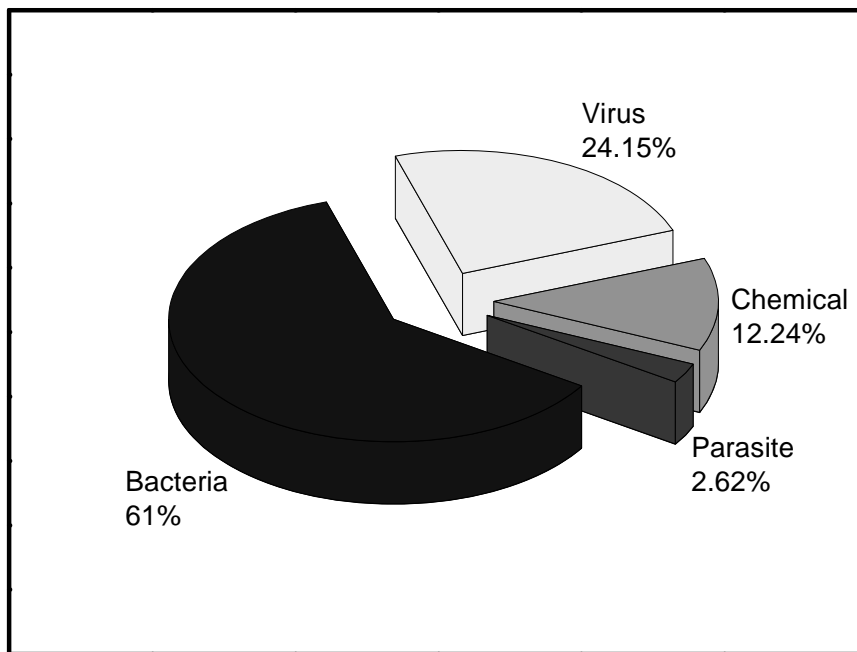


Fig. 2-2 Breakdown of Foodborne outbreaks by its source from 1993 to 2002

Bacterial pathogens by virtue of their ability to multiply remains *the* most common cause of foodborne outbreaks worldwide compared to virus or any other sources of contamination. During the above reported period, bacteria were responsible for 61% of identified outbreaks resulting in millions of illness (Fig2-2). Among bacterial pathogens, *Salmonella* serotype Enteritidis accounted for largest number of outbreaks (24%) followed by *Clostridium* (11%) and *Staphylococcus* (8%). *Escherichia coli* O157:H7 (6%) and *Campylobacter* (3%) were responsible for multi-state outbreak in US. Three-fourth of outbreak caused by bacteria linked to beef, pork, dairy, eggs and poultry products. During the same period viral related outbreaks increased at an alarming rate from mere 6% (reported during 1993 to 1997) to 33% (reported during 1998 to 2002). This is mainly because of enhanced molecular detection methods for norovirus, a major source of viral outbreak emphasizing the importance of novel detection methodologies.

2.2. *Staphylococcus aureus* (*S.aureus*)

Staphylococcus aureus is an important causative agent of food poisoning because it can contaminate food products both during preparation and processing. They are gram positive, non-spore forming; non-motile bacteria belong to the genus *Staphylococci* of Micrococcaceae family. They are spherical in shape with a diameter of 0.5-1.5 μ m and can occur as single cells, in pairs or as clusters. *Staphylococci* are broadly classified in to two groups: coagulase positive & coagulase negative. *S.aureus*, a coagulase positive species is the most common of staphylococcus genus associated with diseases in humans and animals. They can be differentiated from other staphylococci on the basis of gold pigmentation of colonies (hence the name aureus) and positive results of coagulase, catalase, deoxyribonuclease tests and anaerobic fermentation of glucose & mannitol.

These species are aerobes or facultative anaerobes that typically grow within the temperature between 7 and 48 °C, with an optimum of 35-40°C [5]. These characteristics allow them to flourish in a wide variety of food products.

2.3. Pathogenesis of *S.aureus* diseases

S.aureus is part of the common micro flora found on the nares, pharynx and/or skin of the host. It is a very interesting organism having a diverse arsenal of components and products (Table 2-1) causing multiple diseases in humans and animals. Apart from the toxins, proteins and adhesins present on the surface of *S.aureus* aids in the attachment to host tissue promoting colonization. These virulence factors cause several diseases including skin lesions, urinary tract infections, gastroenteritis, pneumonia, mastitis, phlebitis, meningitis, osteomyelitis and endocarditis. The clinical manifestation associated with the infection depends on the complex interplay between *S.aureus* products and host defense mechanisms following a breach of the skin or access to the bloodstream [6].

Toxins	Enzymes
Cell Membrane damaging toxins:	Coagulase
α-toxin	Staphylokinase
β-toxin	Proteases
γ-toxin	Phospholipase
δ-toxin	Lipase
leucocidin	DNase
Epidermolytic toxin	Hyaluronidase
Toxic shock syndrome toxin-1	Phosphatase
Enterotoxin	β-Lactamase
Pyrogenic exotoxin	

Table 2-1 Extracellular virulence factors produced by *S.aureus*

Humans are always at risk of becoming infected with *S.aureus* strains since nearly 30 to 50% of humans are colonized with this bacteria on their skin or in nose along with other micro flora. The introduction of penicillin during 1940's saw a decline in mortality associated with *S.aureus* infections. However, by 1950's nearly 50% of hospital isolates developed resistance against penicillin. A semi-synthetic variant of penicillin's such as methicillin, oxacillin were introduced in 1960's only to find out these pathogens developed resistance to the new antibiotic within a span of two years. Today approximately 60% of clinical strains are methicillin resistant leaving vancomycin as our last line of defense against this deadly pathogen. However, the outlook of the treatment options looks limited as strains with intermediate resistance to vancomycin is reported in Japan in 1996 followed by vancomycin resistant strains few years later [7]. As this bacterium evolving at much faster rate physicians and microbiologists have yet to completely understand its mechanism of infection and are racing against the time to discover new line of antibiotics that can overcome the bacterial resistance.

Due to high rate of colonization on humans, both methicillin-sensitive (MSSA) and methicillin resistant (MRSA) strains lead to the spread of staphylococcal infections in the hospital setting. Most of the nosocomial (hospital-related) infections originate from the hands of health care workers or from infected patients. Recognized 50 years ago, MRSA becomes more persistent in hospitals in last 20 years. Apart from causing mild skin infections, they are responsible for fatal illness such as toxic shock syndrome. Once exclusively associated with hospitals, these antibiotic resistant strains are now common cause of community-assisted MRSA infections (known as staph infections) infecting more than 2 million Americans.

The relative prevalence of *S.aureus* in animals poses a serious threat to our food safety. For example, it is estimated that nearly 90% dairy herds are carriers of *S.aureus* which may transmit this organism through various dairy products. *S.aureus* causes food poisoning mainly by producing enterotoxins. There are 14 different enterotoxins designated as staphylococcal enterotoxin A (SEA), SEB, SEC, SED, SEG, SHE, SEI, SEJ, SEK, SEL, SEM, SEN and SEO [8-10].

Many intrinsic and extrinsic factors such as temperature, pH, nitrite concentration and water activity (a_w) determine the growth of *S.aureus* and staphylococcal enterotoxin (SE) production. The bacterial growth and toxin production largely depends on the nutritional availability. Several amino acids such arginine and cysteine are necessary for both bacterial growth and SE production. However, the presence of other organisms in the food products has a huge impact on *S.aureus* growth and hence on enterotoxin formation. Common spoilage agents such as pseudomonas, lactobacilli and streptococcus will limit the growth at almost any temperature. Even though this bacterium will be outnumbered in the presence of competing microbes, *S.aureus* developed a strategy to grow under extreme conditions such as water activity (a_w) of 0.83, which is too low for any bacteria to even survive (Table 2-2). They are very tolerant to the presence of solutes such as salts and sugars and can easily replicate over a range of water activity from 0.83 to >0.99 [11, 12].

Organisms	Minimum	Maximum	Optimum
<i>Campylobacter spp.</i>	0.98		0.99
<i>Shigella spp.</i>	0.97		
<i>Yersinia enterocolitica</i>	0.97		
Enterohemorrhagic <i>E.coli</i>	0.95		0.99
<i>Salmonella spp.</i>	0.94	>0.99	0.99
<i>Vibrio parahaemolyticus</i>	0.94	0.99	0.98
<i>Bacillus cerus</i>	0.93		
<i>Clostridium perfringens</i>	0.943	0.97	0.95-0.96
<i>Listeria monocytogenes</i>	0.92		
<i>Staphylococcus aureus</i> growth	0.83	0.99	0.98
<i>Staphylococcus aureus</i> toxin	0.88	0.99	0.98

Table 2-2 Approximate water activity (a_w) of selected bacterial pathogens associated with food illness [13]

The toxins produced by *S.aureus* are single polypeptide chains of low molecular-weight proteins (26 – 34 kDa) comprising large amounts of lysine, tyrosine, aspartic and glutamic amino acids. Almost all of the SE has a disulfide bridge in the middle of the molecule to stabilize its structure. These enterotoxins are the members of the toxin super family secreted by *S.aureus* and are responsible for gastroenteritis. It exhibit resistance against heat, irradiation and some proteolytic enzymes such as trypsin, chymotrypsin, rennin and papain (pH > 2.0). Especially, their enhanced resistance against common processing techniques (heat, irradiation & enzymes) in complex food matrix compared to laboratory conditions explains why these SE able to remain active after ingestion or remain active for several years [8, 12, 14].

Hence, the supply of inadequately processed food contaminated with *S.aureus* and SE jeopardize the food safety. With the high possibility of recontamination from a human

& animal source coupled with ability of this organism to grow in inanimate object where water is scarce reveals the challenges in food inspection for this pathogen and the necessity to maintain proper sanitation.

2.4. Biosensors

Biosensor is defined by IUPAC [15, 16] as a self-contained analytical device capable of providing quantitative or semi-quantitative information about the system under investigation using a biological recognition element retained in direct contact with a transduction element. The schematic of a typical biosensor is shown in Fig. 2-3.

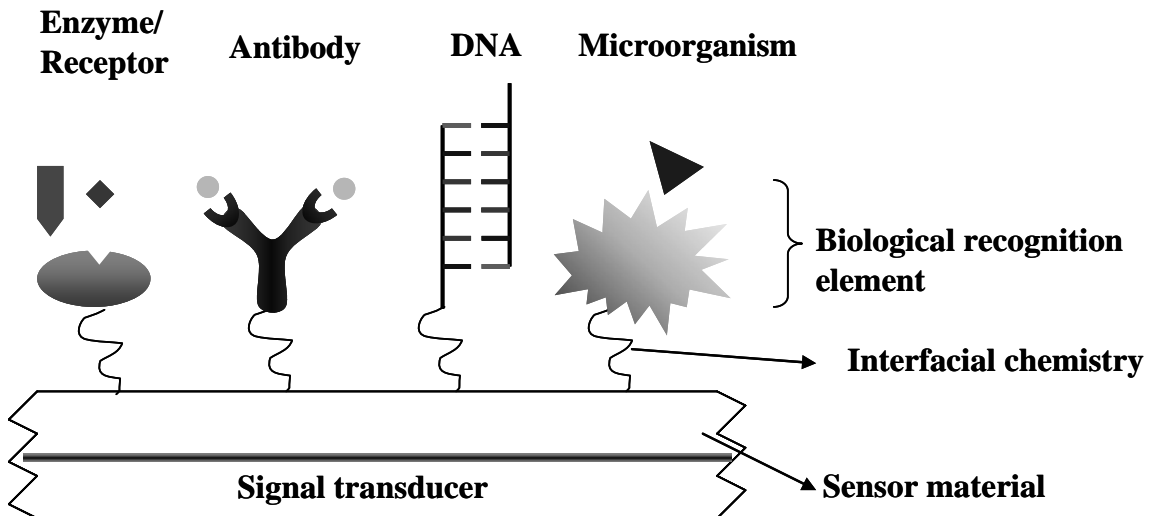


Fig. 2-3 Schematic representation of a biosensor

Biosensors are usually classified into various groups either by type of transducer employed (electrochemical, optical, piezo-electric, and thermal) or by the kind of bio recognition element utilized (antibody, enzymes, nucleic acids, and whole cells). Both components of the biosensor, namely, bio recognition element (referred as a ‘receptor’) and transduction platform (referred as a ‘transducer’) play an important role in the construction of a sensitive and specific device for the analyte of interest (referred as a

‘target’). The operational characteristics of a biosensor are influenced by both receptor and transducer each having its inherent advantages and disadvantages over others.

Advancement in the fields of engineering, molecular and micro biology provides us with the tools to develop new techniques to monitor molecular interactions on solid-state devices under physiological conditions. Especially, breakthroughs in the field of nanotechnology and microelectronics allow us to miniaturize all components of physical systems such as pumps and valves into sensing devices creating a disposable lab-on-chip. Hence, coupling the ingenious sensitivity and specificity of biomolecules with electronic devices creates a simple, inexpensive analytical device capable of providing molecular information which was once existed as hypotheses. Potential application areas of biosensor include molecular diagnostics in patient health care, pharmaceutical industry, food and beverage industry, environmental and ecological monitoring, bioprocess monitoring and in military/anti-terrorism. Due to the immense growth in various technologies, this review is not intended to be comprehensive. However, main emphasis will be on selection of probes and on the advancement of transducer technology for bacterial sensor application.

2.5. Recognition elements

2.5.1. Enzyme sensors

Based on receptors, biosensing mechanism can be sub-divided in to two categories: catalytic and non-catalytic (affinity based). Nearly all of the catalytic sensors employ enzymes as their receptors while some of the new formats use whole microorganisms. A popular example for enzyme based biosensor is the glucose (bio) sensor for diabetes management which utilizes glucose oxidase enzyme. This enzyme

oxidizes blood glucose to glucono-lactone and hydrogen peroxide which in turn oxidized to produce measurable signal. Glucose biosensors are mostly electrochemical in nature as the mechanism involves oxidation and reduction of sample and enzyme respectively [17].

Other common application of enzymes in biosensors involves in the detection and decontamination of pesticides and potential chemical warfare agents. Our group has developed battery of biosensor platforms for detection of organophosphate pesticides and chemical warfare agents using organophosphorus hydrolase as enzyme receptors [18-22]. Even though enzymes are most widely used in biosensor design, several factors affect its spectrum of application such as large scale production, expensive purification procedures, requirement of co-factors for its appropriate catalytic activity and limitation to detect small molecules and metabolites. The presence of multiple enzymes and co-factors within the whole microorganisms offers an inexpensive route for biosensor applications. In addition, its ability to detect wide array of chemical substances, mutability, broad operating pH and temperature range may overcome some of the issues associated with selectivity of microbial biosensors. More detailed application of microbes in biosensor can be found in extensive reviews and in their references [23]. In common, enzyme based biosensors are highly selective, fairly fast-acting and suffer from loss of activity over time due to denaturation.

2.5.2. Affinity sensors

Second class of biosensors based on selective interaction between immobilized receptors and its partner molecule through affinity are called as affinity biosensors. Common affinity sensing mechanism involves antigen-antibody interaction, DNA hybridization and other receptors-target interaction with or without labels. This versatility

of affinity biosensing has the advantage of utilizing almost all the transducers for transforming its interactions to measurable signals.

Identification assays for the agent's are improved dramatically in past 20 years because of technological innovations in molecular and microbiology. Detection of these agents can be either genotype or phenotype (Fig. 2-4).

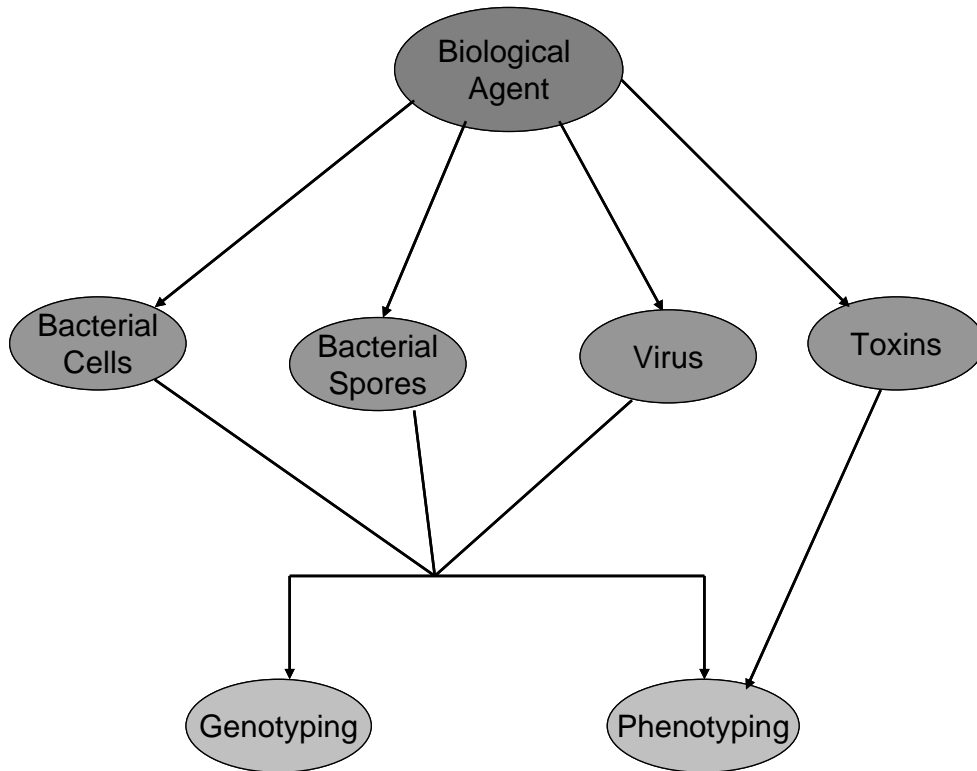


Fig. 2-4 Biological threat agents and detection schemes

The fact that infection causing agents express surface receptors or ligands that is specific for complimentary biomolecular ligands or receptors forms the basis of molecular detection & identification. Immunological detections based on antibody are one of the oldest and most versatile detection mechanisms widely utilized in sensing and clinical applications. This detection mechanism can be employed for virtually any compounds as most of the antigen elicits an immune response immediately after invasion

in to an animal or human body. Antibodies employed in biosensors are usually polyclonal or monoclonal antibodies. The affinity constant associated with antigen-antibody reactions can range from weak (10^5 M^{-1}) to very strong (10^9 M^{-1}) interactions in addition to their specificity and selectivity similar to enzymes. Despite of this advantage, polyclonal antibodies suffer major limitations such as “heterogeneity” because of their reactivity towards all antigens to which the animal has been exposed in the past and use of expensive methods such as affinity purification to produce a polyclonal antibody for specific application. On the other hand, monoclonal antibodies are selective but they (including polyclonal) are sensitive to field conditions such as harsh chemicals, pH, temperature [24, 25].

Apart from antibodies, specific base-pairing between complimentary DNA and RNA strands (commonly known as nucleic acids) forms an important class of affinity biosensors. From molecular recognition standpoint, DNA is a very special structure serving as the central icon of modern biology. The specific interactions between complimentary strands determine the flow of genetic information which modulates the biological function in unicellular as well as multicellular organisms.

In principle, nucleic acid detections are based on the hybridization of complimentary base pair of the target probe to capture probe immobilized on a solid support forming Watson-Crick base pairs. Detection of pathogens based on genomic analysis involves two process often carried out in conjunction: 1) amplification and 2) detection of pathogen-specific gene fragments. In case of nucleic acid based detection (genotyping), virtually any biological agent can be identified as every agent expresses a unique nucleic acid sequence (DNA or RNA). The only exceptions are prions - a protein

particle that lacks nucleic acid, which are believed to be the cause of various infectious diseases in nervous systems (like Bovine Spongiform Encephalopathy aka mad-cow disease). Even though nucleic acid detection is more specific and sensitive (up to femtomolar concentration), they have their inherent limitations such as time consuming and tedious pre-hybridization sample preparation procedures [24].

2.6. Bacteriophage as an alternative probe for biosensors

The design of a robust biosensor demands the choice of the molecular probes to be specific, selective and stable for longer shelf life. However, the system based on traditional receptors such as antibody, enzymes and nucleic acid probes require *a priori* knowledge of the target under investigation, which becomes problematic when high-throughput screening of plethora of different targets is required.

Mother Nature developed its own way of combating bacterial pathogens using bacteriophages. Bacteriophages are viruses, harmless to humans but capable of infecting and replicating within bacteria. They are integral part of the microbial communities on earth. They come in different shapes and sizes, have many different lifestyles and live everywhere. Phage typing, where a panel of phages was used to discriminate between different isolates of bacteria is one of earlier known method for discriminating bacterial strains. Many strains of *Salmonella*, *Listeria*, and *Staphylococcus* were still identified by phage typing [26, 27]. Because of their ability to replicate within their host bacterium accompanied by their narrow host range, bacteriophage based therapy are currently considered to treat infections, including skin, gastrointestinal, pulmonary, wound and abscess infections. Last year, FDA approved the use of mixture of six phages specific

against *Listeria monocytogenes* to be sprayed on ready-to-eat meat products to control the growth of 170 different strains of *L. monocytogenes* [28].

The therapeutic nature of bacteriophage in treating infectious disease discovered by Felix d'Herelle in 1917 [29] and phage display technique pioneered by Smith in 1985 [30] revolutionized phage application in modern science and technology. The engineering of phage by phage display technique using recombinant DNA & molecular selection procedures allow us to modify the protein architecture of the phage virion by inserting a piece of foreign DNA within phage genome. Phage is so robust that insertion of foreign DNA will not alter its basic property i.e., to infect bacteria. Using this technique, theoretically a phage can be selected against any material either organic or inorganic. Recently, it was shown that filamentous phage scaffold (phage fd) fused with foreign random peptides could serve as a substitute for antibodies against various antigens. The foreign peptide is identical in all 4,000 copies major coat proteins pVIII leading to multivalent binding sites for antigens. In addition, the surface area of the phage particles is extremely high (300-400 m²/g) surpassing best-known absorbents or catalyst [25].

Recently several reports have been published for the identification of pathogenic bacteria using phage as molecular probe. For example, Goodridge *et al* [31] demonstrated a novel flow cytometric assay employing a fluorescent-tagged bacteriophage for *Escherichia coli* O157:H7. Using this technique, they were able to detect *E.coli* cells as low as 10² cells/ml. For staphylococcal enterotoxin B, a Cy5 labeled M13 bacteriophage were selected by phage display method. A combination of enzyme-linked immunosorbent assay (ELISA) and fluorescence method was used and labeled phages were able to detect 1.4ng/well [32]. Similarly, Mosier-Boss *et al* [33] reported detection of *Salmonella*

typhimurium LT2 using phage P22 modified with highly sensitive nucleic acid stain, SYBR gold modified.

2.7. Transducers

If the characteristics of the recognition element determine the selectivity and specificity of a biosensor, its sensitivity is defined by how rapid the transducer responds to the “host-guest” interactions. Rapidity of a transducer element determines the response time – one of the important characteristics of a biosensor. The transducer converts the observed changes (physical or chemical) due to biological interactions in to measurable signals. Table 2-3 summarizes transducer technologies currently employed for biosensor application which are classified solely on the mechanism by which the change is observed.

Types of Transducer	Techniques
Electrical and/or Electrochemical	Potentiometric, Voltammetric, Conductometric, Capacitive and FET based sensors
Optical	Absorption spectroscopy, Fluorescence spectroscopy, Luminescence spectroscopy, Attenuated Total Internal Reflection, Surface Plasmon Resonance (SPR) spectroscopy and Light scattering
Piezo-electric	Thickness-shear mode (TSM), surface acoustic wave (SAW), Love wave sensor, Flexural plate wave (FPW), Shear-horizontal acoustic wave (SH-APW)
Thermal	Thermistors, Catalytic gas sensors, Thermal Conductivity devices

Table 2-3 Type of transducers employed in biosensor applications

Surface plasmon resonance (SPR) biosensors based on optical transduction are particularly attractive for the above applications as they offer “label-free” detection and “near real-time” monitoring of interactions. The principle and application of this technique has been described extensively in the literature [34-37]. Briefly, SPR uses the

principle of total internal reflectance (TIR) occurring at the interface between materials with differing refractive indices. An evanescent wave penetrates the interface (modified with a thin layer of gold) and couples with surface plasmons (oscillating free electrons). The interaction causes a change in reflectivity and a concurrent change in resonance angle, which correlates to the refractive index (RI) of the adjacent medium. The RI is therefore directly related to changes in surface concentration of interacting ligands. The change in RI is continuously monitored to produce a sensogram of refractive index unit (RIU) as a function of time. Typically, a response of 1000 RIU or 0.1° change in angle corresponds to a change in surface protein concentration of 1 ng/mm^2 [36]. SPR has proven to be particularly useful for the analysis of biological systems as labeling of ligands or receptor molecules are not required and can be used to determine kinetic parameters of the interacting molecules [36-39]. Combined with high sensitivity, this technique has been widely employed for the detection of various bacteria [40-42], toxins [43, 44], and viruses [45]. The use of SPR for biological systems however, generally requires the development of specific methods to attach biomolecules on the sensor surface and orient the molecules for optimal biological activity.

2.8. Commercial kits for *S.aureus* detection

Apart from conventional culturing and staining methods, the tube coagulase test using rabbit plasma remains the “gold standard” for the identification of *S.aureus* [46]. This involves the interaction between the extracellular free coagulase of *S.aureus* and the prothrombin in the plasma, which results in the formation of fibrinopeptides forming fibrin clots. However, long incubation period, false positive results from non-*S.aureus* and false negative results from coagulase-negative *S.aureus* decrease the reliability of the

above test. To overcome the problems of specificity, commercial agglutination kits were developed to contain two or more properties of *S.aureus* to perform clinical studies (Fig. 2-5) [47, 48]. The current commercial kits available for the detection of *S.aureus* focus mainly on the three strategies [49, 50]:

1. First generation test kits were created to identify clumping factor using rabbit fibrinogen.
2. Second generation test kits targeted organisms possessing clumping factor and/or protein A. Human fibrinogen and antibody was used to identify clumping factor and protein A respectively.
3. Third generation test kits include an additional detection scheme using an antibody against *S. aureus* capsular polysaccharides (capsule type 5 and 8) in addition to schemes described in second generation kits.

Based on different detection schemes employed, the commercial methods have sensitivities between 77.6 and 86.9%, which is attributed to the inefficiency in detecting strains without clumping factor, protein A or capsule type 5 and 8 [50]. Also, methicillin resistant *S.aureus* (MRSA) strains deficient in clumping factor [51] and protein A [52, 53] were detected only by third generation kits [54]. Although, several commercial test kits detect *S.aureus* with high sensitivity, the kits did not identify all of the staphylococcal isolates. Hence, a second test, the tube coagulase test has to be performed in order to confirm the presence or absence of the isolates [50, 54]. In addition, most of the commercial kit requires *S.aureus* concentration to be greater than 10^5 cfu/ml [50], which is on the limit of the infectious dose for this organism [38, 55].

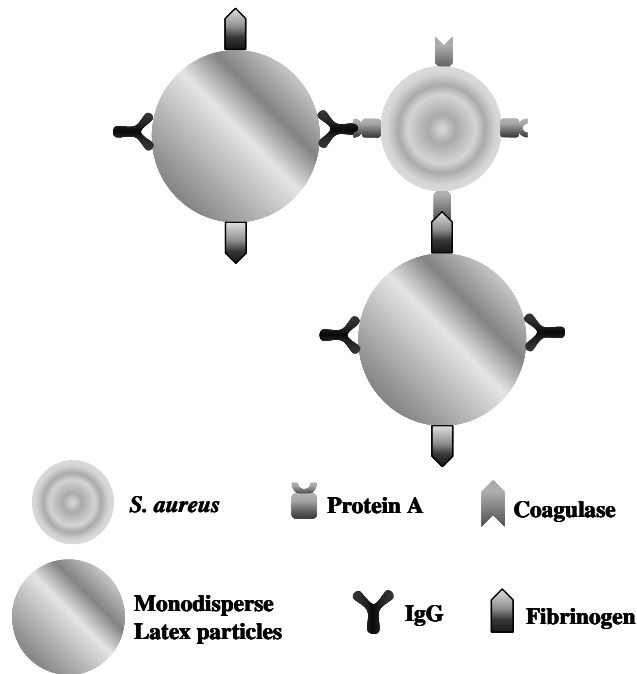


Fig. 2-5 Principle of *S.aureus* detection using commercial agglutination test kits

2.9. *S.aureus* biosensors

Biosensors for direct detection of *S. aureus* are rare compared to traditional microbiological methods such as real-time polymerase chain reaction (RT-PCR), which target the amplification of specific gene corresponding to particular strain of interest. However, handful of reports has been published for direct *S.aureus* detection. For example, Si *et al* [56] reported an piezoelectric immunosensor for direct *S. aureus* detection having linear range from 10^5 to 10^9 cells/ml. Subramanian *et al* [57] reported a surface plasmon resonance (SPR) based detection of *S.aureus* cells by anti-*S.aureus* antibody immobilized on mono and dithiol self-assembled monolayers. A sensitivity of 10^7 cfu/ml was reported for direct assay while amplification with secondary antibody improves the sensitivity to 10^5 cfu/ml. Rishpon and Ivnitski [58] reported an amperometric enzyme-channeling immunosensor for *S.aureus* detection. Even though,

sensor has a detection limit of 1000 cells/ml, this method is very complicated. It requires both anti-*S.aureus* antibody and glucose oxidase (GOx) to be immobilized on the electrode surface and an enzyme labeled anti-*S.aureus* to be added with test solution. Combination of antigen-antibody interaction and hydrolysis of glucose by GOx produces signal. Thus, invariably all the reported biosensors for *S.aureus* detection requires antibody for specific detection.

2.10. Antimicrobial reactive coatings/surfaces

If biosensors mediate the detection of pathogens, antimicrobial surfaces on the other hand allow us to eliminate pathogens. Surfaces exposed to air and moisture is a vibrant reservoir for adherence and proliferation of infection-causing microorganisms and thereby becoming a potential source for disease spread. Disease spread through surfaces is especially common in hospital settings, food processing industries (e.g. conveyor belts) and also in house-holds due to commonly shared surfaces such as kitchen countertops, door knobs, computer keyboards etc. For example, the recent pandemic caused by severe acquired respiratory syndrome (SARS) was thought to spread through contaminated surfaces, known as fomites [59]. A similar study found that this virus can survive on dried inert surface such as telephone in nursing stations and in patient's bedrail [60]. The extent to which the surface contamination plays a role in nosocomial infections is unknown; however, it is estimated that 1 in 10 patients acquire infection after admission resulting in a substantial annual economic burden of \$6.7 billion in US alone [61]. Typically, antimicrobial liquids and detergents are used to clean and sanitize the surface. Though this procedure immediately reduces pathogenic bacterial population it does

require frequent cleaning to prevent further contamination and it is not commonly applied to inert surfaces like stethoscopes and telephones.

On the other hand, materials/surfaces that inhibit bacterial colonization over long period of time offer an effective strategy to combat surface assisted infection. Therefore, there is a great interest to modify surface properties to make them resistance to bacterial colonization or even better to make it antimicrobial. This not only renders the surface antiseptic but also inhibit bacterial metabolism and discourage the growth of bacteria thus preventing disease transmission. There is a long list of antibacterials available in the literature ranging from chemical food preservatives like simple salt to natural food antimicrobials like lysozyme to complex antimicrobial agents like silver or copper ions and quaternary ammonium compounds.

2.10.1. Nanomaterial for antimicrobial applications

Because of their enhanced properties at the nanoscale, nanomaterials play a significant role in many technological innovations. As exquisitely put forth by Dr. Feynman [62], there are several fundamental advantages by limiting the size of the material in the nanoscale. Nanoscale materials differ from their bulk counterparts not only in size but they have fundamentally different physical and chemical properties. Although their properties can be defined using classical physical laws, this definition ceases to exist at some level as quantum-mechanical laws outweigh the classical counterparts. Biology offers innumerable examples of nanomaterial and devices; rods and cones of retina acts as optical sensors and ion channels which control the flow of specific ions to cells are some of the bioengineering marvelous at the nanoscale dimensions.

2.10.2. Bio-inorganic hybrid materials for antimicrobial applications

Mother Nature has developed numerous antimicrobial agents in plants and animals as a first line of defense against harmful infections and diseases. In fact, many civilizations have used herbs, oils and spices to preserve food materials with or without the knowledge of their antimicrobial properties. Starting with fermentation of cheese and milk products, these natural antimicrobials have found its way in to modern medicines.

One of the best examples of naturally derived antimicrobial is lysozyme which was first discovered by Sir Alexander Fleming in 1922 [63]. This enzyme is evolved to specifically lyse β -1, 4 linkages between N-acetylmuramic acid (NAM) and N-acetyl glucosamine (NAG) in the peptidoglycan of Gram-positive bacterial cell wall. However, the spectrum of action could be widened to Gram-negative bacteria with the addition of chelating agents such as EDTA. It is commonly found in human tears, saliva, urine and milk at a significant amount (0.1 to 2.6 m/ml). Because it is endogenous to plants & animals accompanied by its bacteriostatic and bacteriolytic property, lysozyme has been used extensively for preservation of food products such as cheese, chewing gums, candies and mouthwashes. Since lysozyme is stable in wide range of temperature & pH and still maintains its antimicrobial efficacy [64], it has been combined with various polymers and biomaterials to produce food packaging films with antimicrobial quality [65]. Such packaging materials extend the shelf-life of food products by preventing bacterial growth [66]. In addition, due to its cationic property it has been studied to form antimicrobial thin films in combination with anionic polyelectrolyte's or other biomaterials using a technique called "layer-by-layer" assembly. Typically, these films would release

lysozyme to its environment and the amount of release could be controlled depending of the mechanism of action [67].

Similar antimicrobial releasing coatings were developed extensively using inorganic nanoparticles. Colloidal silver, copper and zinc are most promising for antimicrobial applications along with photocatalytic property of TiO₂ nanoparticles [68]. Compared to other inorganic strong antimicrobials such as mercury, arsenic and cadmium, they are biologically less toxic. With respect to antimicrobial application, inorganic nanoparticles have wide spectrum of action killing both harmful pathogens and benign bacteria.

Due to its unique properties, single-walled carbon nanotubes (SWNTs) have been recognized as attractive building blocks for the realization of numerous technological innovations in biomedical field [69]. However, similar to other nanomaterials, application of carbon nanotubes (CNTs) is limited by the associated cytotoxicity. Recently, purified SWNT were shown to exhibit strong antibacterial activity towards *E. coli* [70]. Though the mechanism of antibacterial action is not very well understood, it was speculated that direct contact between SWNT and *E. coli* damages the cell wall. This process was found to be size dependent as shorter SWNT interacts more compared to longer ones [71].

Hybrid materials combining biomolecular specificity along with nanomaterial properties shows promise for developing multifunctional smart materials. Such composites of bio-inorganic nature have the properties of both materials by working in synergy. For example, by combining with biomolecules and polymers, researchers were able to utilize SWNT as drug-carriers [72].

2.11. Thesis organization

Potential health benefits can be attained by eliminating pathogenic bacteria at the source which would go a long way in the battle to combat disease transmission. Nature has developed her own variant of antimicrobial strategy by developing lytic bacteriophage which is hypothesized as the “next-generation” therapy in the battle against rapidly evolving antibiotic resistance bacterial strains. However, application of lytic bacteriophage for direct detection of bacteria is very minimal. Hence, proof-of-concept was developed to demonstrate that a biosensor based on immobilized lytic bacteriophage indeed can serve as bacterial capturing agent without losing its lytic activity. Non-specific adsorption is a critical problem in developing a sensitive and specific biosensor for any diagnostics. Poly(ethylene glycol) based polymers have been exploited to address this issue on various surfaces. It is hypothesized that reduction of non-specific adsorption could directly/indirectly influence the sensitivity of detection, hence the performance of the biosensor. Finally, the subtlety of biological systems could be exploited to solve intriguing engineering problems associated with nanomaterials. One such example is the dispersion of carbon nanotubes which is limiting successful transfer of individual CNT to macroscopic systems. This integration would allow us to produce complex, hybrid materials from “bottom up” with critical control.

Thus, the main objectives of the present study were:

- I. To investigate the prospects of lytic bacteriophage as bacterial capturing agent on SPR sensor platform and examine the sensitivity and specificity for the detection of *S. aureus*

- II. To improve the sensitivity of SPR biosensor by preventing non-specific adsorption on biosensor surface using poly(ethylene glycol) based copolymer
- III. To develop an effective strategy to immobilize and remove biomolecules from gold surface as a way to modulate biological interfaces focusing on biosensor applications
- IV. To exploit favorable interactions of biomolecules with carbon nanotubes in developing mechanically strong antimicrobial coatings.
 - To develop DNA and Lysozyme (LYZ) enabled dispersion of single-walled carbon nanotube
 - To fabricate thin films of DNA-SWNT and LYZ-SWNT with critical control over coating thickness and nanotube orientation

2.12. References

1. *Foodborne Illness*. [cited 2008 February 10]; Available from: http://www.cdc.gov/ncidod/dbmd/diseaseinfo/foodborneinfections_g.htm#whatoutbreak.
2. *Managing Food Safety: A Manual for the Voluntary Use of HACCP Principles for Operators of Food Service and Retail Establishments*. 2006 [cited; Available from: <http://www.cfsan.fda.gov/~dms/hret2-4.html>].
3. Olsen, S.J., et al., *Surveillance for Foodborne Disease Outbreaks - United States, 1993-1997*. Morbidity and Mortality Weekly Report, 2000. **49**(SS01): p. 1-51.
4. Lynch, M., et al., *Surveillance for Foodborne-Disease Outbreaks --- United States, 1998--2002*. Morbidity and Mortality Weekly Report, 2006. **55**(SS10): p. 1-34.

5. Varnam, A.H. and M.G. Evans, *Foodborne Pathogens: An Illustrated Text*. 1991: Mosby-Year Book.
6. Arbuthnott, J.P., D.C. Coleman, and J.S.d. Azavedo, *Staphylococcal toxins in human disease*. Journal of Applied Microbiology Symposium Supplement, 1990. **69**(s19): p. 101S-107S.
7. Chang, S., et al., *Infection with Vancomycin-Resistant Staphylococcus aureus Containing the vanA Resistance Gene*. 2003. p. 1342-1347.
8. Dinges, M.M., P.M. Orwin, and P.M. Schlievert, *Exotoxins of Staphylococcus aureus*. Clinical Microbiology Reviews, 2000. **13**(1): p. 16-34.
9. Honeyman, A.L., H. Friedman, and M. Bendinelli, *Staphylococcus aureus Infection and Disease*. Infectious Agents and Pathogenesis. 2001: Kluwer Academic/Plenum Publishers.
10. Le Loir Y, Florence Baron, and M. Gautier, *Staphylococcus aureus and food poisoning*. Genetics and Molecular Research, 2003. **2**(1): p. 63-76.
11. Soriano, J.M., et al., *Enterotoxigenic staphylococci and their toxins in restaurant foods*. Trends in Food Science & Technology, 2002. **13**(2): p. 60-67.
12. Tranter, H.S. and R.D. Brehm, *Production, purification and identification of the staphylococcal enterotoxins*. Journal of Applied Microbiology Symposium Supplement, 1990. **69**(s19): p. 109S-122S.
13. Busta, F.R., et al., *Evaluation and Definition of Potentially Hazardous Foods, A Report of the Institute of Food Technologists for the Food and Drug Administration of the U.S. Department of Health and Human Services* 2001, IFT/FDA.

14. Mossel, D.A.A. and P.v. Netten, *Staphylococcus aureus and related staphylococci in foods: ecology, proliferation, toxinogenesis, control and monitoring*. Journal of Applied Microbiology Symposium Supplement, 1990. **69**(s19): p. 123S-145S.
15. Thevenot, D.R., et al., *Electrochemical biosensors: recommended definitions and classification*. Biosensors & Bioelectronics, 2001. **16**(1-2): p. 121-131.
16. Thevenot, D.R., et al., *Electrochemical biosensors: Recommended definitions and classification - (Technical Report)*. Pure and Applied Chemistry, 1999. **71**(12): p. 2333-2348.
17. Wang, J., *Electrochemical glucose biosensors*. Chemical Reviews, 2008. **108**(2): p. 814-825.
18. Luckarift, H.R., et al., *Enzyme-encapsulated silica monolayers for rapid functionalization of a gold surface*. Colloids and Surfaces B-Biointerfaces, 2007. **58**(1): p. 28-33.
19. Ramanathan, M. and A.L. Simonian, *Array biosensor based on enzyme kinetics monitoring by fluorescence spectroscopy: Application for neurotoxins detection*. Biosensors & Bioelectronics, 2007. **22**(12): p. 3001-3007.
20. Simonian, A.L., A.W. Flounders, and J.R. Wild, *FET-based biosensors for the direct detection of organophosphate neurotoxins*. Electroanalysis, 2004. **16**(22): p. 1896-1906.
21. Simonian, A.L., et al., *Nanoparticle-based optical biosensors for the direct detection of organophosphate chemical warfare agents and pesticides*. Analytica Chimica Acta, 2005. **534**(1): p. 69-77.

22. Viveros, L., et al., *A fluorescence-based biosensor for the detection of organophosphate pesticides and chemical warfare agents*. Sensors and Actuators B-Chemical, 2006. **115**(1): p. 150-157.
23. Lei, Y., W. Chen, and A. Mulchandani, *Microbial biosensors*. Analytica Chimica Acta, 2006. **568**(1-2): p. 200-210.
24. Iqbal, S.S., et al., *A review of molecular recognition technologies for detection of biological threat agents*. Biosensors and Bioelectronics, 2000. **15**(11-12): p. 549-578.
25. Petrenko, V.A. and V.J. Vodyanoy, *Phage display for detection of biological threat agents*. Journal of Microbiological Methods, 2003. **53**(2): p. 253.
26. Kutter, E. and A. Sulakvelidze, *Bacteriophages - Biology and Applications*. 2004: CRC Press.
27. Waldor, M.K., D.I. Friedman, and S.L. Adhya, *Phages: their role in bacterial pathogenesis and biotechnology*. 2005, Washington DC: ASM Press.
28. Bren, L., *Bacteria-eating virus approved as food additive, in FDA consumer magazine*. 2007.
29. D'Herelle, F., *Sur un microbe invisible antagoniste des bacilles dysentériques*. Comptes Rendus de l'Academie des Sciences, Serie D: Sciences naturelles, 1917. **165**: p. 373.
30. Smith, G.P., *Filamentous Fusion Phage - Novel Expression Vectors That Display Cloned Antigens on the Virion Surface*. Science, 1985. **228**(4705): p. 1315-1317.

31. Goodridge, L., J.R. Chen, and M. Griffiths, *Development and characterization of a fluorescent-bacteriophage assay for detection of Escherichia coli O157 : H7*. Applied and Environmental Microbiology, 1999. **65**(4): p. 1397-1404.
32. Goldman, E.R., et al., *Phage-displayed peptides as biosensor reagents*. Journal Of Molecular Recognition, 2000. **13**(6): p. 382-387.
33. Mosier-Boss, P.A., et al., *Use of fluorescently labeled phage in the detection and identification of bacterial species*. Applied Spectroscopy, 2003. **57**(9): p. 1138-1144.
34. Green, R.J., et al., *Surface plasmon resonance analysis of dynamic biological interactions with biomaterials*. Biomaterials, 2000. **21**(18): p. 1823.
35. Homola, J., *Surface Plasmon Resonance Sensors for Detection of Chemical and Biological Species*. Chemical Reviews, 2008. **108**(2): p. 462-493.
36. Myszka, D.G., *SPR biosensors as biophysical research tools*. Faseb Journal, 2000. **14**(8): p. A1511-A1511.
37. Rich, R.L. and D.G. Myszka, *Advances in surface plasmon resonance biosensor analysis*. Current Opinion in Biotechnology, 2000. **11**(1): p. 54-61.
38. Leonard, P., et al., *Advances in biosensors for detection of pathogens in food and water*. Enzyme and Microbial Technology, 2003. **32**(1): p. 3.
39. Melendez, J., et al., *A commercial solution for surface plasmon sensing*. Sensors and Actuators B: Chemical, 1996. **35**(1-3): p. 212.
40. Bokken, G.C.A.M., et al., *Immunochemical detection of Salmonella group B, D and E using an optical surface plasmon resonance biosensor*. FEMS Microbiology Letters, 2003. **222**(1): p. 75.

41. Koubova, V., et al., *Detection of foodborne pathogens using surface plasmon resonance biosensors*. Sensors and Actuators B: Chemical, 2001. **74**(1-3): p. 100.
42. Leonard, P., et al., *A generic approach for the detection of whole Listeria monocytogenes cells in contaminated samples using surface plasmon resonance*. Biosensors and Bioelectronics, 2004. **19**(10): p. 1331.
43. Medina, M.B., *A biosensor method for a competitive immunoassay detection of staphylococcal enterotoxin B (SEB) in milk*. Journal Of Rapid Methods And Automation In Microbiology, 2005. **13**(1): p. 37-55.
44. Naimushin, A.N., et al., *Detection of Staphylococcus aureus enterotoxin B at femtomolar levels with a miniature integrated two-channel surface plasmon resonance (SPR) sensor*. Biosensors and Bioelectronics, 2002. **17**(6-7): p. 573.
45. Boltovets, P.M., et al., *Detection of plant viruses using a surface plasmon resonance via complexing with specific antibodies*. Journal of Virological Methods, 2004. **121**(1): p. 101.
46. Gerhardt, P., et al., *Methods for general and molecular bacteriology*. 1994, Washington D. C.: American Society for Microbiology.
47. Boerlin, P., et al., *Methods for identification of Staphylococcus aureus isolates in cases of bovine mastitis*. Journal of Clinical Microbiology, 2003. **41**(2): p. 767-771.
48. Smole, S.C., et al., *Sensitivity and specificity of an improved rapid latex agglutination test for identification of methicillin-sensitive and -resistant Staphylococcus aureus isolates*. Journal of Clinical Microbiology, 1998. **36**(4): p. 1109-1112.

49. van Griethuysen, A., et al., *International multicenter evaluation of latex agglutination tests for identification of Staphylococcus aureus*. Journal of Clinical Microbiology, 2001. **39**(1): p. 86-89.
50. Zschock, M., A. Nessler, and I. Sudarwanto, *Evaluation of six commercial identification kits for the identification of Staphylococcus aureus isolated from bovine mastitis*. Journal of Applied Microbiology, 2005. **98**(2): p. 450-455.
51. Lally, R. and B. Woolfrey, *Clumping Factor Defective Methicillin-Resistant Staphylococcus-Aureus*. European Journal of Clinical Microbiology & Infectious Diseases, 1984. **3**(2): p. 151-152.
52. Rossney, A.S., L.F. English, and C.T. Keane, *Coagulase Testing Compared with Commercial Kits for Routinely Identifying Staphylococcus-Aureus*. Journal of Clinical Pathology, 1990. **43**(3): p. 246-252.
53. Neville, L.O., et al., *Methicillin Resistant Staphylococcus-Aureus without Clumping Factor, Protein-a, and Dnase*. Lancet, 1991. **338**(8765): p. 518-518.
54. Gupta, H., et al., *Comparison of six rapid agglutination tests for the identification of Staphylococcus aureus, including methicillin-resistant strains*. Diagnostic Microbiology and Infectious Disease, 1998. **31**(2): p. 333-336.
55. USFDA, *Bad bug book: Foodborne Pathogenic Microorganisms and Natural Toxins Handbook*. 1992.
56. Si, S.H., et al., *Electrochemically modified piezoelectric crystal biosensor for detection of Staphylococcus aureus*. Chinese Journal of Chemistry, 1996. **14**(3): p. 222-227.

57. Subramanian, A., J. Irudayaraj, and T. Ryan, *Mono and dithiol surfaces on surface plasmon resonance biosensors for detection of Staphylococcus aureus*. *Sensors and Actuators B-Chemical*, 2006. **114**(1): p. 192-198.
58. Rishpon, J. and D. Ivnitski, *An amperometric enzyme-channeling immunosensor*. *Biosensors & Bioelectronics*, 1997. **12**(3): p. 195-204.
59. Gerberding, J.L., *Faster . . . but Fast Enough? Responding to the Epidemic of Severe Acute Respiratory Syndrome*. *The New England Journal of Medicine*, 2003. **348**(20): p. 2030-2031.
60. Dowell, S.F., et al., *Severe Acute Respiratory Syndrome Coronavirus on Hospital Surfaces*. *Clinical Infectious Diseases*, 2004. **39**(5): p. 652.
61. Graves, N., *Economics and preventing hospital-acquired infection*. *Emerging Infectious Diseases*, 2004. **10**(4): p. 561-566.
62. Feynman, R.P. *There's Plenty of Room at the Bottom*. 1959 [cited March 15th 2008]; Available from: <http://www.zyvex.com/nanotech/feynman.html>.
63. Fleming, A., *On a remarkable bacteriologic element found in tissues and secretions*. *Proceedings of the Royal Society of London, (Series B)*, 1923. **93**: p. 306.
64. Proctor, V.A. and F.E. Cunningham, *THE CHEMISTRY OF LYSOZYME AND ITS USE AS A FOOD PRESERVATIVE AND A PHARMACEUTICAL*. *Crc Critical Reviews in Food Science and Nutrition*, 1988. **26**(4): p. 359-395.
65. Appendini, P. and J.H. Hotchkiss, *Review of antimicrobial food packaging*. *Innovative Food Science & Emerging Technologies*, 2002. **3**(2): p. 113-126.

66. Appendini, P. and J.H. Hotchkiss, *Immobilization of Lysozyme on Food Contact Polymers as Potential Antimicrobial Films*. Packaging Technology and Science, 1997. **10**(5): p. 271-279.
67. Buonocore, G.G., et al., *A general approach to describe the antimicrobial agent release from highly swellable films intended for food packaging applications*. Journal of Controlled Release, 2003. **90**(1): p. 97-107.
68. Matsunaga, T., et al., *Photoelectrochemical sterilization of microbial cells by semiconductor powders*. FEMS Microbiology Letters, 1985. **29**(1-2): p. 211-214.
69. Yang, W.R., et al., *Carbon nanotubes for biological and biomedical applications*. Nanotechnology, 2007. **18**(41).
70. Kang, S., et al., *Single-walled carbon nanotubes exhibit strong antimicrobial activity*. Langmuir, 2007. **23**(17): p. 8670-8673.
71. Kang, S., et al., *Antibacterial Effects of Carbon Nanotubes: Size Does Matter!* Langmuir, 2008.
72. Feazell, R.P., et al., *Soluble single-walled carbon nanotubes as longboat delivery systems for Platinum(IV) anticancer drug design*. Journal of the American Chemical Society, 2007. **129**(27): p. 8438-8439.

3. SURFACE PLASMON RESONANCE – PRINCIPLE & EXPERIMENTAL SETUP

3.1. Optical biosensors

Optical transduction techniques have played a vital role in the development of biosensors over the last three decades. They offer some unique advantages from other transduction methods such as, high sensitivity. Optical methods are capable of measuring surface concentration as low as 10^{12} molecules/cm², which is very low in case of medium sized protein such as avidin [1]. In addition, they exploit surface-specific optical phenomena (e.g. evanescent wave technique in SPR) to interrogate the properties of the surfaces while excluding the bulk effects to a large extent. Finally, they offer non-destructive method of analysis which is important in order to obtain real-time measurements giving kinetic information.

Optical transducers are commonly developed using two basic approaches for signal transduction, 1) direct detection which involves probing of surface for minute change in refractive index by evanescent wave techniques such as waveguide or surface plasmon resonance (SPR) spectroscopy or by reflection/interference techniques such as ellipsometry, and 2) labeling method such as fluorescence assays.

3.2. Direct detection based on guided wave

The fact that biological molecules have a higher refractive index (RI) than water led to the development of optical transducers which monitors the refractive index close to the transducer surface. At wavelengths close to 600nm, the RI of water is about 1.333.

Adsorption or binding of biological molecules such as proteins to the surface changes the effective refractive index of the medium immediately next to the surface and this minute change alters the propagation properties of the guided wave (such as evanescent wave in SPR) leading to direct detection of biological interactions on surfaces. Thus, transducers developed using guided wave principles are effectively high sensitive refractometers capable of measuring refractive index of the solution close to the guided (sensor) surface.

3.3. Biomolecules and refractive index

de Feijter et al [2] showed that at constant temperature and salt concentration, the bulk refractive indexes of the protein solutions are proportional to the mass concentration of dissolved protein. The increase in RI with respect to concentration is thus give as

$$\frac{dn}{dc} = 0.188ml.g^{-1} \quad (3.1)$$

where n - RI of the solution

c - protein concentration, g/ml

Even though the exact nature of RI of an aqueous solution depends on the various parameters such as concentration of the biomolecule, total salt concentration and temperature, these transducers can accurately “sense” the optical thickness of the adsorbing protein layer if the bulk RI of the solution remains constant (or accurately known).

Based on this, the surface concentration Γ (surface coverage, ng/mm^2) of proteins bound to the surface can be calculated in terms of experimentally measurable quantities such as refractive index in accordance with the approach proposed by de Feijter for homogeneous or inhomogeneous surface adlayers [2]

$$\Gamma = (dn_{\infty}/dc)^{-1} * (n_a - n_l) * d \quad (3.2)$$

where Γ - surface coverage, ng/mm²

n_{∞} - RI of the protein at infinite distance from the surface,

c - protein concentration, g/ml

n_a - effective RI of the adsorbed layer (adlayer),

n_l - effective RI of the solution

d - mean thickness within the adlayer

3.4. Surface plasmon

The field of plasmonics studies the confinement of electromagnetic radiations within nanostructures having dimensions on the order of or smaller than their wavelength. It plays a critical role in the development of *nanophotonics*, a branch of photonics dealing with the enhanced optical properties at sub-wavelength dimensions.

The history of *surface plasmon* is very old dating back as early as 1900s when mathematical descriptions were developed for propagation of radio waves on the surface of conducting material (known as *Sommerfeld's surface waves*). This was followed by observation of *anomalous* drop in the reflected light intensity from metallic gratings in the visible region by Wood in 1902 [3], a phenomenon largely went unnoticed. However, it was not until mid-century, a theory was described to explain this phenomenon in the visible region [4] followed by the re-discovery of similar *loss* phenomena by Ritchie in 1957 [5].

3.4.1. Surface plasmon polaritons (SPPs) at metal/dielectric interfaces

Surface plasmons are electromagnetic excitations evanescently propagating at the interface between a dielectric and a conductor in perpendicular direction. They arise due to the coupling of electromagnetic fields to oscillations of the conductor's electron

plasma. The interaction of electromagnetic fields with conductors (such as metals) can be described using Maxwell's classic equations:

$$\nabla \cdot \mathbf{D} = \rho, \quad (3.3.1)$$

$$\nabla \cdot \mathbf{B} = 0, \quad (3.3.2)$$

$$\nabla \times \mathbf{E} = -\frac{\partial \mathbf{B}}{\partial t}, \quad (3.3.3)$$

$$\nabla \times \mathbf{H} = \mathbf{J} + \frac{\partial \mathbf{D}}{\partial t} \quad (3.3.4)$$

These equations link the four macroscopic fields \mathbf{D} (the dielectric displacement), \mathbf{B} (the magnetic induction or magnetic flux density), \mathbf{E} (the electric field), \mathbf{H} (the magnetic field) with the external charge and current densities ρ and \mathbf{J} , respectively.

In case of linear, isotropic, non-magnetic media like Au, Ag, ρ & \mathbf{J} are zero. Then

Maxwell equations translates to

$$\nabla \cdot \mathbf{D} = 0, \quad (3.4.1)$$

$$\nabla \cdot \mathbf{B} = 0, \quad (3.4.2)$$

$$\nabla \times \mathbf{E} = -\frac{\partial \mathbf{B}}{\partial t}, \quad (3.4.3)$$

$$\nabla \times \mathbf{H} = \frac{\partial \mathbf{D}}{\partial t} \quad (3.4.4)$$

The above Maxwell equations are related to the “material equations” describing the propagation of electromagnetic wave through a medium by

$$\mathbf{D} = \epsilon \epsilon_0 \mathbf{E}, \quad (3.5.1)$$

$$\mathbf{B} = \mu \mu_0 \mathbf{H} \quad (3.5.2)$$

where ϵ_0 and μ_0 are the electrical permittivity of free space or vacuum ($\epsilon_0 = 8.85 \times 10^{-12}$ farad per meter, F/m) and magnetic permeability of free space ($\mu_0 = 1.257 \times 10^{-6}$ H/m).

The optical constants of the material are contained in the coefficients ϵ and μ .

Combining equations (3.4.3) & (3.5.2) and (3.4.4) & (3.5.1), we get

$$\nabla \times E = -\mu\mu_0 \frac{\partial H}{\partial t} \quad (3.6.1)$$

$$\nabla \times H = \varepsilon\varepsilon_0 \frac{\partial E}{\partial t} \quad (3.6.2)$$

The physical properties of surface plasmons polaritons (SPPs) can be investigated by applying above developed Maxwell equations to a flat interface between a conductor (metal) and a dielectric as shown in the figure 3-1

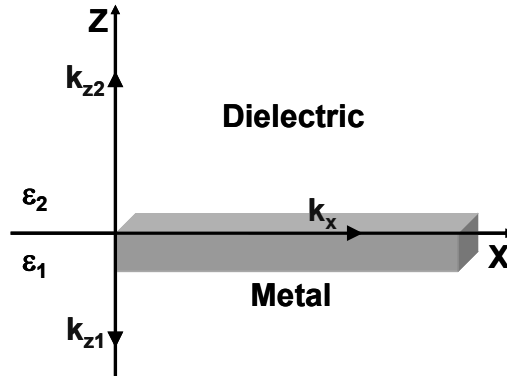


Fig. 3-1 Definition of planar waveguide geometry. The waves propagate along the x-direction in the Cartesian coordinate system

Applying vector identity, $\nabla \times \nabla \times E \equiv \nabla(\nabla \cdot E) - \nabla^2 E$ to (6.1) and $(\partial/\partial t)$ to (6.2) followed by substitution back to (6.1), yields

$$\nabla^2 E = \mu\mu_0\varepsilon\varepsilon_0 \frac{\partial^2 E}{\partial t^2} \quad (3.6.3)$$

A general solution to the above electromagnetic wave equation takes the form

$$E = E_0 e^{i(kr - \omega t)} \quad (3.7)$$

where E_0 is the maximal value of the electric field strength, r is the position vector, k is known as propagation constant of the traveling wave corresponding to the wave vector in

the direction of propagation, ω is the angular frequency defined as $2\pi\nu$, where ν is the frequency and t is the time.

After substitution and differentiation of (3.7) in to (3.6.3) yields the magnitude of the wave vector, k given by

$$k = \sqrt{\mu\mu_0\epsilon\epsilon_0\omega^2} \quad (3.8.1)$$

In case where the dielectric is air, $\epsilon = 1$, $\mu = 1$ and since $\lambda = 2\pi c / \omega$, $k = 2\pi / \lambda = \omega / c$, then equation (3.8.1) become

$$c = \frac{1}{\sqrt{\mu_0\epsilon_0}} \quad (3.8.2)$$

The free electrons of the metal can interact electrostatically with light of proper photon energy to perform coherent fluid like oscillations, known as *surface plasma oscillation*. A dispersion relation $\omega(k)$ governs the relationship between the frequency, ω of these longitudinal oscillations with wave vector, k . These oscillations are accompanied by a mixed longitudinal and transverse oscillations which vanishes as $z \rightarrow \infty$ on the both sides of metal/dielectric interface, having a maximum at $z = 0$. This explains their sensitivity towards the surface properties of the interface, a typical property of surface waves.

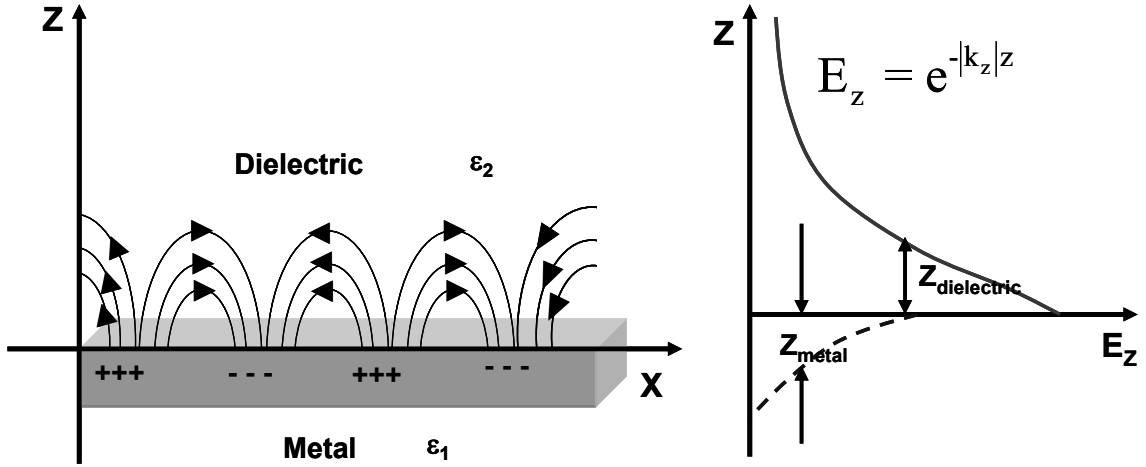


Fig. 3-2 Schematic representation of charges and surface plasmon fields propagation. The exponential dependence of E_z is shown in the right [6].

3.4.2. Dispersion relations of SPP

The dispersion relation of SPPs propagating at the interface can be obtained by applying boundary conditions to the Maxwell equation (3.6.3) along with the continuity relations. Since, for the non-magnetic materials, transverse electric (TE or s) modes are not supported. For transverse magnetic (TM or p) mode, the electromagnetic field is given by

$$E = E_0^{\pm} \exp[+i(k_x x \pm k_z z - \omega t)] \quad (3.9)$$

with + for $z \geq 0$, - for $z \leq 0$ and the wave vector $k_x = 2\pi / \lambda_p$ lies parallel to the x direction, where λ_p is the wavelength of the plasma oscillation. Continuity at the interface demands,

$$D_0 = \frac{k_{z1}}{\epsilon_1} + \frac{k_{z2}}{\epsilon_2} = 0 \quad (3.10.1)$$

together with

$$\epsilon_i \left(\frac{\omega}{c} \right)^2 = k_x^2 + k_{zi}^2 \quad (3.10.2)$$

yields the dispersion relation of SPPs propagation

$$k_x = \frac{\omega}{c} \left(\frac{\epsilon_1 \epsilon_2}{\epsilon_1 + \epsilon_2} \right)^{1/2} \quad (3.11)$$

3.4.3. Prism Coupler

The dielectric constant of the electron gas according to the free electron model is given by

$$\epsilon(\omega) = 1 - \frac{\omega_p^2}{\omega^2} \quad (3.12.1)$$

$$\text{where } \omega_p^2 = \frac{e^2 N_f}{4\pi^2 \epsilon_0 m} \quad (3.12.2)$$

The frequency ω_p is often called as *plasma frequency*, where e is the electronic charge density, N_f is the number of electrons, and m is the mass of the electron. For light, the dispersion line is given by $\omega = k * c$. Similarly, for SPP, the dispersion line can be drawn using (11) and the comparison of dispersion relation between light line and SPP is shown in figure 3-3. It is clear that SPP dispersion curve lies to the right of light line confirming that SPP cannot transform into light, hence remains “non-radiative” electromagnetic wave. Converse is also true (i.e.) the fact that k_x of SPP lies to the right of light line prohibits the phase matching between light wave vector and SPP wave vector and hence cannot be excited directly by light beams.

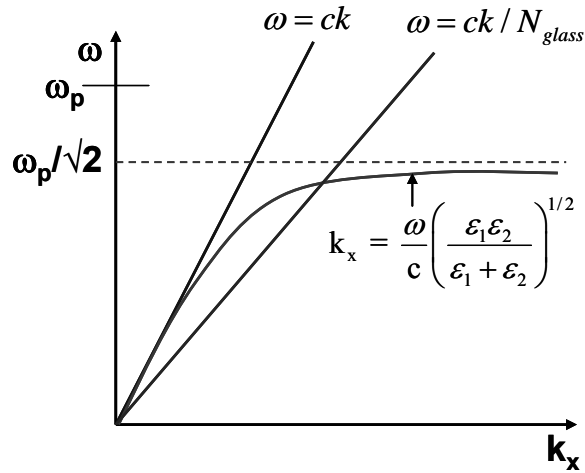


Fig. 3-3 Comparison of dispersion relation between light and SPP [6]

The phase-matching of the SPP and incoming light wave vector can be achieved in a three-layer system proposed by Kretschmann-Raether [7] and Otto [8]. Here, a thin metal film is sandwiched between two insulators of different dielectric constants such that the incoming photon energy is increased by Δk_x in order to “transform” photons into SPPs.

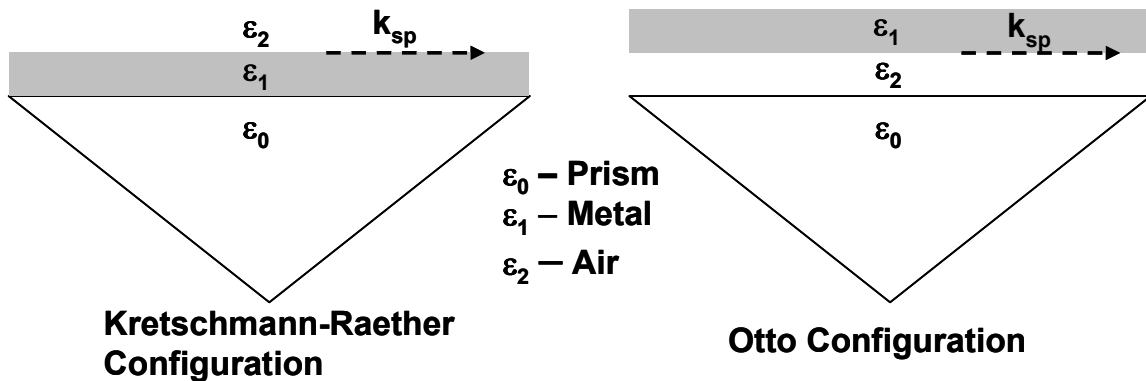


Fig. 3-4 Prism coupling to SPPs using two configurations

Typically a prism with higher dielectric constant (ϵ_0) is used compared to the second insulator, mostly air ($\epsilon_2 = 1$). In case of Kretschmann configuration where a thin metal film is evaporated on top of a glass prism, the incoming light will be total internally

reflected at the interface between prism and the metal. This light will have an in-plane momentum, $k_x = \sqrt{\varepsilon_0} \frac{\omega}{c} \sin \theta$ sufficient to excite SPPs at the metal/air interface (fig. 3-3).

This scheme of coupling is commonly known as attenuated total internal reflection, which involves the tunneling of the excited beam to the metal/air interface where SPP oscillations takes place.

In Otto configuration, the metal layer is separated by a distance of λ from higher dielectric constant by a medium of lower dielectric constant, usually air. Again, SPPs are created at metal/air interface via tunneling of total internally reflected light. Due to difficulty in experimental setup, Otto configuration is mostly used when direct contact to the metal surface is undesirable, for example to study the quality of single crystal.

3.5. SPREETA - Commercial surface plasmon resonance (SPR) sensor

SPREETA™ sensors developed by Texas Instrument (TI) will be used for SPR experiments. Small dimensions (4 cm × 1.3 cm × 2.8 cm), robustness, the availability of two channels, and cost (US\$ 25/channel) are some of the advantages of SPREETA™ (fig.3-5). The sensitivity of the system ($\sim 3 \times 10^{-6}$ RI) is comparable to other commercially available SPR systems. The whole SPR kit is comprised of a multi-channel SPR sensor, a flow cell, and a 12-bit three-channel DSP electronic control box (ECB). SPREETA™ sensor is a highly integrated SPR system, which incorporates a light emitting diode (840 nm) with a polarizer, reflecting mirror, and Si-photodiode array. An optically clear material encases the entire assembly while the sensor is coated with an opaque material to block out external light (with the exception of the sensing region). The sensing region is coated with a semi-transparent gold film (~ 50 nm) with a Cr-adhesion

layer (1–2 nm). The presence of wider gold surface compared to the single-channel prototype allows for the introduction of a second channel; thus, one channel can be dedicated for target analyte detection and the second channel can be used as a reference channel for temperature and non-specific signal compensation. In our experiments, a two-channel polypropylene flow cell with $\sim 10 \mu\text{l}$ volume/channel is used to establish a flow system along with an Ismatec peristaltic pump (Cole-Parmer Instrument Co., Chicago, IL, USA) at a flow rate of $100 \mu\text{l}/\text{min}$. A 12-bit three-channel electronic control box completes the interface between the sensor and a PC. Multi-channel SPREETA™ software provided by TI monitors the changes in RI near the sensing surface, calculates the statistical noise in the signal and displays the results. The signal is generally displayed in the response unit (RU) ($1 \text{ response unit} = 10^{-6} \text{ refractive index unit}$).

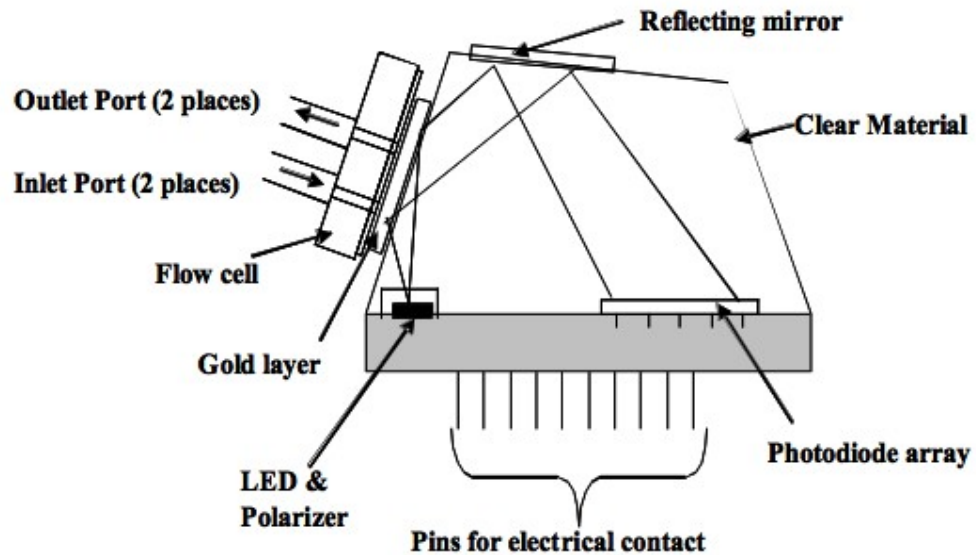


Fig. 3-5 Schematic of SPREETA™ sensor used in the study

3.5.1. Protocol for sensor setup:

The following protocol is routinely used to prepare SPREETA™ sensor for biosensor experiments.

1. Clean the gold surface of the sensor with piranha solution (**Caution:** *Piranha solution is dangerous and should be handled with proper protections*)
2. Wash with copious amount of DI water
3. Blot the surface with ethanol using Kim wipe (**Caution:** *Do not expose the body of the sensor with ethanol. Clean only the gold surface*)
4. Sonicate the sensor in DI water for 3 ~ 4 minutes. Remove all the water and air-dry the sensor
5. Clean the sensor in air-plasma for ~ 5 minutes
6. Dock the sensor in the SPR-system
7. Flush the flow block against the sensor and tighten with screws
8. Install the inlet and outlet tubes
9. Open MultiSPR.exe (**version:** 10.83)
10. Initialize the sensor in air and water. Save the results
11. Perform a cleaning step with NaOH-Triton-X (*recommended by manufacture*)
12. Again initialize with water and save the data
13. Start monitoring the signal in water and let it stabilize (~5 minutes)
14. After baseline stabilization, introduce solutions serially and follow the change in RI vs. time
15. Record the data in the data sheet and report the results

3.6. Reference

1. Brecht, A. and G. Gauglitz, *Recent developments in optical transducers for chemical or biochemical applications*. Sensors and Actuators B: Chemical, 1997. **38**(1-3): p. 1-7.
2. Defeijter, J.A., J. Benjamins, and F.A. Veer, *Ellipsometry as a Tool to Study Adsorption Behavior of Synthetic and Biopolymers at Air-Water-Interface*. Biopolymers, 1978. **17**(7): p. 1759-1772.
3. Wood, R.W., *On a Remarkable Case of Uneven Distribution of Light in a Diffraction Grating Spectrum*. Proceedings of the Physical Society of London, 1902. **18**: p. 269-275.
4. Fano, U., *The theory of anomalous diffraction gratings and of quasi-stationary waves on metallic surfaces (Sommerfeld's waves)*. Journal of the Optical Society of America, 1941. **31**(3): p. 213-222.
5. Ritchie, R.H., *Plasma Losses by Fast Electrons in Thin Films*. Physical Review, 1957. **106**(5): p. 874.
6. Raether, H., *Surface Plasmons on Smooth and Rough Surfaces and on Gratings*. Springer Tracts in Modern Physics; 111. 1988, Berlin: Springer-Verlag.
7. Kretschmann, E. and H. Raether, *Radiative decay of non-radiative surface plasmons excited by light*. Zeitschrift für Naturforschung A, 1968. **23A**: p. 2135-2136.
8. Otto, A., *Excitation of nonradiative surface plasma waves in silver by the method of frustrated total reflection*. Zeitschrift für Physik A Hadrons and Nuclei, 1968. **216**: p. 398-410.

4. LYTIC PHAGE PROBE ON SURFACE PLASMON RESONANCE BIOSENSOR FOR DETECTION OF STAPHYLOCOCCUS AUREUS

4.1. Introduction

Responsible for both community acquired and hospital acquired staphylococcus aureus (*S.aureus*) infection for over 100 years, multi-drug resistant *S.aureus* remains a threat to the human population [1-3]. It is one of the common causes of confirmed bacterial food poisoning in the US with over 50 outbreaks involving multiple cases [4]. An antibiotic-resistant strain of *S.aureus* was also the cause of an outbreak in a UK hospital in the year 2000. Up to 30-50% of humans carry *S.aureus* in nostrils and on skin surfaces, thus contamination of food products is a direct result of poor handling and sanitation of processed goods. *S.aureus* can cause multiple illnesses such as urinary tract infections, pneumonia, gastroenteritis, respiratory diseases, bronchial diseases, abdominal cramps and diarrhea.

Staphylococcus aureus produces a variety of highly stable toxic proteins, such as different staphylococcal enterotoxins and the toxic shock syndrome toxin [5-7]. The production of these toxins occur in between 10 and 46°C and as early as 4-6 hours after contamination of food products, while most common food borne pathogens need longer incubation periods ranging from ten hours to several days [8]. To elicit food poisoning, a minimum staphylococcal enterotoxin E dose of 1µg is required and can be produced with a bacterial population as low as 10⁵ cfu per gram [2, 9]. During major outbreaks,

S. aureus was specifically identified by traditional microbiological laboratory procedures, which involve culturing the bacteria followed by either specific genotype or phenotype diagnostic assays [10]. Even though these methods are specific and sensitive, they often take 24 to 48 hours to confirm the results. Hence, a rapid and simple method of detection is required to identify low quantities of bacteria and toxins.

The advent of modern technologies led to the development of analytical devices such as chemical and biological sensors, which changed the way pathogens are identified. These analytical devices offer near-real-time monitoring coupled with rapid and specific detection of the analyte of interest. A biosensor is comprised of a physical transducer (electrochemical, optical, mass, and thermal) and a specific bio-probe (antibody, enzymes, nucleic acids, receptors and whole cells) in which the biospecific interaction between the probe and target of interest is converted to a measurable signal by the physical transducer [11-14]. The sensitivity and specificity of the overall system depends on the transduction technique employed and the type of bio-probe used. Surface plasmon resonance biosensors based on optical transduction are particularly attractive for the above applications as they offer “label-free” detection and “near real-time” monitoring of interactions. Combined with high sensitivity, this technique has been widely employed for the detection of various bacteria [15-17], toxins [18, 19], and viruses [20].

Surface plasmon resonance (SPR) is an optical phenomenon, which occurs when TM-polarized light undergoes total internal reflection (TIR) at certain angles of incidence (resonance angle) at the interface of two media of different refractive indices (RI), generating a non-radiative evanescent wave. If the interface is modified with a thin layer of metal (Au/Ag ~50nm) and a monochromatic p-polarized light is used as a source, a

minimum in reflectivity is observed at the resonance angle. The resonance angle (or position) of this minimum is very sensitive to minute changes in the RI of the adjacent medium, which is directly related to the change in surface concentration of interacting ligands. This change in RI is continuously monitored to produce a sensorgram having RIU (refractive index unit) as y-axis and time as x-axis. Typically, a response of 1000 RIU or 0.1° change in angle corresponds to a change in surface protein concentration of 1ng/mm^2 [21-24].

The design of a robust biosensor demands the choice of the molecular probes to be specific, selective and stable for longer period of shelf life. Most of the affinity-based biosensing assays currently utilize monoclonal or polyclonal antibody for specific antigen detection. Even though these antibodies, in many cases are specific and selective, both formats of the antibodies suffer from environmental instabilities and require laborious and expensive procedures for isolation and purification [25]. In addition, polyclonal antibodies are limited by their heterogeneity towards other species or strains and bring forth the need for alternative probe selections [26, 27]. Bacteriophages are ever-present components of the microbial communities on earth [28]. Their specificity coupled with resistance to environmental stresses makes them an excellent molecular probe for the detection of pathogenic bacteria. This recognition ability has been exploited in several ways, namely in phage typing where a panel of phages were used to discriminate between different isolates of bacteria. Many strains of *Salmonella*, *Listeria*, and *Staphylococcus* were still identified by phage typing method as it is inexpensive and easy to use [29]. Several articles demonstrate the potential for development of fluorescent tagged bacteriophage for *E.coli O157:H7* [30], and *Salmonella typhimurium* LT2 detection [31]

and phage-displayed peptides labeled with the dye Cy5, for staphylococcal enterotoxin B detection [26]. However, involvement of labeling by fluorophore dyes or more complicated labeling by the dsDNA of phage bound to specially design gold particles, with further collection of phage-infected bacteria by filters and fluorescence microscope image analysis, make these approaches multi-step and complicated.

Earlier we reported the highly sensitive detection of model antigen β -galactosidase by SPR biosensor (up to 0.41nM) using a filamentous phage as a bio-probe selected by phage-display technique [32].

In this study we are reporting the use of lytic phage as a bio-recognition element and SPREETA™ sensor as a detection platform, for label-free direct measurement of *S. aureus* in low concentrations. Specificity of the detection assay was tested by an inhibition assay, while selectivity of phage-*S.aureus* interaction was examined using non-specific *Salmonella typhimurium*.

4.2. Materials and Methods

4.2.1. Bacterium

Staphylococcus aureus subsp. *aureus* ATCC 12600 was used as the bacterium and was obtained from American Type Culture Collection (Manassas, VA). The strain was cultured in a NZY medium (g/l - NZ amine A, 10; yeast extract, 5; NaCl, 5; pH 7.5) at 37°C for 18-24 hours.

4.2.2. Bacteriophage and propagation

The lytic phage (bacteriophage 12600) was selected from the commercial mixture of phages by incubation with the *S. aureus* ATCC 12600 strain. Selected phage infects wide spectrum of *Staphylococcus* isolates. To obtain the suspension of phage, an

overnight culture of *S. aureus* ATCC 12600 was used. Five ml of the bacterial culture was incubated with the phage in a 500 ml NZY medium in a 2 L flask on shaker-incubator at 37°C overnight. The culture was centrifuged at 4,424 x g for 10 minutes at 4°C. Supernatant was re-centrifuged at 11,325 x g for 10 minutes at 4°C. Solution of PEG/NaCl was added and the suspension was stored in overnight refrigeration. Precipitated phage was collected at 11,325 x g for 40 minutes at 4°C, dissolved in PBS and centrifuged at 19,837 x g for 10 minutes to clear. Serial dilutions of such phage suspension were prepared in a NZY medium. Overnight culture of host strain *S. aureus* ATCC 12600 was plated onto the plates with a NZY agar (NZY medium with Bacto agar, 15 g per liter). After the surface dries, a sample (10 µl) of appropriate phage dilution was spotted on the surface of the plate. Four samples were placed on each plate. Plates were incubated at 37°C for 18-24 hours and then examined for the formation of plaques. The phage titer was calculated from the number of plaques produced by a dilution of phage suspension.

4.2.3. Reagents

Phosphate buffered saline (PBS), pH 7.4 containing 0.138 M NaCl and 0.0027 M KCl dry powder sachet was obtained from Sigma, Bovine Serum Albumin (BSA), Tween-20, Triton-X were obtained from Fisher Scientific.

4.2.4. Phage Immobilization

A gold surface of SPR sensors were carefully cleaned with piranha solution (*Caution: Piranha solution is dangerous and should be handled with proper protections*) followed by Ar-plasma cleaning. The cleaning of the sensor was confirmed by the return of RI to 1.333 for water. Immediately following the surface cleaning, the sensor was

docked with the flow cell and background signals were made in air and water. An *in-situ* NaOH-Triton-X cleaning was performed as recommended by the manufacturer. A baseline was established with PBS for 5 minutes followed by the flushing of 1×10^8 cfu/ml of phage to the sensing channel. Non-specific sites on the sensing and control channel surfaces were blocked with BSA (1mg/mL in PBS) followed by a detergent wash (PBS-0.1% Tween). All the immobilization procedures were carried out at room temperature ($22 \pm 0.5^\circ\text{C}$) using flow system as described in Fig. 4-1. During the course of phage immobilization and BSA blocking, the change in RI was monitored over time using SPREETA™ software. The running buffer (PBS) was used to remove unbound phage.

4.2.5. Detection of bacteria

Different concentrations of overnight cultured *S. aureus* diluted in PBS were pumped simultaneously through the sensing and control channels. To determine the limit of detection, *S. aureus* bacteria was serially diluted from 10^8 to 10^1 cfu/ml and introduced sequentially through both channels. Each successive dilution of bacteria was introduced only when a previous addition resulted in the saturation of binding curve. Between additions of aliquots of different concentrations, unbound bacterial cells were washed with PBS. The difference between the initial PBS baseline and the corresponding after-binding PBS signals were calculated to determine responses elicited by aliquots of particular concentration of bacteria. The net response was finally calculated by subtracting signals of the sensing and control channels. All calculations and analysis were carried out “off-line” with OriginPro 7.5 (*OriginLab Corporation, MA, USA*) software. Waste solutions were collected in beaker containing 70% ethanol and finally, the system

was decontaminated with 70% ethanol. To visualize bacteria on the sensor surface, suspensions of *S. aureus* at different concentrations (10^1 to 10^7 cfu/ml) were injected over both the immobilized phage and the control surface. After washing with PBS, the sensor was removed and the gold surface was air dried and the surface was then examined by a Nikon Eclipse L150 optical microscope. ImageJ software (<http://rsb.info.nih.gov/ij/>) was used for surface coverage quantification and analysis.

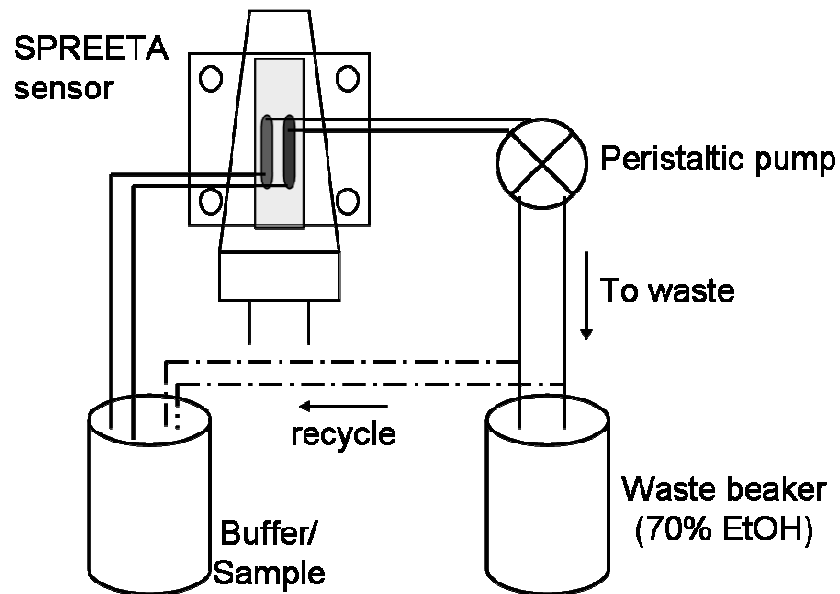


Fig. 4-1 Experimental setup. A SPREETA™ sensor is docked with fluidics part to set up a flow using peristaltic pump. A polypropylene flow cell (FC) containing two independent flow channels with gasket installed on the face of SPREETA™ sensor. Silicone tubing of 0.64mm ID was inserted to the two inlet and two outlet ports. The sensor is first initialized with air and water and the references are saved for future use. The data from the sensor is fed through the control box to the computer.

4.2.6. Binding Kinetics

The interaction between immobilized lytic phage and *S.aureus* can be quantitatively described using known binding equations with some considerations. Since, the phage-*S.aureus* surface receptors are unknown, as well as their stoichiometry of their interaction, the interaction between them can be by the equation:



where n represents Hill-coefficient which may represent the number of phage particles bound to *S.aureus* receptor and S represents selected *S.aureus*. Because of the multivalent nature of the interaction, n can take 1, 0.5 or $1/k$, where k is the valency of binding. From the law of mass action,

$$K_b = \left[\frac{\text{SP}_n}{[\text{S}][\text{P}]^n} \right] \quad (4.2)$$

The total number of *S.aureus* receptors (S_p) is simply the summation of occupied and unoccupied sites (neglecting sites occupied by non-specific molecules), then

$$S_p = [\text{S}] + [\text{SP}_n] \quad (4.3)$$

By combining (4.2) and (4.3), the fraction of receptor occupied site can be found,

$$Y = \frac{[\text{SP}_n]}{S_p} = \frac{K_b [\text{P}]^n}{(1 + K_b [\text{P}]^n)} \quad (4.4)$$

From this the ratio of occupied and unoccupied binding sites can be defined,

$$\frac{Y}{(1-Y)} = K_b [\text{P}]^n \quad (4.5)$$

By taking logarithm,

$$\log\left(\frac{Y}{1-Y}\right)=\log K_b+n\log [P] \quad (4.6)$$

The plot of the equation (4.6) is called Hill plot which provides a linear regression to the non-linear binding data, much similar to Lineweaver-Burk Plot for Michaelis-Menten kinetics. From the slope, n the Hill constant and hence the valency of the binding can be determined. Using the valency, the effective dissociation constant (K_d) can be determined. The values obtained from this analysis will allow us to directly compare the interaction kinetics at different experimental setup.

4.2.7. Specificity and selectivity of *S. aureus* recognition

The specificity of the phage binding to *S. aureus* was examined in a blocking experiment in which *S. aureus* cells at concentration of 1×10^6 cfu/ml were pre-incubated with the different concentrations (10^1 to 10^6 pfu/ml in PBS) of selected phage, and sensors were exposed to each bacterial suspension. PBS was used to remove the unbound cells between injections. The response for the particular phage concentration was calculated as described above. For selectivity experiments, sensor surface were exposed to different concentrations of *Salmonella typhimurium* for a period of 30 minutes with in-between PBS washing steps. The system was decontaminated by flowing 70% ethanol solution following the bacterial exposure.

4.3. Results and Discussion

4.3.1. Phage immobilization

Biosensor probes are commonly immobilized through well developed covalent linkages or avidin/biotin chemistry [33, 34]. Recently, we have shown that bacteriophage

can be reliably immobilized on the gold surface via direct physical adsorption which makes the whole process of immobilization much easier [32, 35]. To facilitate the accessibility of phage to the sensor surface, the phage solution was introduced at a flow rate of 100 μ l/min in a recycling mode. A small decrease in signal was observed after washing with buffer due to the removal of loosely bound molecules. We speculate that since the lytic phage head has a polyhedral structure it might be positioned and packaged on the gold surface with high density and regularity. Fig. 4-2 shows the change of interfacial refractive index (Δ RI) as a function of time, as the phage physically adsorbs to the gold surface. The surface coverage of phage adsorption was calculated from the method described by Jung et al [36] and Naimushin et al [19]:

$$d_a = \left(\frac{l_d}{2} \right) \frac{(n_{eff} - n_b)}{(n_a - n_b)} \quad (4.7)$$

The following parameters were used for surface coverage calculation: thickness of the adlayer (d_a), characteristic decay length (l_d) = 307 nm, effective refractive of the adlayer from SPR signal (n_{eff}), refractive index of water, n_b = 1.333, refractive index of adlayer (protein), n_a = 1.57. Using this method, the surface coverage density was found to be 2.68 \pm 0.12 ng/mm².

Table 4-1 Surface coverage for different phage immobilization times

Method of immobilization	Thickness, (d), nm	Surface coverage ¹ , ng/mm ²
Short-term	2.06 \pm 0.09	2.68 \pm 0.12
Long-term	2.37 \pm 0.08	3.10 \pm 0.11

¹Surface coverage for both assays were calculated using the formula 1

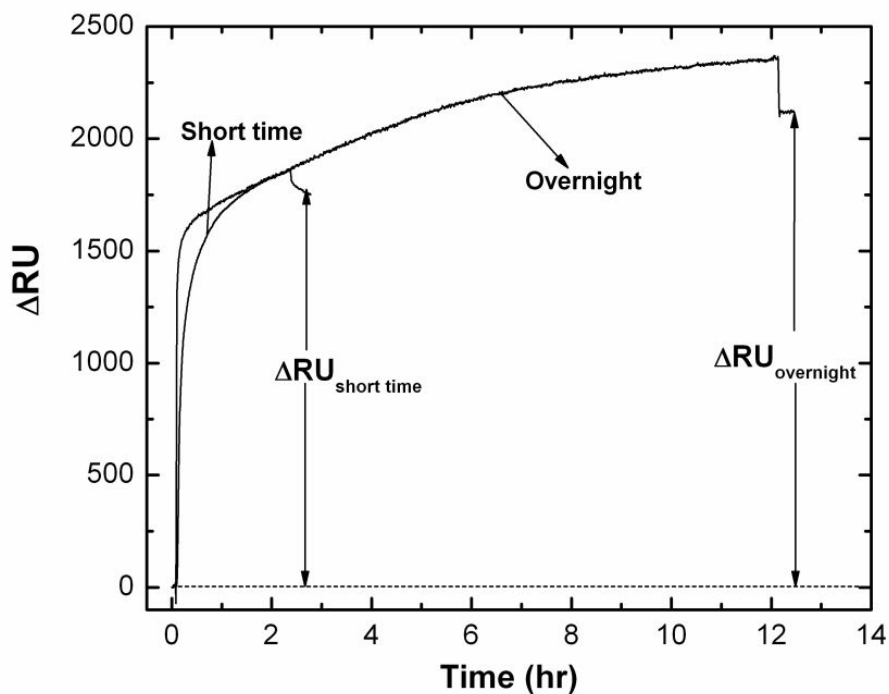


Fig. 4-2. Sensor response for different time length of phage immobilization. The net change in RI for particular immobilization is calculated by subtracting the subsequent PBS baselines. The phage surface coverage was calculated using the formula 1.

4.3.2. Bacterial detection

The SPR sensor described above was tested at flow mode to detect *S. aureus* in direct assay. The uniqueness of SPREETA™ allows simultaneous monitoring of the specific interactions between the partners using sensing and reference channels. Graded concentrations of *S. aureus* were prepared in a PBS buffer and pumped sequentially over both channels. After the surface saturates with particular concentration of bacteria, the loosely bound bacteria were washed with PBS running buffer. This allows the elimination of the signal generated due to non-specific adsorption of cells to the sensor surface, as well as change in RI due to bulk refractive index of the solution. Optical microscopic images of both sensing and control channels after exposure to the 10^7 cfu/ml

of *S. aureus* are shown in the Fig. 4-3. It is apparent that the surface of sensing channel is covered with much higher number of bacteria (~ 62 particles/ μm^2) than the surface of the control channel (~ 12 particles/ μm^2).

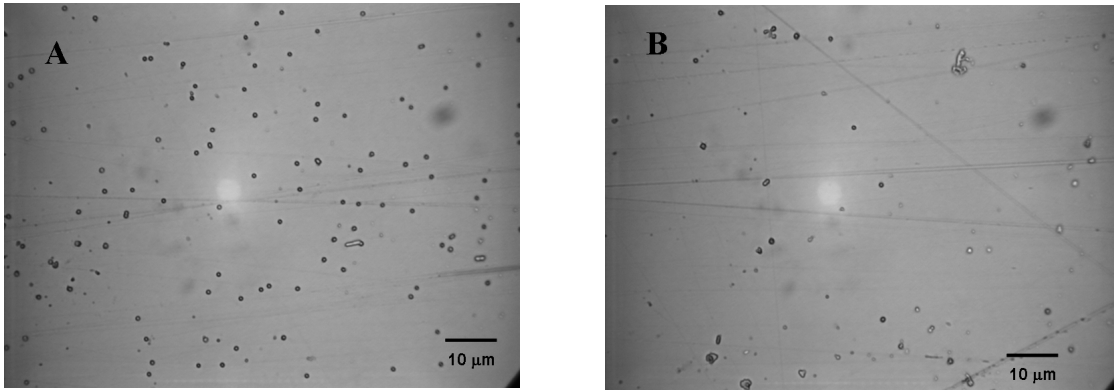


Fig. 4-3 Optical microscope image of the sensor surface after exposure to the suspension of *S. aureus* at 10^7 cfu/ml. A – Sensing channel; B – reference channel.

Fig. 4-4 depicts a characteristic dose-response curve obtained for *S. aureus* recognition by lytic phage. The data were approximated to a sigmoidal fit according to the binding kinetics described earlier [27, 37]. The limit of detection for this assay was found to be 10^4 cfu/ml. This was determined as the lowest concentration of *S. aureus* that produced a distinguishable net response (signal/noise ≥ 3).

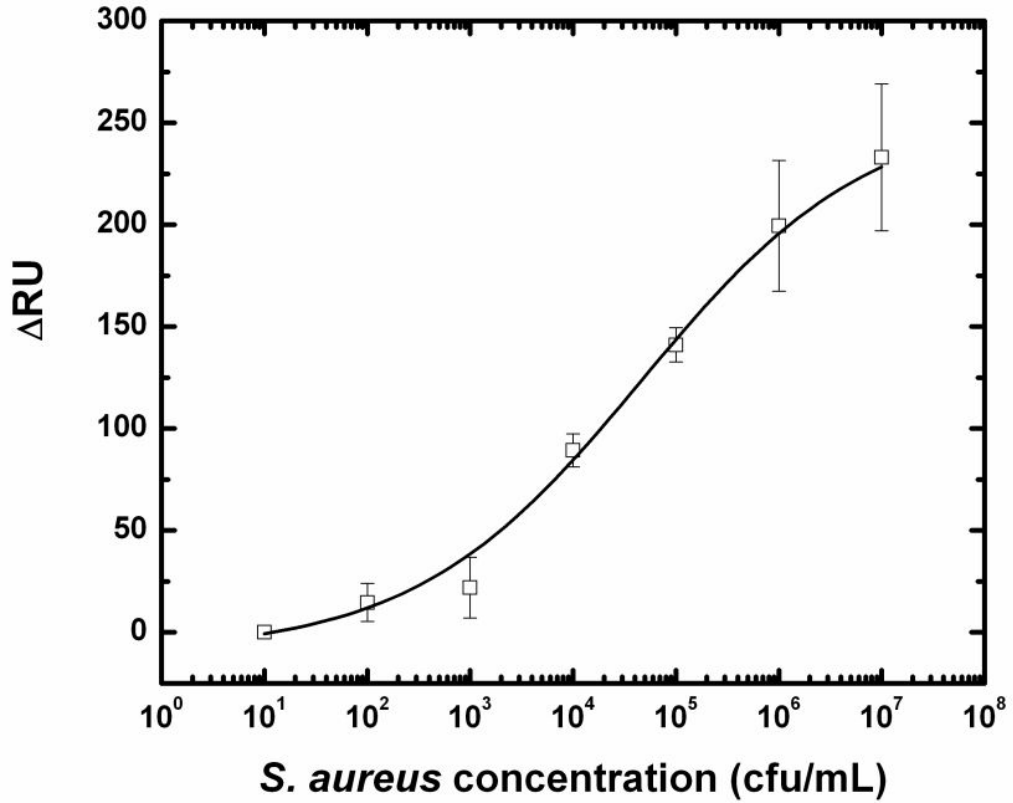


Fig. 4-4 Dose-Response curve for *S. aureus* detection by lytic phage. The net response curves were plotted after adjusting for non-specific binding and bulk RI change from control channel. The detection limit of 1×10^4 cfu/ml was calculated as the lowest *S. aureus* concentration producing distinguishable net response (signal/noise ≥ 3). Mean values (n=3) of Δ RU vs. aureus concentration is plotted. Bars are SD. Points are experimental data while curve is sigmoidal fit ($\chi^2 = 0.59$, $R^2 = 0.988$).

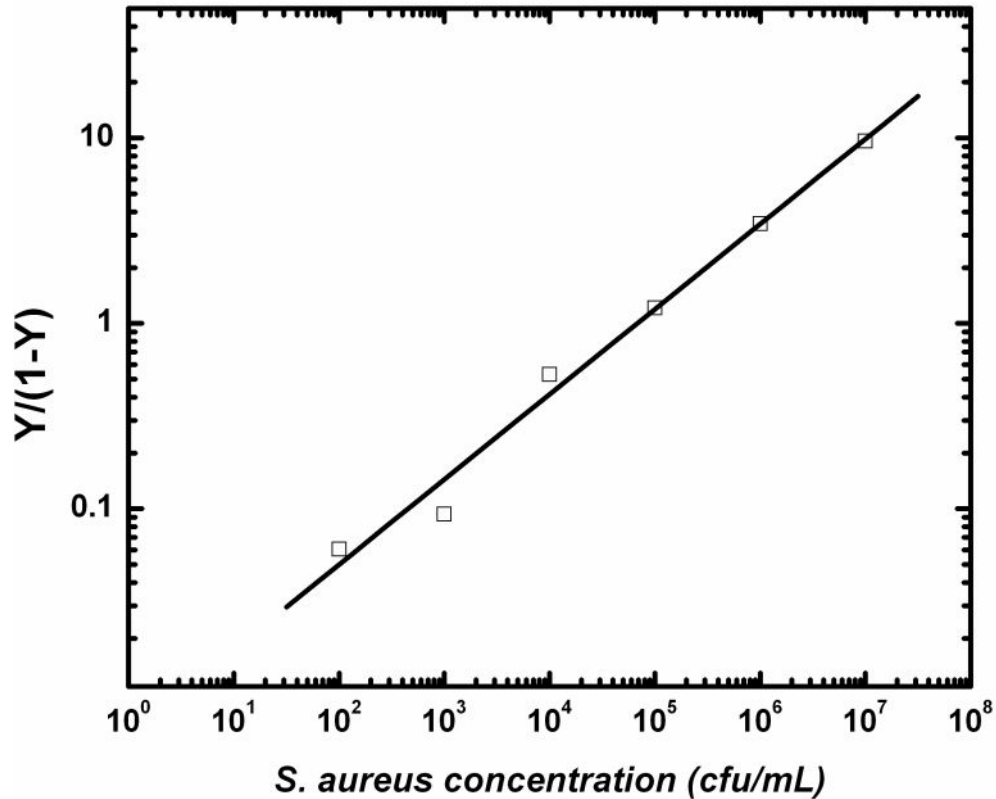


Fig. 4-5 Hill Plot of binding isotherm. Hill coefficient was found to be 0.46. Dissociation constant for phage-bacteria complex was found to be 0.66×10^5 cfu/ml. Points are experimental data while line is linear least-square fit ($R = 0.99$, slope = 0.46 ± 0.03).

The binding parameters between the phage-bacteria complex were calculated using the law of mass action under special considerations. Plots was made between the bacterial concentration and the fractional occupied phage binding sites to estimate the dissociation constant and was found to be 0.66×10^5 cfu/ml (Fig. 4-5). The above assay was repeated with long-term immobilization of phage (12h) which produces ~16% more surface coverage (Table 4-1) than was obtained via short-term immobilization (see Fig. 4-2). However, the different surface coverage of phage did not have a significant effect on the sensitivity of the detection (data not shown for overnight assay). We assume that

this may be due to the non-favorable orientation and to the phage-to-phage interaction of phage in a long-term immobilization assay, which results in blocking of bacterial adhesion sites on the phage. It might be assumed as well that change in RI immediately to the surface is influenced by various factors such as compression of visco-elastic layers due to bacterial adhesion. In addition, various factors influence the response of a SPR assay while detecting bacterial cells in solution. Surface plasmon resonance phenomenon occurs at the metal-liquid interface under the influence of total internal reflection in which the generated evanescent wave can travel up to ~300nm in the z-direction [36]. Since the diameter of *S. aureus* is 0.5- 1 μ m, only a portion of the cell may directly interfere with evanescent wave to generate the response. Nevertheless, the generated SPR signal is enough to provide reliable detection of low concentration of *S. aureus*.

4.3.3. Specificity and selectivity of the sensor response

The detection of the pathogenic bacteria should be specific and selective in order to discriminate the real signals from false-positive signals. Here, the specificity was demonstrated by competitive inhibition assay. For this, different concentrations of phage were pre-incubated with a known concentration of *S. aureus* for 1 hour to block the receptor sites from binding, and the solutions were introduced through the sensor. Fig. 4-6 shows an actual response for the competitive inhibition assay in which the response of sensor decreases as the concentration of phage increases. The responses were calculated after accounting for non-specific binding from the control channel and the net response for each concentration were calculated. With increasing phage concentration in the incubation solution, the number of available bacterial receptor sites decreases and hence results in a decrease in signal. This further confirms that the signal obtained in direct

detection mode (Fig. 4-4) was not due to non-specific binding. The selectivity of the *S. aureus* detection was verified with non-specific *Salmonella typhimurium* at various concentrations. Fig. 4-7 clearly shows the selectivity of the assay as even high concentration of *Salmonella* 1×10^7 cfu/ml failed to produce any significant response.

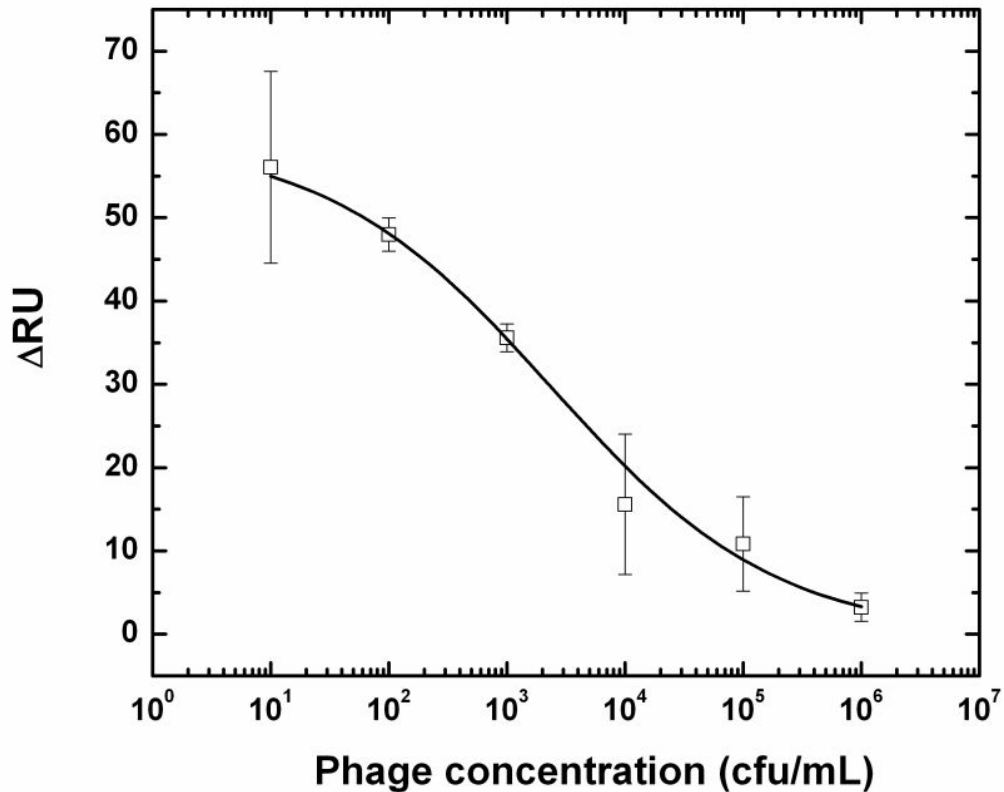


Fig. 4-6 The response curve for the inhibition assay showing the specificity of *S. aureus* detection by lytic phage. Different concentration of phage were pre-incubated with a known concentration of *S. aureus* for 1 hr to block the receptor sites for binding, and the solutions were flown through the sensor. As a free phage concentration increases, the more binding sites on the bacterial surface are blocked and less number of bacteria is able to bind on the sensor surface. Squares are experimental data, and bars are SD (n=3). The smooth curve is sigmoidal fit of experimental data ($\chi^2 = 0.216$, $R^2 = 0.99$).

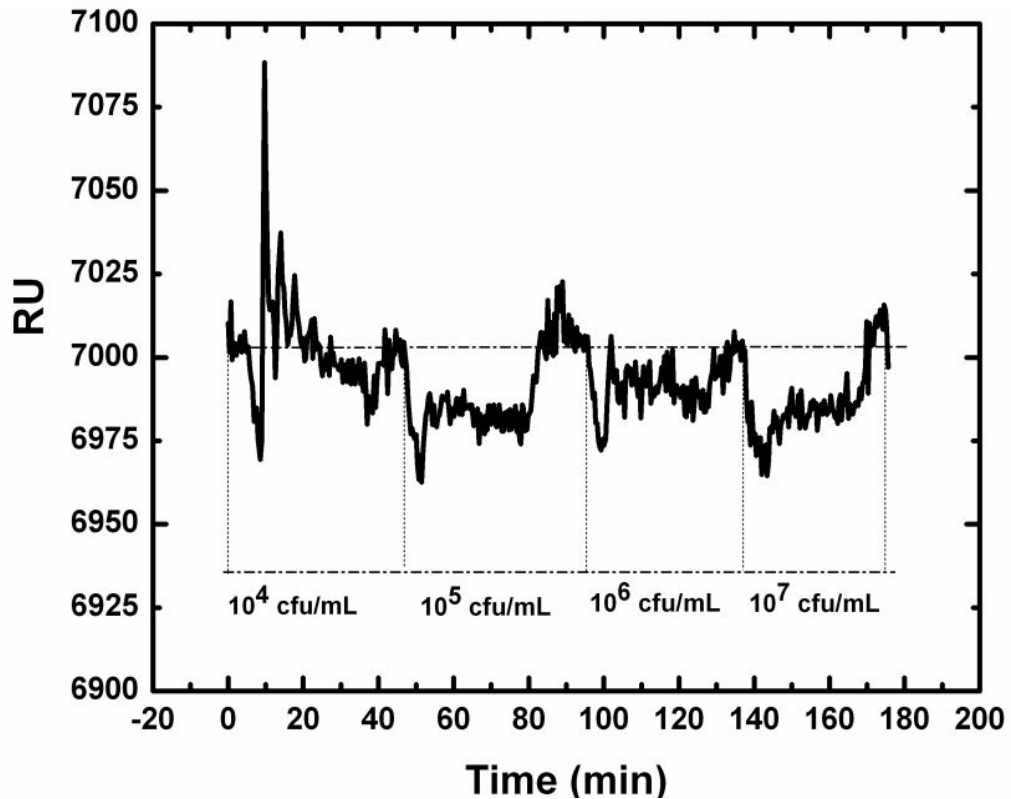


Fig. 4-7 Selectivity of *S. aureus* detection by lytic phage was demonstrated by cross-examining with non-specific *Salmonella typhimurium*. The figure shows the response obtained with alternative application of incrementally increasing concentrations of *Salmonella typhimurium*. Even for the high concentrations *Salmonella typhimurium* failed to produce any significant signal and the response returns to the baseline after washing with PBS buffer.

4.4. Conclusions

We have shown here the use of lytic phage as recognition element and surface plasmon resonance spectroscopy as a platform of biosensor for *S. aureus* detection. Because of the phage remarkable specificity and high affinity towards *S. aureus*, this phage-based biosensor was able to identify as low as 10^4 cfu/ml in direct detection mode without any labeling and amplification steps. It is pertinent to note that lytic phage was

immobilized on the gold surface of SPREETA™ sensor via trouble-free direct physical adsorption, which allows avoiding complex and expensive surface chemistry and phage modification. Biosensor demonstrates high specificity through competitive inhibition assay and selectivity was illustrated with non-specific *Salmonella typhimurium* experiments. Further experiments are underway to improve the sensitivity by amplification assay with phage and to test the biosensor for direct detection of bacteria in real samples.

4.5. References

1. Aucken, H.M., et al., *A new UK strain of epidemic methicillin-resistant Staphylococcus aureus (EMRSA-17) resistant to multiple antibiotics*. 2002. p. 171-175.
2. Jay, J.M., *Modern Food Microbiology*. 6th ed. 2000: Aspen Publication.
3. Lowy, F.D., *Staphylococcus aureus Infections*. N Engl J Med, 1998. **339**(8): p. 520-532.
4. Labbe, R.G. and S. Garcia, *Guide to Foodborne Pathogens*. Wiley Publishers, Inc., 2001.
5. Arbuthnott, J.P., D.C. Coleman, and J.S.d. Azavedo, *Staphylococcal toxins in human disease*. 1990. p. 101S-107S.
6. Jarraud, S., et al., *A highly prevalent operon of enterotoxin gene, forms a putative nursery of superantigens in Staphylococcus aureus*. Journal of Immunology, 2001. **166**(1): p. 669-677.
7. Lina, G., et al., *Toxin involvement in staphylococcal scalded skin syndrome*. Clinical Infectious Diseases, 1997. **25**(6): p. 1369-1373.

8. Mead, P.S., et al., *Food-related illness and death in the United States*. Emerging Infectious Diseases, 1999. **5**(5): p. 607-625.
9. Honeyman A.L, Friedman H., and B. M., *Staphylococcus aureus Infection and Disease*. Infectious Agents and Pathogenesis. 2001: Kluwer Academic/Plenum Publishers.
10. Stepan, J., R. Pantucek, and J. Doskar, *Molecular diagnostics of clinically important staphylococci*. Folia Microbiologica, 2004. **49**(4): p. 353-386.
11. Hall, R.H., *Biosensor technologies for detecting microbiological foodborne hazards*. Microbes and Infection, 2002. **4**(4): p. 425.
12. Hobson, N.S., I. Tothill, and A.P.F. Turner, *Microbial detection*. Biosensors and Bioelectronics, 1996. **11**(5): p. 455.
13. Ivnitski, D., et al., *Biosensors for detection of pathogenic bacteria*. Biosensors and Bioelectronics, 1999. **14**(7): p. 599.
14. Leonard, P., et al., *Advances in biosensors for detection of pathogens in food and water*. Enzyme and Microbial Technology, 2003. **32**(1): p. 3.
15. Bokken, G.C.A.M., et al., *Immunochemical detection of Salmonella group B, D and E using an optical surface plasmon resonance biosensor*. FEMS Microbiology Letters, 2003. **222**(1): p. 75.
16. Koubova, V., et al., *Detection of foodborne pathogens using surface plasmon resonance biosensors*. Sensors and Actuators B: Chemical, 2001. **74**(1-3): p. 100.
17. Leonard, P., et al., *A generic approach for the detection of whole Listeria monocytogenes cells in contaminated samples using surface plasmon resonance*. Biosensors and Bioelectronics, 2004. **19**(10): p. 1331.

18. Medina, M.B., *A biosensor method for a competitive immunoassay detection of staphylococcal enterotoxin B (SEB) in milk*. Journal Of Rapid Methods And Automation In Microbiology, 2005. **13**(1): p. 37-55.
19. Naimushin, A.N., et al., *Detection of Staphylococcus aureus enterotoxin B at femtomolar levels with a miniature integrated two-channel surface plasmon resonance (SPR) sensor*. Biosensors and Bioelectronics, 2002. **17**(6-7): p. 573.
20. Boltovets, P.M., et al., *Detection of plant viruses using a surface plasmon resonance via complexing with specific antibodies*. Journal of Virological Methods, 2004. **121**(1): p. 101.
21. Green, R.J., et al., *Surface plasmon resonance analysis of dynamic biological interactions with biomaterials*. Biomaterials, 2000. **21**(18): p. 1823.
22. Myszka, D.G., *SPR biosensors as biophysical research tools*. Faseb Journal, 2000. **14**(8): p. A1511-A1511.
23. Rich, R.L. and D.G. Myszka, *Advances in surface plasmon resonance biosensor analysis*. Current Opinion in Biotechnology, 2000. **11**(1): p. 54-61.
24. Simonian, A.L., et al., *Characterization of oxidoreductase-redox polymer electrostatic film assembly on gold by surface plasmon resonance spectroscopy and Fourier transform infrared-external reflection spectroscopy*. Analytica Chimica Acta, 2002. **466**(2): p. 201.
25. Pancrazio, J.J., et al., *Development and application of cell-based biosensors*. Annals Of Biomedical Engineering, 1999. **27**(6): p. 697-711.
26. Goldman, E.R., et al., *Phage-displayed peptides as biosensor reagents*. Journal Of Molecular Recognition, 2000. **13**(6): p. 382-387.

27. Petrenko, V.A. and V.J. Vodyanoy, *Phage display for detection of biological threat agents*. Journal of Microbiological Methods, 2003. **53**(2): p. 253.
28. Paul, J.H., et al., *Coliphage and indigenous phage in Mamala Bay, Oahu, Hawaii*. Appl. Environ. Microbiol., 1997. **63**(1): p. 133-138.
29. Kutter, E. and A. Sulakvelidze, *Bacteriophages - Biology and Applications*. 2004: CRC Press.
30. Goodridge, L., J.R. Chen, and M. Griffiths, *Development and characterization of a fluorescent-bacteriophage assay for detection of Escherichia coli O157 : H7*. Applied and Environmental Microbiology, 1999. **65**(4): p. 1397-1404.
31. Mosier-Boss, P.A., et al., *Use of fluorescently labeled phage in the detection and identification of bacterial species*. Applied Spectroscopy, 2003. **57**(9): p. 1138-1144.
32. Sokkalinga Balasubramanian S.G., V.A. Petrenko, and A.L. Simonian. *Prevention of Non-specific binding as a way to increase sensitivity of SPR-based biosensors*. in *206th Meeting of The Electrochemical Society*. 2004. Honolulu, Hawaii.
33. Pradier, C.M., et al., *Specific binding of avidin to biotin immobilised on modified gold surfaces - Fourier transform infrared reflection absorption spectroscopy analysis*. Surface Science, 2002. **502**: p. 193-202.
34. Willner, I. and E. Katz, *Integration of layered redox proteins and conductive supports for bioelectronic applications*. Angewandte Chemie-International Edition, 2000. **39**(7): p. 1180-1218.

35. S.G. Sokkalinga Balasubramanian, V.A. Petrenko, and A.L. Simonian. *Prevention of Non-specific binding as a way to increase sensitivity of SPR-based biosensors.* in *206th Meeting of The Electrochemical Society*. 2004. Honolulu, Hawaii.
36. Jung, L.S., et al., *Quantitative interpretation of the response of surface plasmon resonance sensors to adsorbed films.* Langmuir, 1998. **14**(19): p. 5636-5648.
37. Sorokulova, I.B., et al., *Landscape phage probes for Salmonella typhimurium.* Journal of Microbiological Methods, 2005. **63**(1): p. 55.

5. BIOSENSOR SENSITIVITY IMPROVED BY PREVENTING NON-SPECIFIC ADSORPTION USING PLL-g-PEG BLOCKERS

5.1. Introduction

Biosensor is a sub-set of chemical sensor incorporating biological entities as probes on a transducer surface producing measurable signals upon interaction with the target species. The analyte can be either organic (biological) or inorganic (chemical) depending up on the application. If the characteristics of a probe determine the specificity of a biosensor, its sensitivity is determined by how transducer distinguishes “specific” interactions from “non-specific” interactions. In biosensor application, one of the components must be immobilized in order to interact with its partner. Hence, prevention of non-specific protein adsorption is particularly useful for the specificity of the biosensor.

The surfaces that resist protein and/or cell adsorption are referred as “non-fouling surfaces” (NFS) or “stealth” surfaces. NFS found applications in many *in vivo* as well as *in vitro* applications. Some of the *in vivo* applications includes implanted devices, blood compatible materials and many *in vitro* applications such as diagnostic assays, biosensors, affinity separations and also in non-medical applications such as biofouling-resistant heat exchangers & ship bottom [1]. In addition, the design of medial devices and implants in contact with the blood needs a stable protein-resistant surface for long-term *in vivo* applications. In case of bioaffinity sensing applications, the protein-resistant surfaces are mandatory in order to validate the selectivity & specificity of the sensor [2, 3].

BSA and milk proteins such as gelatin and casein are the typical blocking agents used extensively in immunoassays and biosensor development. As these proteins are purified from serum, they are often contaminated with IgG and other low-molecular weight contaminants like enzymes, salts and heavy metals [4]. These contaminants interfere with target of interest and cross-react with secondary antibodies producing high background signals. Most of the research in creating NFS has been devoted to the coatings developed using relatively simple polymer, ethylene glycol, $(-CH_2CH_2O-)_n$. When $n = 2-15$, polymer is called oligo(ethylene glycol) (OEG). When $n = 15$ to 3500 (MW = 400 to 100,000 Da), poly (ethylene glycol) (PEG) designation is used. When the molecular weights are greater than 100,000 Da, the polymers are commonly referred as poly (ethylene oxide). Protein-resistant surfaces from PEG are well-established strategy for reducing non-specific adsorption on various materials and particularly suitable for biosensor application [5]. PEG can be immobilized to the surface either by coupling to previously immobilized functional groups or by grafting PEG as side chains to polymer backbone, forming a comb-like structure.

Huang et al [3, 6] developed a strategy based on PEG grafted to Poly-L-Lysine (PLL) backbone for protein-resistant applications. Since, PLL is cationic at physiological pH, it can be electrostatically adsorbed to negatively charged surfaces. Derivatizing surfaces with such grafted polymers offer several advantages over conventional blocking agents like BSA and milk proteins. As it is inherently hydrophilic, it provides wide range of applications including resistance to interfering proteins and bacterial contaminants. In addition, some of the PEG chains in PLL-g-PEG can be end functionalized to which

capture molecules are immobilized. This allows us to have a critical control over the biosensing interfaces by creating mixed monolayers with different functionalities.

With respect to biosensor development, there are several advantages in using bacteriophage as sensor recognition molecule. In first, detection involving bacteriophages are affinity-based which is similar to widely employed immunosensing methods. However, they differ by virtue of their innate stability in harsh conditions which are lacking in antibody based systems [7]. By the advent of phage display method [8], scientist have found a way to engineer these phages such that they can express 4000 copies of antigen binding sites. On the contrary, only two sites are available on antibody to bind the antigen and they would also suffer from “heterogeneity”, if the selected antibody is polyclonal in nature [9]. The amount of surface area available to bind antigen is about 300-400 m²/g which sometimes surpasses best known adsorbents or catalyst [10]. Compared to antibodies, phage can be produced relatively inexpensively in large quantities and they are stable over long period without significant loss in their activity [7].

Here, the application of PLL-g-PEG as blocking buffer in reducing the bacterial fouling on gold surface will be demonstrated. Subsequently, this property will be exploited to develop highly sensitive detection of model target enzyme β -galactosidase using affinity-selected filamentous bacteriophage. Surface plasmon resonance, a surface sensitive biophysical method was used to characterize the non-fouling property of PLL-g-PEG polymer and also for developing phage based biosensor.

5.2. Materials & Methods

5.2.1. Reagents

Escherichia coli β -galactosidase (β -gal) was obtained from Sigma Chemical Co. (G5635) as a lyophilized powder and was resuspended in phosphate buffered saline (PBS) to a final concentration of 3 μ M. Phosphate buffered saline solution (PBS); pH 7.4 containing 0.138 M NaCl and 0.0027 M KCl dry powder sachet, 11-mercaptoundecanoic acid (MUA), Poly-L-Lysine-HBr was obtained from Sigma. Bovine serum albumin (BSA), Casein, Tween-20 and Triton-X were obtained from Fisher Scientific. N-Hydroxysuccinimidyl ester of methoxy poly (ethylene glycol) propionic acid [SPA-PEG] was obtained from Nektar Therapeutics.

5.2.2. Phage

The filamentous bacteriophage with specific affinity towards β -gal was used as a probe in this study (aka working phage, 1G40). It is a virus that possesses a single stranded DNA encapsulated in a protein sheath. It was selected from a library of filamentous phages as described [11, 12]. The protein sheath is made up of both major and minor coat proteins. The target for designing the probe is the major coat protein, pVIII, of which there are several thousand copies. A wild-type phage, F8-5, was used as a reference probe without β -Gal specificity.

5.2.3. Bacterium

S. aureus ssp. *aureus* ATCC 12600 was used as the bacterium and was obtained from American Type Culture Collection (Manassas, VA, USA). The strain was cultured overnight in a NZY medium (g/l – NZ amine A. 10; yeast extract, 5; NaCl, 5; pH 7.5) at

37°C for 18-24 h. The culture was centrifuged at 4424 x g for 10 min at 4°C and the supernatant was discarded. The bacterium was resuspended in PBS for analysis.

5.2.4. Synthesis of PLL-g-PEG

PLL-g-PEG was synthesized by following the procedure described in the literature [3, 6]. In brief, Poly-L-Lysine hydrobromide (82mg, mol wt 7 kDa) was dissolved in 1.05ml of 50mM sodium borate buffer. The SPA-PEG was added to the filter sterilized (0.22µm pore size filter) PLL. The mixture was allowed to incubate for 6hr at room temperature. Then the mixture was dialyzed for ~24hr initially against PBS followed by MilliQ water. The product was then freeze-dried and stored at -20°C.

5.2.5. FTIR

Synthesized PLL-g-PEG samples were grounded with KBr & pressed into a pellet using pellet maker. FTIR measurements were done using Perkin-Elmer spectrometer.

5.2.6. Surface plasmon resonance

Surface plasmon resonance occurs when TM-polarized light undergoes total internal reflection at certain angle of incidence (called resonance angle) at the interface of medium of different dielectric constants generating a non-radiative evanescent wave. If this interface is modified with a thin layer of metal (Au/Ag ~50nm) & a monochromatic p-polarized light is used as a source, a minimum in reflectivity is observed. The resonance angle changes with addition of monolayer/multilayer of biomolecules. The non-radiative evanescent wave is very sensitive to minute changes in the RI of the adjacent medium and the change in RI is directly related to the change in surface concentration of biomolecules. This change in RI is continuously monitored to produce a sensorgram having RU (refractive index unit) as y-axis and time as x-axis. Typically, a

response of 1×10^{-6} RIU corresponds to 1 pg/mm^2 of adsorbed protein [13-17]. Although several companies involved in the development of SPR sensors, SPREETA™ sensor produced by Texas Instrument (TI) is the prime candidate for field application because of its compact size, robustness and also affordable. SPREETA is a dual-channel SPR system such that one channel can be dedicated to the detection of analyte of interest while the second channel can serve as control/reference.

SPR measurements were carried out to analyze the concentration-response curve for selected phage against β -galactosidase. Immediately after surface cleaning, the sensor was docked & background reference signals were obtained in air & water. An in-situ NaOH-Triton-X cleaning was performed as suggested by the manufacturer. Selected phage was loaded on to the sensor surface through flow system after establishing a baseline with PBS. Phage adsorption was carried out non-specifically on the sensor surface since phages were found to adsorb directly to the gold through multitude of weak interactions. This was confirmed by buffer washing after the surface saturates with phage adsorption.

5.2.7. BSA-Casein blocking

After phage loading, the uncovered surfaces were blocked with BSA-Casein (1mg/ml each) mixture for ~1hr. This was then followed by detergent (PBS-0.5% Tween) wash & again with buffer to remove loosely bound molecules on the surface. After these washing steps, sensor was ready for detecting β -galactosidase in buffer. A 3-fold graded concentration was introduced to the sensor surface starting from lowest concentration at 5pM. The SPR response was monitored until the surface saturates ($RI < 5 \times 10^{-6}$) for that concentration & then washed with PBS buffer solution. After this, next higher

concentration was introduced sequentially and responses (change in RI) were monitored & recorded.

5.2.8. PLL-g-PEG blocking

The experimental protocol was same as above except the above synthesized PLL-g-PEG (1mg/mL in PBS) was used instead BSA-Casein blocker. As before detergent & buffer washing was performed after phage loading. β -galactosidase detection was same as above.

5.2.9. Bacterial resistance studies

To our knowledge, there has been no report on PLL-g-PEG as protein resistant on gold surface. So in order to validate the protein resistant property of PLL-g-PEG, a self-assembled monolayer of 11-MUA was initially formed on the one channel of the SPREETA™ sensor. The other channel was left unmodified to compare direct binding of *S. aureus* to the gold surface. To the modified channel, PLL-g-PEG was electrostatically attached, while the other channel left unprotected. After immobilization, the protected and unprotected surfaces were challenged with increasing concentration of *S.aureus* (10^1 to 10^9 cfu/mL) and the responses were monitored.

5.3. Results and Discussion

5.3.1. FTIR Characterization of PLL-g-PEG

PEG grafted with PLL was synthesized and characterized using FTIR spectroscopy. The vibrational modes (Fig. 5-1) and their band assignments are summarized in table 1. A wide band around 3500cm^{-1} accompanied by a small peak at 3299 cm^{-1} is ascribed due to amide bond of the PLL backbone. The asymmetric and symmetric stretching of PEG CH_2 chains gives rise to a strong band at 2887 cm^{-1} with a

shoulder at 2946 cm^{-1} . The strong bands at 1654 and 1547 cm^{-1} are assigned to primary amides and N-monosubstituted amides in solid state respectively while the band at 1467 cm^{-1} was due to stretching of CH_2 . A strong absorption peak at 1108 & 1149 cm^{-1} are associated with C-O-C stretching modes. The band positions at 1343, 1242 and 963 cm^{-1} represents CH_2 wagging, twisting and rocking modes typical for crystalline materials. These results clearly confirm successful grafting of PEG to PLL backbone [6, 18, 19].

Wave number, cm^{-1}	Assignments	Source
3299	-CONH	PLL
2951, 2887	Asymmetric and symmetric CH_2 stretching	PEG
2864	Symmetric CH_2 stretching	PLL
1108, 1147	C-O-C stretching	PLL-PEG
1453	Ether methylene units CH_2 scissoring mode	PEG
1358, 1256, 944	Ether CH_2 wagging, twisting and rocking modes respectively	PLL

Table 5-1 FTIR vibrational mode assignments for PLL-g-PEG

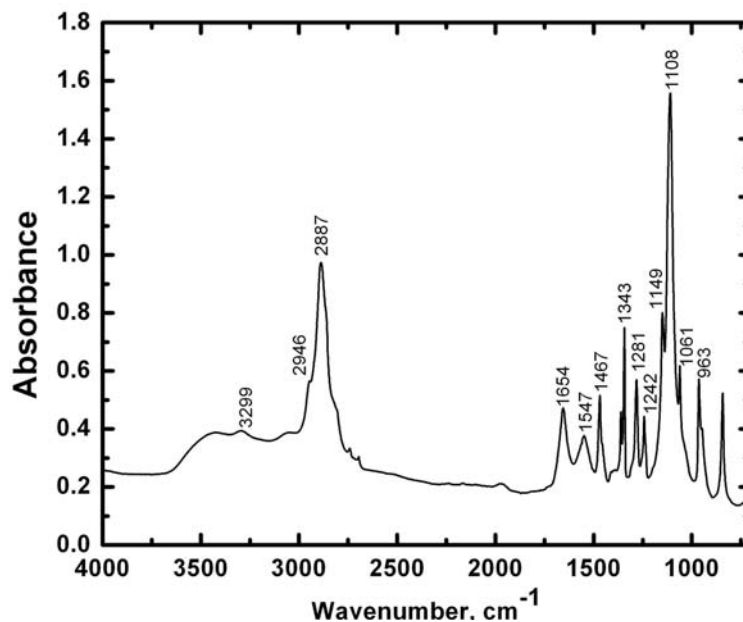


Fig. 5-1 FTIR spectrum showing the vibrational modes of PLL-g-PEG polymer

Fig. 5-2 and 5-3 show the kinetics & schematics of PLL-g-PEG adsorption to modified and unmodified gold surfaces. There is sudden increase in the SPR signal immediately following the injection of PLL-g-PEG solution on both surfaces. This is due to bulk refractive index difference between buffer solution and polymer. Following this, mercaptoundecanoic acid (MUA) modified surface shows faster kinetics of chemisorption compared to unmodified surface. As expected, this is due to the strong electrostatic attraction between PLL-g-PEG polymer and MUA which is negatively charged under neutral or slightly basic pH conditions and hence strongly adsorbs cationic species. The amount of PLL-g-PEG adsorption after final washing with PBS solution suggests that nearly twice the amount of polymer retained to MUA modified surface compared to unmodified gold surface. With respect to the bare gold surface, multiple weak interactions between positively charged PLL backbone and the gold surface were speculated for significant physisorption.

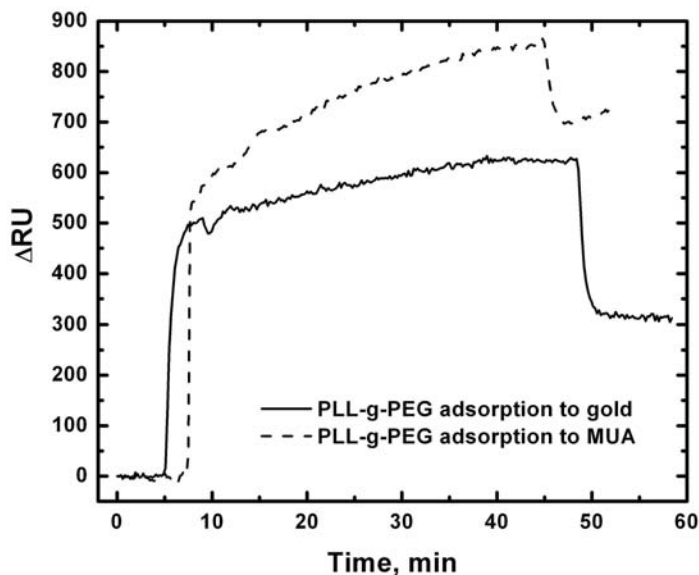


Fig. 5-2 Kinetics of PLL-g-PEG adsorption to MUA modified and unmodified gold surface

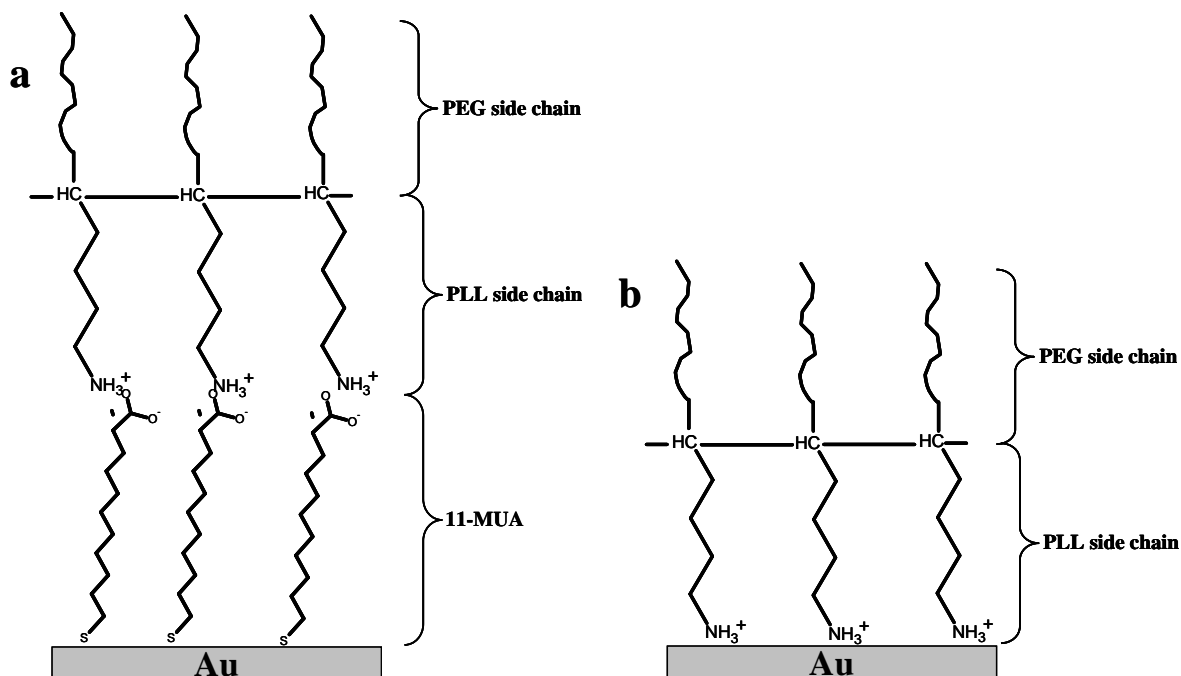


Fig. 5-3 Schematic of PLL-g-PEG adsorption to a).11-MUA modified and b).unmodified surface

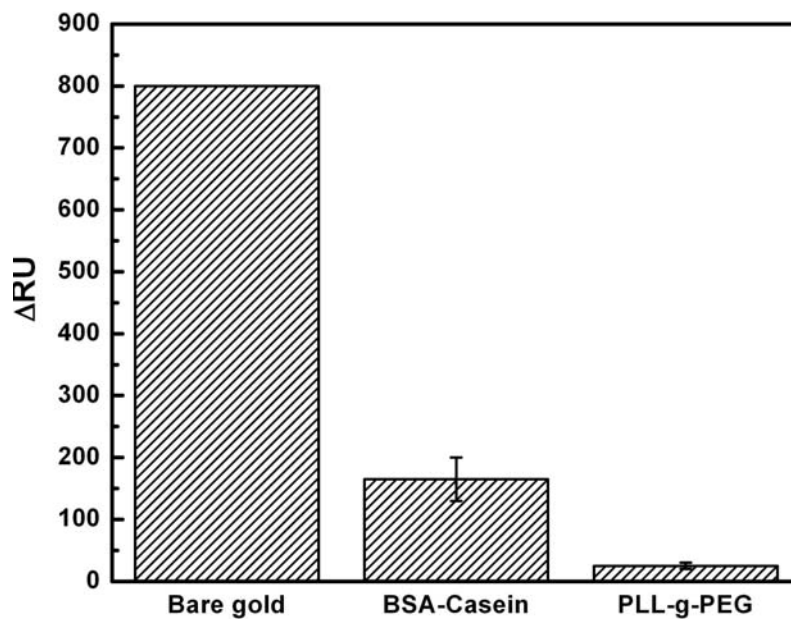


Fig. 5-4 Comparison of *S.aureus* adsorption to PLL-g-PEG, BSA-Casein blocked and unblocked gold surfaces

5.3.2. Antifouling Property

Resistance to bacterial binding is an unsolved issue in biomaterial implants because bacteria tend to adhere & colonize almost on any surfaces. Here, the antifouling property of the synthesized polymer was demonstrated by challenging the polymer modified surface with *S. aureus*. *S. aureus* was selected because of its relevance to pathogenicity & medical-device-related infections. Fig. 5-4 shows that coating of gold surface with this polymer resulted in decrease of bacterial binding by ~97% for PLL-g-PEG modified surfaces. Few bacteria stick to the polymer surface even at very high concentration making it suitable for sensor and biomaterial applications. This antifouling property was imparted to the gold surface by unique hydrophilic nature of PEG surfaces.

5.3.3. Phage based bioaffinity sensing

The application of phage display in microbiological and environmental problems is a fast growing area. This includes analysis of trace substances in pharmaceutical industry, food industry and detection of biowarfare agents. Petrenko et al showed the detection of model antigens like streptavidin from *Streptomyces avidinii* and β -galactosidase from *E.coli* by ELISA and thickness shear mode (TSM) sensors [10, 20]. For biosensors aimed at detecting the analyte at low concentration, it is critical to eliminate the non-specific signals from high background.

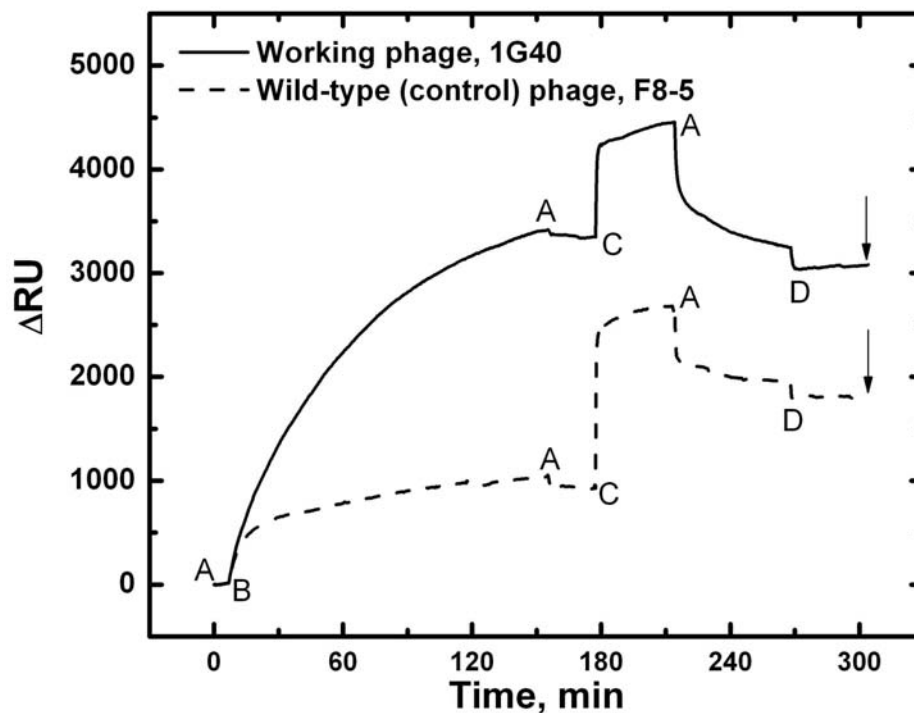


Fig. 5-5 Real time responses obtained for phage immobilization on SPR sensor. Alphabets indicate the time when various solutions were introduced, A - PBS, B – Working (1G40) & Control phage (F8-5), C - BSA and D – PBS-Tween 20 (0.5% v/v).

For the detection of model target enzyme β -gal, the selected phage was directly physisorbed to the SPR gold surface and the adsorption can be confirmed from the real-time SPR response shown in Figure 5-6. A wild-type phage with no affinity towards enzyme β -gal was immobilized on the second channel to serve as a control for non-specific adsorption and signal fluctuations due to pH and temperature change. Fig. 5-5 shows that channels modified with 1G40 and wild-type phage reach saturation around 150 minutes. The response for phage immobilization is repeatable and only a small decrease in signal was observed after buffer washing. This suggest that phage adsorption on gold was very strong involving multiple attractive forces between phage and gold

(including hydrophobic bonding, covalent bond through Cys-SH groups and van der Waals forces).

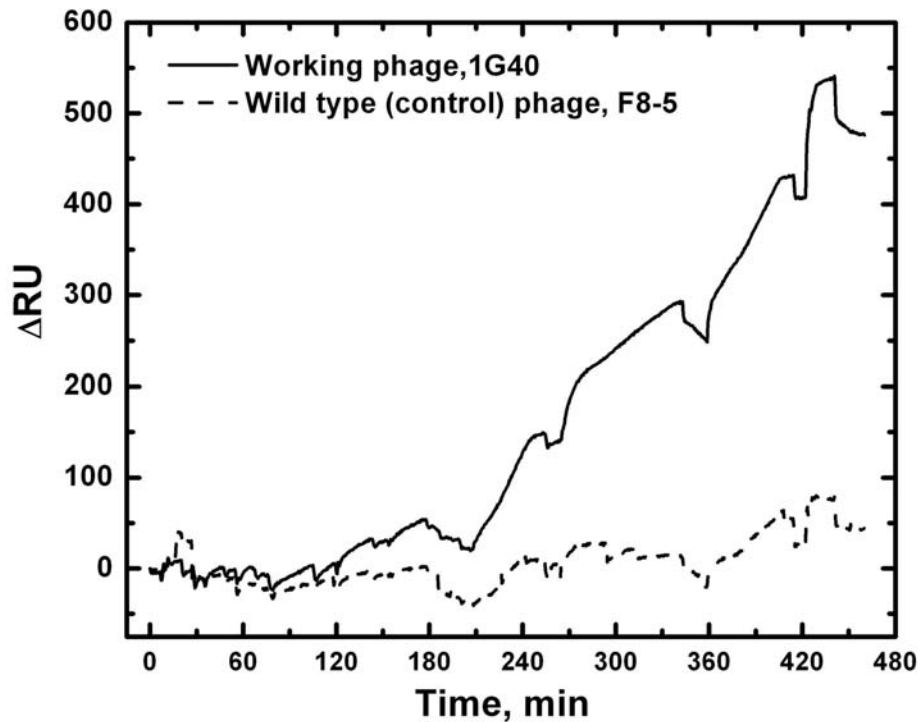


Fig. 5-6 Real-time response for β -gal detection by the selected phage immobilized on the sensor surface. Wild type F8-5 was used as a control phage to show the responses due to non-specific binding of enzyme to the sensor surface. The signal on this fig was normalized to the baseline indicated by arrows in fig. 5-5.

In the first series of experiments, blocking buffers containing equal amount of high molecular weight BSA (66 kDa) & low molecular weight Casein (~22 kDa) were used to block spatially unoccupied sites. Followed by blocking, the phage immobilized surfaces were challenged with sequentially increasing concentration of β -gal (Fig. 5-6). As expected, the β -gal specific phage 1G40 shows a rapid increase in signal as the concentration increases while the wild-type phage showed a minimal response to β -gal

concentrations. This clearly validates the specificity of affinity-selected phage towards β -gal. However, some non-specific adsorptions were observed at low and high target concentration. This causes a reduction in signal-to-noise ratio especially at low target concentration. Detection of low concentration (typically in picomolar level) is critical in many applications including disease diagnosis and food safety.

When the blocking buffer containing BSA and casein were replaced with PLL-g-PEG, the interaction between phage and β -gal shows a dramatic increase in response especially at low concentrations of β -gal. This improved signal to noise ratio at low concentrations directly impact the sensitivity of the detection. Fig. 5-7 & fig. 5-8 unambiguously demonstrates this effect, shifting the lower limit of detection to picomolar range down from nanomolar obtained with BSA-Casein blocking.

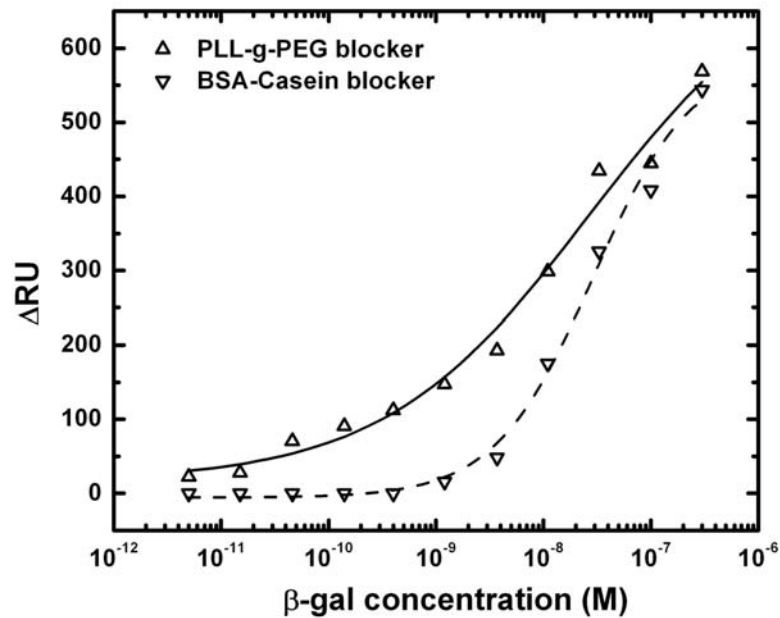


Fig. 5-7 Comparison of response curve for phage based β -gal detection using PLL-g-PEG and BSA-Casein as blockers

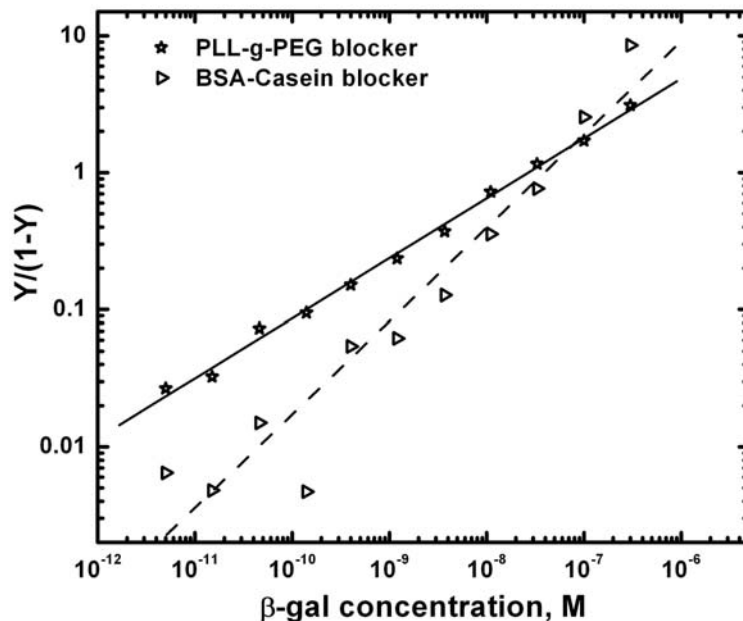


Fig. 5-8 Hill Plot of binding isotherm. The parameters obtained from Hill plot are listed in Table 5-2

Blocking buffer	Dissociation Constant K_d (nM)	Binding Valency
BSA-Casein	67	1.47
PLL-g-PEG	21	2.3

Table 5-2 Effect of blockers on phage- β -galactosidase detections

Why PLL-g-PEG modified surface improved the interaction between β -gal and immobilized phage and hence detection sensitivity is clearly understood. However, we speculate that several factors individually or in concert play a role in this observation. When directly immobilized on the surface, PEG component of PLL-g-PEG is exposed to the buffer containing enzyme. It is necessary to understand how PEG acts as a “protein-resistant” surface. The adsorption of protein causes both bound & free water of hydrated PEG molecule to be released, which is thermodynamically an unfavorable process. Hence, PEG molecules resist the release of its water molecules from the hydrated coil. This

phenomenon is called as *osmotic repulsion*. In addition, this polymer molecules offer resistance to compression because of its tendency to retain the volume of a random coil (*entropic repulsion*) [5, 21, 22]. It is not clear whether PEG of PLL-g-PEG removes water molecules surrounding β -galactosidase exposing its hydrophobic peptides thereby increasing its chances of interaction with immobilized phage molecule. It is well known that affinity interactions like antigen-antibody primarily involve several hydrophobic interactions between the antigen and the active site. Conversely, this hydrophobic interaction might have a role in decreased sensitivity observed with BSA-Casein blockers. This is because BSA and casein have shown to increase the stability of enzyme β -galactosidase compared to other proteins [23]. Here also, the mode of interaction was not clearly understood but speculated that increased hydrophobic bonding due to disruption of water molecules.

5.4. Conclusion

PLL-g-PEG molecules show an excellent resistance towards bacterial fouling. By exploiting this behavior, a highly sensitive biosensor was developed using filamentous bacteriophage as probe molecule. The effect of blocking agents on the sensitivity was studied and found that PLL-g-PEG improved the sensitivity of detection by three orders of magnitude. The reason why PLL-g-PEG improved the sensitivity of detection was not well understood. However, we speculate that exposing hydrophobic domains by disruption of water molecules structure around the enzyme might play a role in the amount of interaction towards immobilized phage.

5.5. References

1. Ratner, B.D., et al., *Biomaterials Science: An Introduction to Materials in Medicine*. 2nd ed. 2004: Academic Press.
2. Leckband, D., S. Sheth, and A. Halpern, *Grafted poly(ethylene oxide) brushes as nonfouling surface coatings*, in *Journal of Biomaterials Science -- Polymer Edition*. 1999, VSP International Science Publishers. p. 1125.
3. Huang, N.P., et al., *Biotin-derivatized poly(L-lysine)-g-poly(ethylene glycol): A novel polymeric interface for bioaffinity sensing*. *Langmuir*, 2002. **18**(1): p. 220-230.
4. *IgG-Free, Protease-Free Bovine Serum Albumin*. [cited May 15th 2008]; Available from: <http://www.jacksonimmuno.com/catalog/catpages/IgG-Free.asp>.
5. Ostuni, E., et al., *A survey of structure-property relationships of surfaces that resist the adsorption of protein*. *Langmuir*, 2001. **17**(18): p. 5605-5620.
6. Huang, N.P., et al., *Poly(L-lysine)-g-poly(ethylene glycol) layers on metal oxide surfaces: Surface-analytical characterization and resistance to serum and fibrinogen adsorption*. *Langmuir*, 2001. **17**(2): p. 489-498.
7. Brigati, J.R. and V.A. Petrenko, *Thermostability of landscape phage probes*. *Analytical and Bioanalytical Chemistry*, 2005. **382**(6): p. 1346-1350.
8. Smith, G.P., *Filamentous Fusion Phage - Novel Expression Vectors That Display Cloned Antigens on the Virion Surface*. *Science*, 1985. **228**(4705): p. 1315-1317.
9. Iqbal, S.S., et al., *A review of molecular recognition technologies for detection of biological threat agents*. *Biosensors and Bioelectronics*, 2000. **15**(11-12): p. 549-578.

10. Petrenko, V.A. and V.J. Vodyanoy, *Phage display for detection of biological threat agents*. Journal of Microbiological Methods, 2003. **53**(2): p. 253-262.
11. Petrenko, V.A. and G.P. Smith, *Phages from landscape libraries as substitute antibodies*. 2000. p. 589-592.
12. Petrenko, V.A., et al., *A library of organic landscapes on filamentous phage*. 1996. p. 797-801.
13. Cooper, M.A., *Label-free screening of bio-molecular interactions*. Analytical and Bioanalytical Chemistry, 2003. **377**(5): p. 834-842.
14. Green, R.J., et al., *Surface plasmon resonance analysis of dynamic biological interactions with biomaterials*. Biomaterials, 2000. **21**(18): p. 1823-1835.
15. Lippa, P.B., L.J. Sokoll, and D.W. Chan, *Immunosensors--principles and applications to clinical chemistry*. Clinica Chimica Acta, 2001. **314**(1-2): p. 1-26.
16. Naimushin, A.N., et al., *Detection of Staphylococcus aureus enterotoxin B at femtomolar levels with a miniature integrated two-channel surface plasmon resonance (SPR) sensor*. Biosensors and Bioelectronics, 2002. **17**(6-7): p. 573-584.
17. Simonian, A.L., et al., *Characterization of oxidoreductase-redox polymer electrostatic film assembly on gold by surface plasmon resonance spectroscopy and Fourier transform infrared-external reflection spectroscopy*. Analytica Chimica Acta, 2002. **466**(2): p. 201-212.
18. Harder, P., et al., *Molecular conformation in oligo(ethylene glycol)-terminated self-assembled monolayers on gold and silver surfaces determines their ability to*

- resist protein adsorption*. Journal of Physical Chemistry B, 1998. **102**(2): p. 426-436.
19. Wang, R.L.C., H.J. Kreuzer, and M. Grunze, *Molecular conformation and solvation of oligo(ethylene glycol)-terminated self-assembled monolayers and their resistance to protein adsorption*. Journal of Physical Chemistry B, 1997. **101**(47): p. 9767-9773.
 20. Petrenko, V.A. and G.P. Smith, *Phages from landscape libraries as substitute antibodies*. Protein Engineering, 2000. **13**(8): p. 589-592.
 21. Golander, C.G., et al., *Properties of Immobilized PEG Films and the Interaction with Proteins: Experiments and Modeling*, in *Poly(ethylene glycol): Chemistry and Biological Applications*, J.M. Harris, Editor. 1992, American Chemical Society
 22. Kingshott, P. and H.J. Griesser, *Surfaces that resist bioadhesion*. Current Opinion in Solid State & Materials Science, 1999. **4**(4): p. 403-412.
 23. Chang, B.S. and R.R. Mahoney, *Enzyme Thermostabilization By Bovine Serum-Albumin And Other Proteins - Evidence For Hydrophobic Interactions*. Biotechnology and Applied Biochemistry, 1995. **22**: p. 203-214.

6. ELECTROCHEMICAL DESORPTION OF PROTEINS FROM GOLD ELECTRODE SURFACE

6.1. Introduction

Precise design of bio-interfacial properties is emerging as a key factor in the fields of biosensing and cellular engineering. Gold is commonly used for fabrication of working electrodes; therefore, defining surface properties of this material is important for electrochemical sensor development and electrical manipulation of cells. Modifying gold surfaces by self-assembly of alkanethiols has been the subject of intense investigation over the past twenty years [1-4]. By synthesizing appropriate alkanethiol molecules, gold surfaces can be rendered non-fouling, through the inclusion of poly(ethylene glycol) molecules, or protein-reactive, by incorporating aliphatic or reactive polar groups[3, 4]. In addition, there is interest in controlling surface properties in a spatial and/or temporal fashion [2, 5-10]. Regional control of surface properties can be exercised by designing substrates composed of different materials and then using self-assembling molecules specific to these materials (e.g. thiols/silane for gold/silicon [9], electrical wiring of proteins by reconstitution of co-factor modified monolayers assembled onto Au-electrodes [11], or thiols/carboxylic acids for gold/ Al_2O_3 [2]). Another approach to controlling spatiotemporal properties of gold electrode surfaces is exemplified by works of Lahann [10] and Mrksich [8] whereby self-assembled monolayer undergoes conformational or compositional changes when electrical potential is applied, thus, resulting in switching of

surface properties. The third approach is based on the ability to strip self-assembled alkanethiols from gold via electrochemical reduction [12]. This method has been used to create molecular and protein concentration gradients on gold [5, 6], as well as, design cell motility assays [7]. While the reports of alkanethiol desorption from gold are common [12-15], studies pertaining to electrochemical removal of large protein molecules covalently immobilized to self-assembled alkanethiols are infrequent.

Therefore, the main goal of the present study was to determine feasibility of removal of model proteins covalently bound to gold electrode surfaces. In order to observe molecular binding events in real-time and to correlate these events to changes in electrical properties of the gold surface, we employed combined electrochemical-surface plasmon resonance (ESPR) instrument described in our prior work[16]. Additional surface characterization was carried out by ellipsometry. Model proteins, bovine serum albumin (BSA) and immunoglobulin G (IgG) were covalently bound to self-assembled mercaptoundecanoic acid (MUA) through carbodiimide (EDAC/NHS) chemistry. Deposition of alkanethiols and proteins was monitored by SPR and confirmed by cyclic voltammetry with potassium ferricyanide serving as a probe molecule. Estimation of the surface coverage based on SPR signals showed formation of densely packed alkanethiol and protein layers. Significantly, electrochemistry and SPR experiments showed that these layers were completely removed from gold surface after applying a reductive potential (-1.2V vs. Pt electrode). The sequence of alkanethiol/protein assembly steps followed by electrochemical stripping could be repeated multiple times, demonstrating the ability to modulate gold electrode properties. Studies described here are envisioned

to have significant applications in the areas of affinity or cell-based biosensing, as well as, in developing tools for micro-patterning and sorting of living cells.

6.2. Materials and Methods

6.2.1. Chemicals

O-[2-(3-Mercaptopropionylamino) ethyl]-*O'*-methylpolyethylene glycol (PEG-thiol), 11-mercaptopundecanoic acid (MUA), 1-ethyl-3-(3-dimethylaminopropyl) carbodiimide (EDC), Phosphate buffered saline (PBS), and absolute ethanol were obtained from Sigma-Aldrich. Bovine serum albumin (BSA), Tris (hydroxymethyl) aminomethane, potassium hydroxide and ethanolamine were purchased from Fisher Scientific. N-hydroxysuccinimide (NHS) and Potassium ferricyanide, $K_3Fe(CN)_6$ (FCN) were obtained from Acros-Organics (through fisher). All the chemicals were used without further purification. Organophosphorous Hydrolase (OPH) enzyme and anti-OPH were obtained from Texas A&M University and was used as is.

6.2.2. Surface preparation and characterization

Sensing surfaces were cleaned using piranha solution (3:1:H₂SO₄ and H₂O₂. *Caution: Piranha solution is dangerous and should be handled with care*) for 5 minutes and rinsed thoroughly with de-ionized (DI) water. The efficacy of cleaning of the sensor surface was confirmed by validating the refractive index (RI) of water as 1.333. Prior to SPR experiments, the sensor surface was made hydrophilic by air-plasma cleaning for 5 minutes (Harrick Scientific). After plasma cleaning, the sensor was docked with the ESPR cell and references were obtained in air and water. For ellipsometry and atomic force microscopy measurements, glass slides were coated with ~ 2 nm chromium adhesion layers followed by ~ 50 nm gold films and was cleaned with piranha solution as

described above. These surfaces were then sonicated in acetone for 5 min., rinsed with DI water, and then sonicated with ethanol for 5 min. After sonication, gold coated glass slides were plasma cleaned in air for 5 minutes and immediately immersed in 1mM ethanolic solution of MUA for ~18 to 20 h. The slides were then rinsed with ethanol and water and modified with proteins as in section 2.4.

Ellipsometric measurements were carried out using a commercially available ellipsometer (Auto ELLE3, Rudolph Research, Inc). The thickness of immobilized multilayer was determined by null ellipsometry with refractive indices taken to be 1.45 for alkanethiols and proteins [17, 18].

6.2.3. Combined electrochemical-SPR setup

For combined electrochemical-SPR studies, SPREETA™ sensors developed by Texas Instrument (TI) were used. This SPR system employs a light emitting diode (840nm) with a polarizer, reflecting mirror, and Si-photodiode array. The sensing region is coated with a semi-transparent gold film (~50 nm) with a Cr-adhesion layer (1-2nm). A 12-bit three-channel electronic control box completes the interface between the sensor and a PC. Multichannel SPREETA software provided by TI monitors the changes in RI near the sensing surface, calculates the statistical noise in the signal and displays the results. The signal is generally displayed in the response unit (RU) (1 Response Unit = 10^{-6} Refractive index unit), and the Spreeta sensor's detection limit is $\sim 10^{-6}$ refractive index units. All the SPR experiments were carried out in batch mode with no flow setup. A custom built electrochemical-SPR cell (ESPR cell) was made of Teflon with openings for inserting both reference electrode (Ag/AgCl, BAS) and platinum counter electrode (Pt foil). Two types of electrochemistry experiments were carried out. Electrochemical

reduction experiments were performed *in situ* in a two or three electrode set-up with SPR sensor gold surface serving as a working electrode (Fig. 6-1). BAS CV-50W potentiostat was used to apply reductive potential. In a second type of electrochemistry experiment, cyclic voltammetric measurements were used to characterize presence of passivating (resistive) layers on the electrode surface. In these experiments, three electrode system consisting of gold working electrode (BAS, $\Phi = 1.6\text{mm}$), Pt foil as counter electrode and Ag/AgCl reference electrode were employed. Initially, the gold electrode was mechanically polished using alumina and rinsed thoroughly with water. Remaining alumina particles were removed by sonication in water for ~ 3 minutes.

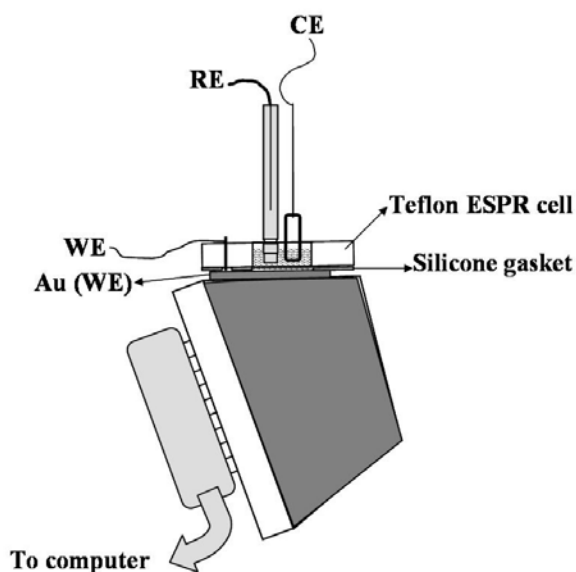


Fig. 6- 1 Combined electrochemical SPR (ESPR) setup. A homemade electrochemical-SPR cell (ESPR cell) was used for all ESPR experiments. SPREETA sensor containing gold electrode was used as working electrode (WE), while Ag/AgCl and Pt foil were used as reference electrode and auxiliary electrode respectively. For two-electrode process, the Ag/AgCl reference electrode (RE) was removed and potential was applied against Pt

counter electrode (CE). The RE and CE leads from the potentiostat were both connected to the Pt electrode in order to use potentiostat as power source.

6.2.4. Adsorption and desorption of proteins from SPR sensor surface

Prior to assembly of molecular components, SPR sensor surface was washed with 0.12N NaOH and 1% Triton X solution. After this washing step, a baseline was obtained in fresh PBS buffer. Clean gold surfaces were modified with self-assembled monolayer (SAM) of 1mM MUA in ethanol for 75 minutes followed by thorough rinsing with ethanol and DI water. Proteins were immobilized on the SAM by activating the carboxylic acid groups of 11-MUA with freshly prepared 0.4M EDC/0.1M NHS in water for 15 minutes. The activated surface was reacted with BSA (1 mg/ml) in PBS (10mM, pH 7.4) to covalently bind this protein to MUA-covered gold surface. After conjugation of BSA for ~ 75 minutes, the surface was rinsed with PBS buffer to remove un-reacted protein molecules. Antibody immobilization occurred by a similar protocol, where 0.1 mg/ml anti-OPH antibody was reacted with activated MUA monolayer for ~ 1 h and washed with PBS buffer. 50mM Tris buffer was used to quench the activated carboxyl groups of MUA to eliminate further chemical reaction with free amines. A low concentration of antigen OPH (35 nM) was introduced and subsequently captured by the immobilized antibody. Unbound OPH molecules were washed away with buffer solution. The above processes are schematically shown in fig. 6-2.

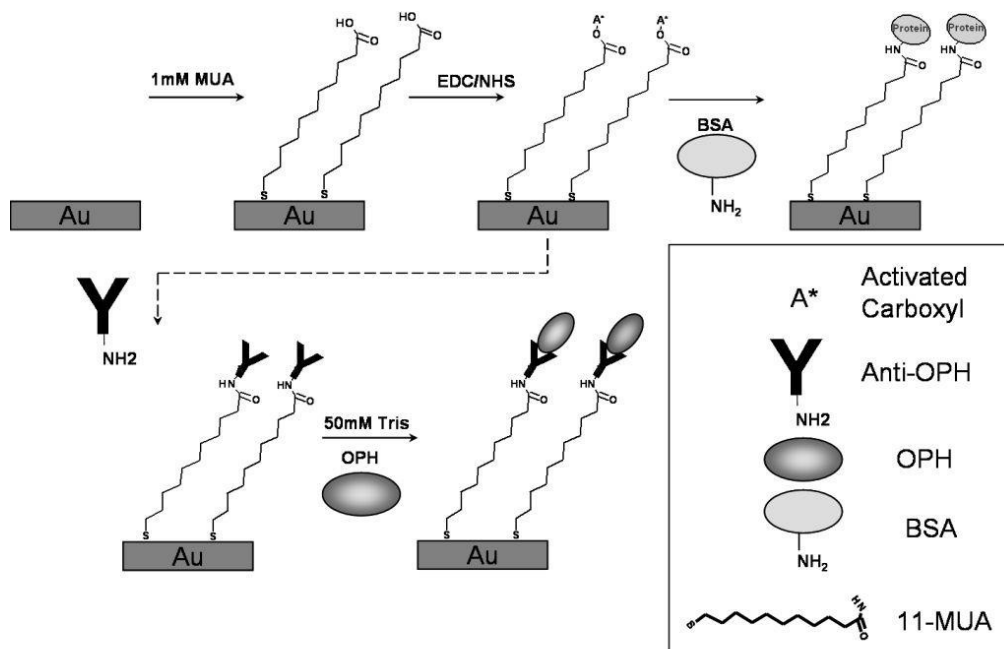


Fig. 6- 2 Schematic of a sequence of surface modification steps employed in the study.

Reductive desorption of immobilized molecules were carried out using two-electrode system. A reductive potential of -1200 mV was applied against Pt counter electrode for 30 seconds and the surface was immediately washed with PBS to avoid re-adsorption of alkanethiol molecules.

The thickness and surface coverage of individual adlayers were calculated assuming ‘linear response regime’ of the evanescent wave, in which the thickness of the adlayers is $d_a \ll l_d$, (l_d is the decay length of the evanescent wave) [19]. Given that the thickness of most of the SAMs and proteins is on the order of few nanometers whereas the decay length of the evanescent wave is on the order of 200 nm [13], this relationship should hold true. Thickness of the adsorbed layer was calculated using Equation 1 shown below:

$$d_a = \left(\frac{l_d}{2} \right) * \frac{(n_{\text{eff}} - n_b)}{(n_a - n_b)} \quad (1)$$

where d_a is thickness of the layer, l_d is characteristic decay length, n_{eff} is effective refractive index measured by SPR, n_b - refractive index of buffer obtained from the buffer baseline before individual assembly step, and n_a - refractive index of adlayer. For proteins and alkanethiols n_a was taken to be 1.45. Once the thickness is known, surface coverage (in g/mm^2 or mole/mm^2) may be derived from bulk density of the molecule. Bulk density values for proteins and MUA were taken to be $1.3 \text{ g}/\text{cm}^3$ [19] and $0.792 \text{ g}/\text{cm}^3$ (from www.sigma-aldrich.com) respectively.

6.3. Results and Discussions

The present study employed coupled electrochemistry-SPR instrument to demonstrate electrochemical removal of proteins covalent bound to the gold electrode surface. Ability to exercise dynamic control over molecular assembly events demonstrated here has important applications in the fields of biosensing and cellular engineering.

6.3.1. Formation of SAM on gold

Ellipsometry, SPR and electrochemistry were used in concert throughout this study to verify assembly and removal of molecules from electrode surfaces. Fig. 6-2 shows diagrammatically, the step-by-step procedure used in this study to immobilize model proteins on Au surfaces. Ellipsometry (Fig. 6-3) was performed to confirm assembly of multiple layers on Au electrode surface. MUA thickness measured by ellipsometry was $\sim 2 \text{ nm}$ which points to formation of a monolayer and is in good agreement with the values of 1.9 nm reported in the literature [20, 21]. The observed

thickness is also in good agreement with values expected for densely packed chains extending away from the surface [1, 22]. By converting SPR signal into thickness (see section 6.2.4 for description of the method) the MUA layer was also determined to be ~ 1.9 nm, confirming our ellipsometry results. The surface coverage was determined from SPR signal to be $(7.04 \pm 0.01) \times 10^{-10}$ mol/cm². This value compares well with literature values of 7.6×10^{-10} mol/cm² and, once again, indicates formation of a tightly packed alkanethiol monolayer [23, 24].

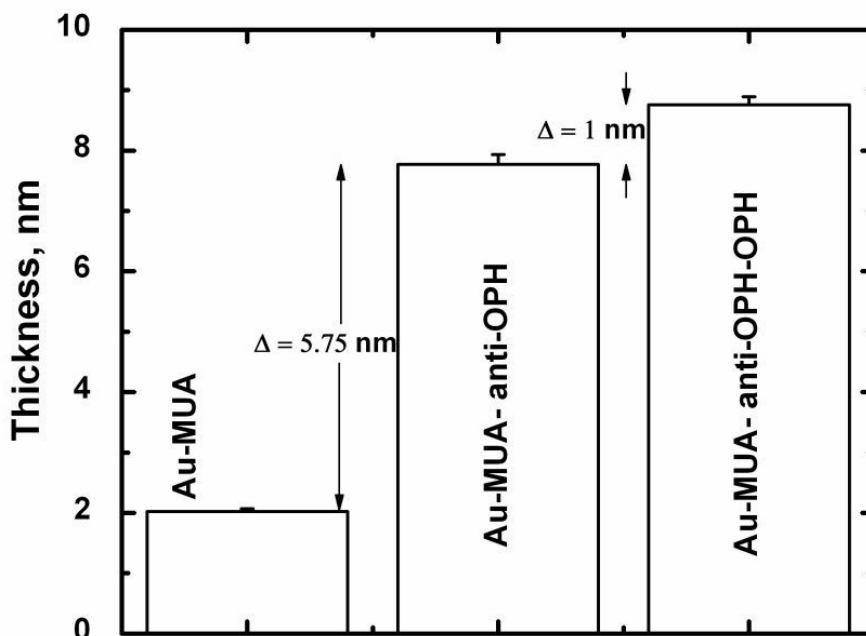


Fig. 6- 3 Ellipsometric thickness measurements for gold surface modified with anti-OPH immobilized on MUA SAM.

6.3.2. Immobilization of proteins on sensing surfaces

Immobilization of proteins was carried out by activating carboxylic acid groups of MUA monolayer with EDC-NHS mixture. Proteins containing amine groups on the surface interact readily with the activated MUA intermediates and form covalent amide

linkages. SPR was used to monitor covalent immobilization of proteins in real time. The thickness of protein layer was calculated according to the Equation 1 and compared to ellipsometry results. Fig. 6-4a shows the real-time binding of BSA to EDC/NHS activated MUA layer. A sharp increase in RI was noticed for EDC/NHS injection, which is due to bulk refractive index change between buffer and EDC/NHS in water. After rinsing with buffer, BSA of 1mg/ml solution was reacted with the surface for ~75 minutes. The surface was then washed with buffer to remove non-specifically or loosely adsorbed molecules. Since, at pH 7.4 BSA carries a net negative charge, non-specific adsorption of BSA to MUA (pKa ~ 6.5 [25]) under neutral pH is not expected to be significant. SPR signal associated with BSA binding, corresponded to surface coverage of (1.08 ± 0.14) ng/mm² or $(9.68 \pm 1.2) \times 10^{11}$ molecules/cm². Similar coverage values (1.2 to 1.8 ng/mm²) were reported in the literature [19, 26]. To determine approximate ideal surface coverage for a given protein, a simple approximation has been shown to work [27]:

$$P_{ideal} \sim \frac{MW}{\pi ab N_a} \quad (2)$$

where, P is surface coverage, MW is molecular weight of the protein, a and b are dimensions of the molecule and N_a is Avagadro's number. Using this relationship and assuming BSA to be a spherical molecule with approximate dimensions of 5 x 5 x 5 nm[28], P_{ideal} was calculated to be 1.4 ng/mm². This translates to ~ 77% surface coverage for BSA molecules.

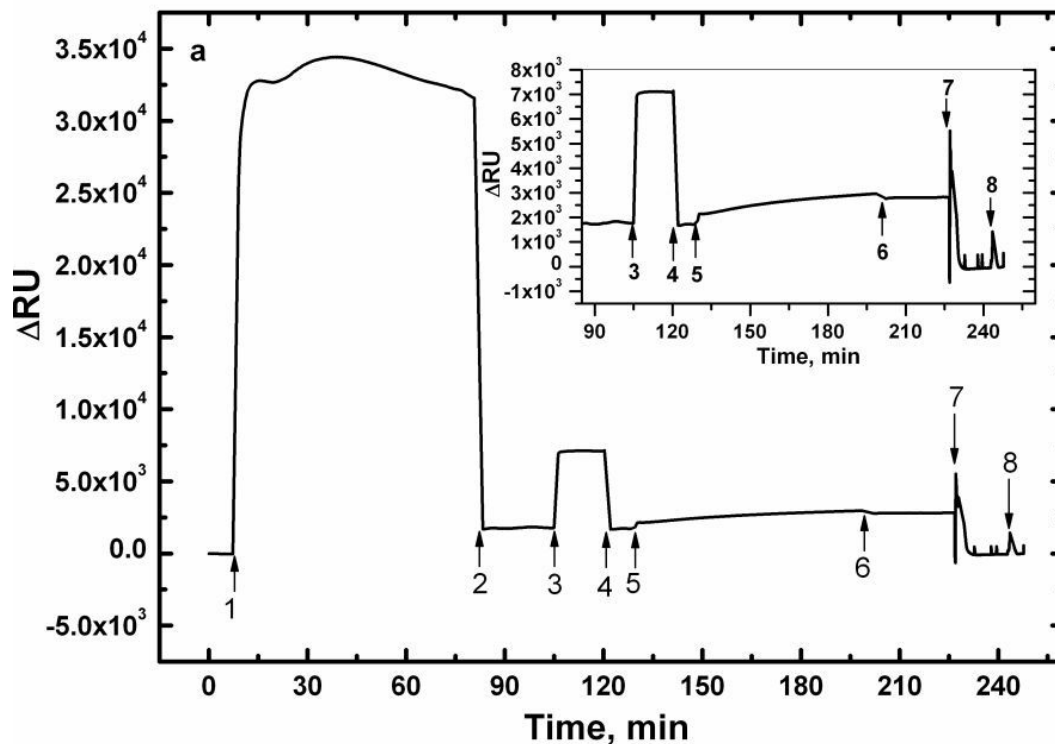


Fig. 6-4.a). Protein immobilization and reductive desorption using SPR. The sequences of the steps are as follows: 1) modification with 1 mM MUA; 2) washing with ethanol and PBS; 3) activation of surface carboxylates using 0.4 M EDC/0.1 M NHS mixture; 4) washing with PBS; 5) covalent immobilization of BSA (1mg/mL) to the activated SAM surface; 6) PBS wash and; 7) reductive desorption of the immobilized molecules at -1200 mV vs. Pt electrode in PBS using two-electrode setup and 8) confirmation of reductive desorption by applying -1200 mV. Insert figure shows the steps 3 to 8.

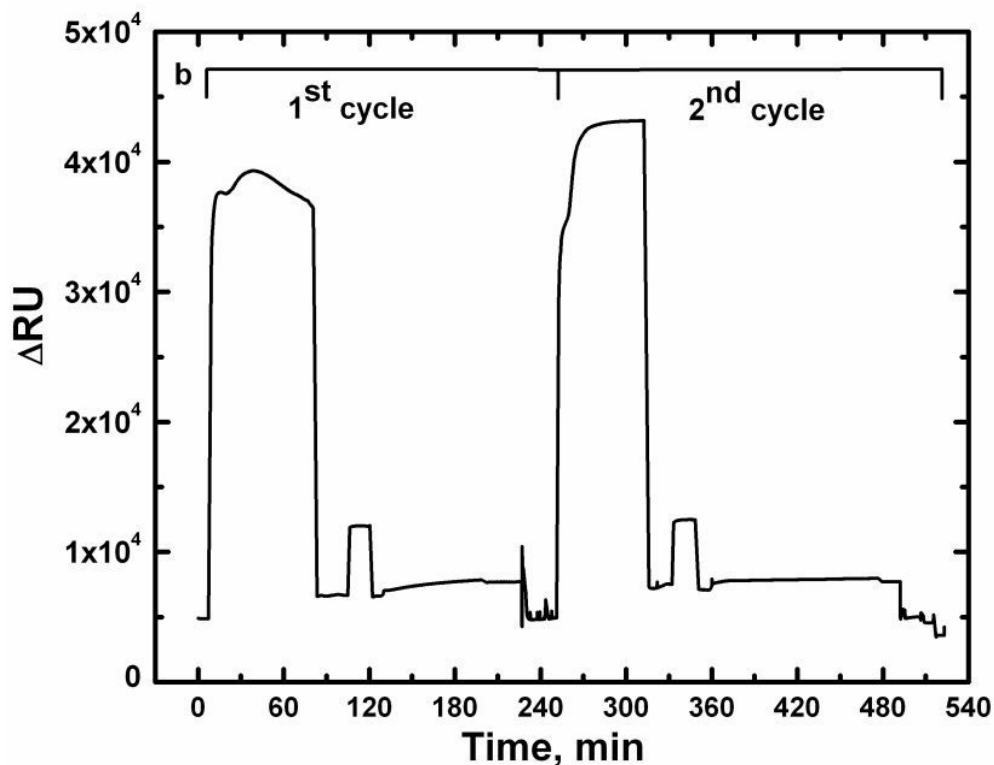


Fig. 6-4 b). Two cycles demonstrating adsorption and desorption of BSA from the electrode surface. These results point to possibility of regenerating electrode surface.

In addition to BSA, we investigated surface deposition and removal of an antibody specific to organophosphorous hydrolase (OPH) – an enzyme hydrolyzing organophosphate neurotoxins. Anti-OPH antibody was reacted for 1 hr with Au surfaces containing EDC/NHS activated MUA layer. Binding of the antibody resulted in an SPR signal of ~ 1500 Δ RU (see Fig. 6-5) compared to ~ 1000 Δ RU for BSA. This difference in signal is expected given the larger size of an IgG molecule (150kDa) compared with BSA (66kDa). After antibody immobilization, unconjugated active carboxyl groups of MUA were quenched with Tris buffer (50mM) followed by PBS washing. Binding of the antibody resulted in a significant SPR signal (~ 600 Δ RU). Injection of OPH (35nM) followed by buffer washing produced an additional signal of ~ 500 Δ RU (see inset of Fig.

6-5). SPR signal from antibody binding was converted to surface coverage of in a fashion similar to that described for BSA. The surface coverage for antibody was found to be $9.69 (\pm 2.3) \times 10^{11}$ molecules/cm² or 1.67 ng/mm² whereas OPH had $1.61(\pm 0.05) \times 10^{12}$ molecules/cm². Therefore, each antibody molecule was bound to roughly 1.6 OPH molecules, which is expected given that this bivalent antibody captures two antigen molecules. These results offer a direct proof that covalently bound antibody retained activity and ability to bind its antigen.

Using Equation 2, taking dimensions of the antibody to be 14.5 x 8.5 nm [29], and assuming ellipsoidal projection onto a plane, P_{ideal} for IgG protein (MW 150000 Da) is approximated to be 0.64 ng/mm². Given the actual surface density of 1.67 ng/mm² determined by SPR measurements and Equation 1, the surface coverage for IgG is ~260%, pointing to some possibility of multilayer formation. This value may not be precise as it hinges on the approximate relationship described in Equation 2 and assumes that antibody molecule creates an elliptical projection onto an x-y plane. However, our surface coverage estimations do point to formation of dense layers of IgG and BSA molecules on the gold electrode surface.

Adlayer	Adlayer thickness, (nm, SPR)	Surface coverage, molecules/cm ²	Adlayer thickness (nm, ellipsometry)
MUA	1.9±0.18	4.15 (±0.4) x 10 ¹⁴	2.02±0.05
BSA	0.83±0.1	9.68 (±1.2) x 10 ¹¹	–
MUA	1.98±0.13	4.33 (=0.29) x 10 ¹⁴	2.05±0.08
Anti-OPH	1.86±0.45	9.69 (±2.3) x 10 ¹¹	5.75±0.2
OPH	1.48±0.05	1.61 (=0.05) x 10 ¹²	1±0.02

Table 6- 1 Thickness and surface coverage calculation

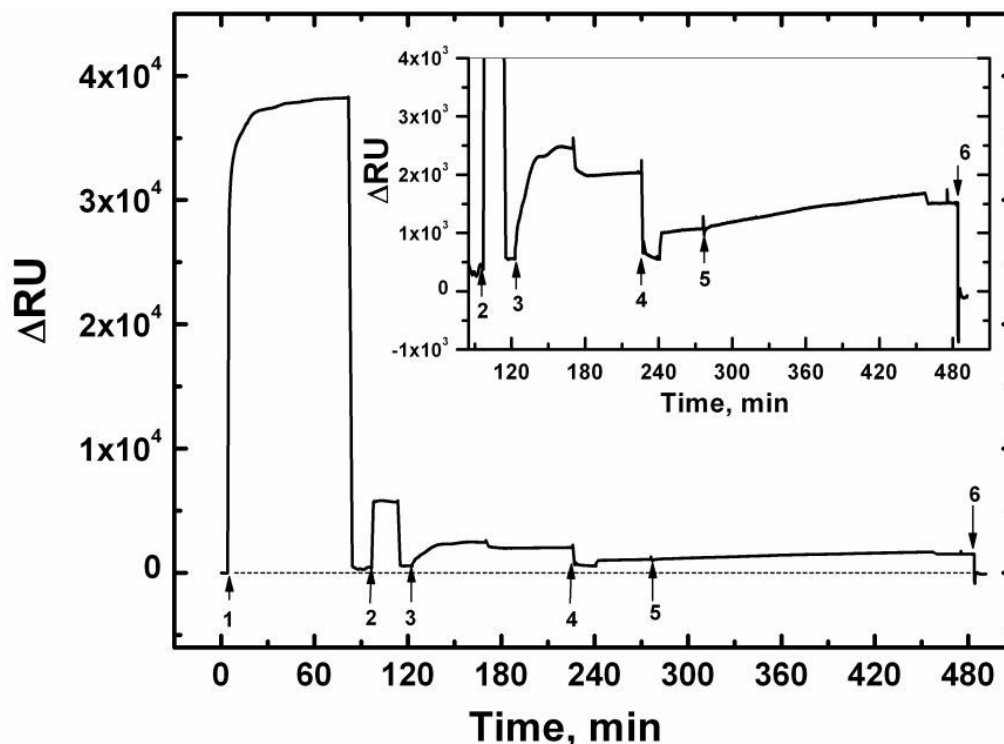


Fig. 6-5 Anti-OPH antibody immobilization and reductive desorption using SPR. The sequences of the steps are follows: 1) modification with 1 mM MUA, 2) activation of surface carboxylates using 0.4 M EDC/0.1 M NHS mixture, 3) covalent immobilization of anti-OPH (0.1 mg/mL) to the activated SAM surface, 4) quenching with 50 mM Tris buffer, 5) injection of OPH (35 nM), and 6) Reductive desorption of the immobilized molecules at -1200 mV vs. Pt electrode in PBS using two electrode setup. Insert figure represents the steps from 2 to 6.

6.3.3. Reductive desorption of immobilized proteins through SAM

Preceding sections ascertained formation of a densely packed alkanethiol and protein layers on gold. Question central to this study was whether proteins could be removed by reductive desorption of the underlying alkanethiol monolayer? Electrochemical-SPR (ESPR) instrument is a perfect tool for probing such questions.

This instrument allows to monitor molecular assembly events in real-time, to apply electrical potential *in situ* and then to observe subsequent changes in the composition of the biointerface. Prior to performing protein-stripping experiments, ability to perform electrochemistry on the SPR sensor surface was demonstrated. Fig. 6-6.a shows a representative cyclic voltammetry experiment performed in HClO₄ solution using SPR sensor surface as working electrode. The shape of the curve is similar to results reported previously for Au (111) in HClO₄ solution [30-32]. The region from 0.2 to 0.92 V corresponds to the double layer charging effect while the oxidation of gold electrode commences at 0.96 V. The two peaks denoted as OA I (1.1 V) and OA II (1.19 V) have previously been attributed to two-electron transfer involved in the oxidation of gold to gold oxide[30, 31]. There is also dependence of the SPR curve on the applied potential as shown in Fig. 6-6.b. The peaks OA I and OA II can be observed in the ΔRI vs. potential curve while the sharp reduction in the current vs. potential curve (Figure 6.a) is seen as sudden drop in ΔRI occurring around 0.89 V. These changes in SPR response for interfacial process on the bare electrode have been reported in the literature [33, 34]. It is important to note that the SPR signal is only affected by the electrical field while the potential is being applied. It stabilizes once the electrochemical experiment is stopped. Effects of applied potential on the SPR readout are manifested by sharp drops in ΔRI signal seen for example in step 7 of Fig. 6-4, where reductive potential is applied. However, as one can see from this figure, SPR signal stabilizes afterwards.

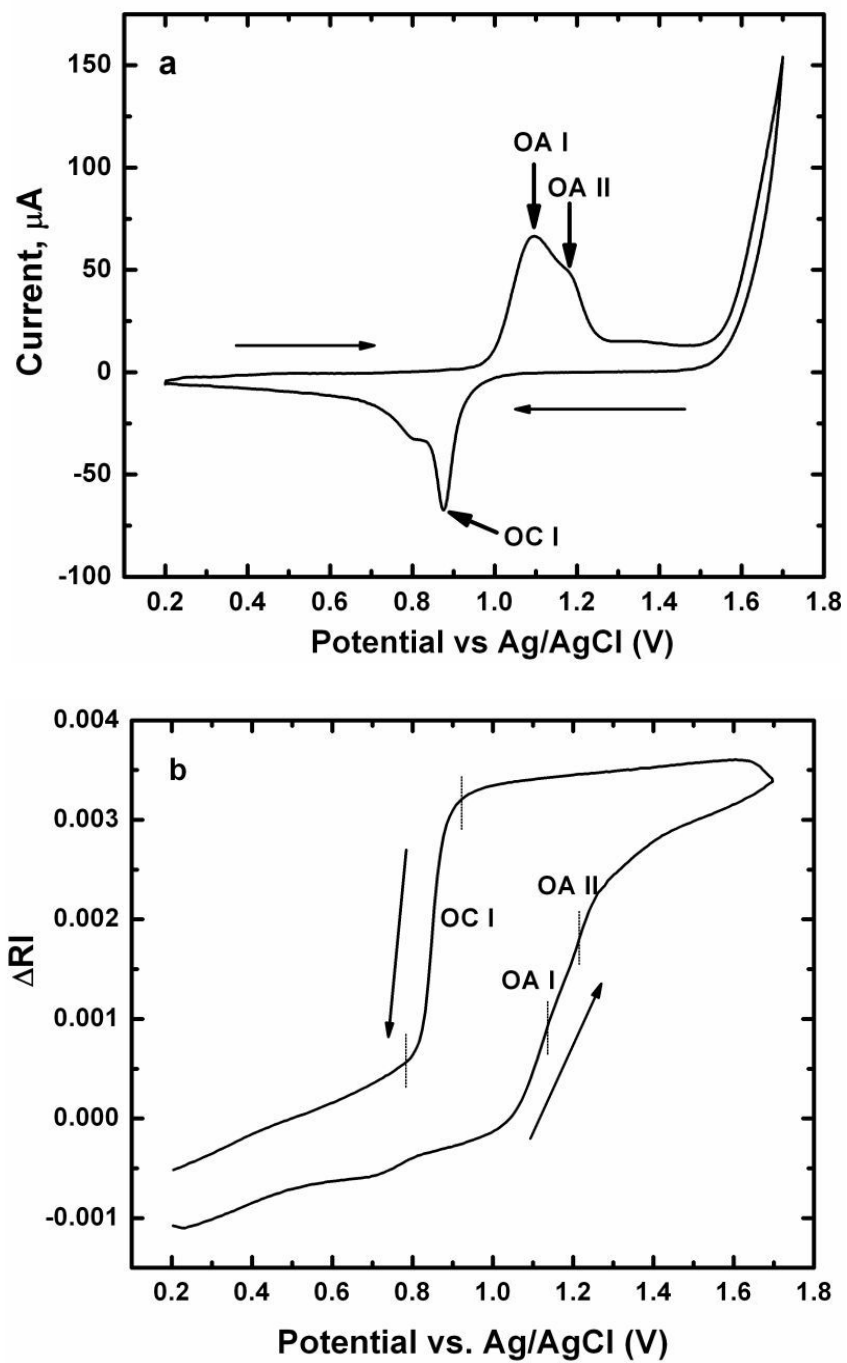


Fig. 6-6 Cyclic voltammogram of 0.1 M HClO₄ from combined ESPR setup. a) Cyclic voltammogram collected using ESPR device; b) DRI vs. E, i.e., potential-dependent change in SPR response.

After validating ESPR instrument, electrochemistry experiments were performed *in situ* using SPR sensor as a working electrode. These experiments were used to complement SPR sensograms. Fig. 6-5 shows SPR sensogram of assembly of anti-OPH antibody on activated alkanethiol monolayers. Results shown in this figure can be correlated with fig. 6-7 where surface properties of the SPR sensor are characterized by cyclic voltammetry (CV) with potassium ferricyanide as redox species. As seen from fig. 6-7, assembly of MUA followed by the antibody immobilization passivates the electrode surface, prevents electron exchange between the redox molecule and the electrode, and almost completely eliminates anodic/cathodic redox peaks of potassium ferricyanide. Time-based amperometry was used to remove this resistive molecular layer and to regenerate the electrode surface. Previous studies reported that reductive desorption of alkanethiols from Au occurred at -0.9 V [14, 35] vs. Ag/AgCl reference electrode. To ensure that both the alkanethiol and protein layers are removed, the gold electrode was biased at -1.2 V (vs. Pt electrode) for 30 s in PBS buffer. Desorption of MUA and antibody layers was verified by CV with ferricyanide. Fig. 6-7.d demonstrates regeneration of the electrode surface and appearance of ferricyanide redox peaks similar in magnitude to an unmodified electrode. Additional desorption experiment carried out at -1.4 V for 30 s in PBS only slightly improved the shape of the ferricyanide CV as shown in fig. 6-7.e.

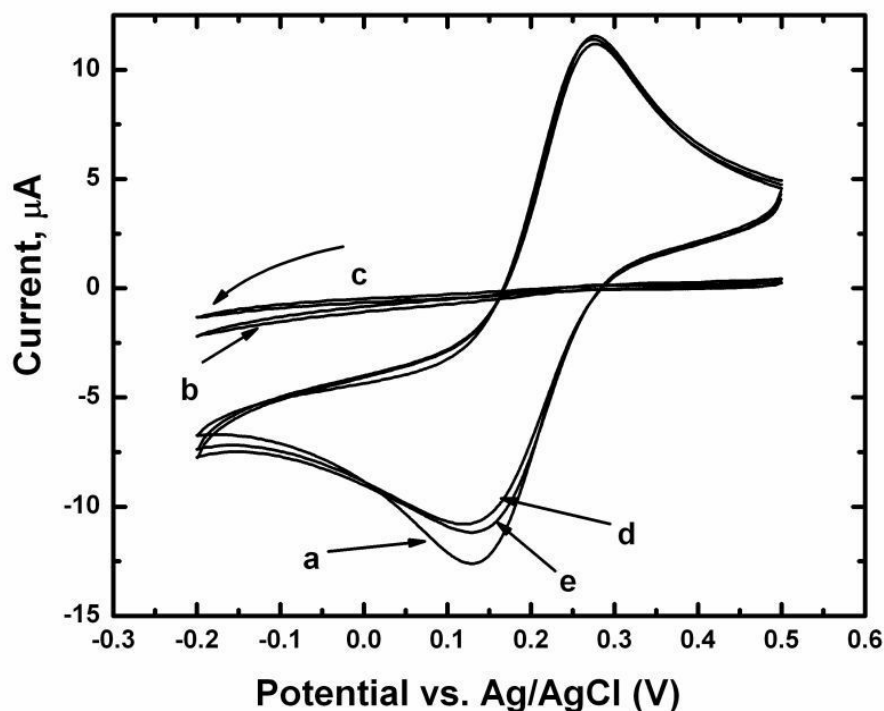


Fig. 6-7 Cyclic voltammogram of commercial BAS electrode modified with SAM and antibody. All the CV's were performed in 5mM FCN solution prepared in 10 mM PBS, pH 7.4. a) Bare gold electrode; b) gold electrode modified with 1mM MUA for 20 h; c) gold electrode modified with antibody (1 h) after SAM activation with EDC/NHS mixture; d) after reductive desorption using two-electrode system at -1200 mV vs. Pt electrode; and e) after reductive desorption using two-electrode system at -1400 mV vs. Pt electrode.

Combined ESPR experiment using BSA confirm the above results (see Fig. 6-4 a&b). After covalent immobilization of BSA to chemisorbed SAMs, the SPR gold electrode was polarized at -1.2 V vs. Pt electrode. After reductive electrochemical desorption, SPR response returns to its initial baseline, demonstrating the complete removal of BSA/MUA layers (see Fig. 6-4.a, step 7). A second application of -1.2 V did

not significantly change the SPR response (Fig. 6-4.a, step 8). Assembly and removal of protein molecules coupled to alkanethiols is repeatable, as demonstrated by fig. 6-4.b which shows two cycles of BSA/MUA adsorption and desorption. Thus, the electrochemical desorption enables regeneration of the electrode surface for further use modification.

Similar desorption experiments were performed to remove antigen-antibody couple from the electrode surface. Fig. 6-5 shows representative ESPR curve for these experiments. After immobilizing the anti-OPH antibody through EDC/NHS chemistry, antigen (OPH) was introduced to interact with anti-OPH. Antibody-antigen pair was removed from the surface by electrochemical desorption of underlying alkanethiol by applying reductive potential of -1.2 V vs. Pt electrode in PBS. As seen in the fig. 6-5 (insert, step 6) SPR signal drops sharply after reductive desorption and reaches its starting baseline (fig. 6-5, main, step 6). Results presented in fig. 6-5 demonstrate that active antibodies can be immobilized on the electrode surfaces and subsequently removed by applying reductive potential. These results are important as a demonstration of electrode surface regeneration. In addition, removal of biomolecules from the electrode surface may be coupled with a fluidic delivery and down stream sample analysis in the future.

6.4. Conclusions

While electrochemical stripping of alkanethiols has been reported widely as a method of biointerface engineering, removal of large protein molecules covalently bound to alkanethiols has not been demonstrated. This study employed electrochemistry and SPR techniques to assemble model proteins, BSA and IgG, on alkanethiol-modified gold electrode surfaces. SPR characterization of the molecular assembly pointed to formation

of a densely packed MUA layer followed by covalent attachment of model proteins. Surface coverage for BSA and IgG was estimated being 77% and 260% respectively, pointing to the abundance of protein molecules present on gold. Complete removal of proteins through reductive desorption of underlying MUA was verified by electrochemical-SPR instrument and by cyclic voltammetry performed in parallel. Controlled desorption of proteins from the gold surface demonstrated in this study represents simple and effective method for designing electrode surface properties. Approach presented here will be applicable in biosensor development, where it may be used to assemble different sensing elements onto individually addressable gold microelectrodes. Controlling protein deposition and removal also defines the surface as cell-adhesive or non-adhesive. Therefore, electrochemistry methods presented here may be used to pattern multiple cells on the surface or to remove cells that are interacting with surface-bound proteins.

6.5. References

1. C. D. Bain, E. B. Troughton, Y. T. Tao, J. Evall, G. M. Whitesides, R. G. Nuzzo, *J. Am. Chem. Soc.* 1989, **111**, 321.
2. P. E. Laibinis, J. J. Hickman, M. S. Wrighton, G. M. Whitesides, *Science* 1989, **245**, 845.
3. J. C. Love, L. A. Estroff, J. K. Kriebel, R. G. Nuzzo, G. M. Whitesides, *Chem. Rev.* 2005, **105**, 1103.
4. K. Prime, G. M. Whitesides, *Science* 1991, **252**, 1164.
5. S. T. Plummer, Q. Wang, P. W. Bohn, R. Stockton, M. A. Schwartz, *Langmuir* 2003, **19**, 7528.

6. R. H. Terrill, K. M. Balss, Y. Zhang, P. W. Bohn, *J. Am. Chem. Soc.* 2000, **122**, 988.
7. X. Y. Jiang, R. Ferrigno, M. Mrksich, G. M. Whitesides, *J. Am. Chem. Soc.* 2003, **125**, 2366.
8. M. N. Yousaf, B. T. Houseman, M. Mrksich, *Proc. Natl. Acad. Sci.* 2001, **98**, 5992.
9. S. Lan, M. Veiseh, Y. Zhang, *Biosens. Bioelectron.* 2005, **20**, 1697.
10. J. Lahann, S. Mitragotri, T. N. Tran, H. Kaido, J. Sundaram, I. S. Choi, S. Hoffer, G. A. Somorjai, R. Langer, *Science* 2003, **299**, 371.
11. I. Willner, V. HelegShabtai, R. Blonder, E. Katz, G. L. Tao, *J. Am. Chem. Soc.* 1996, **118**, 10321.
12. V. M. Mirsky, *Trends Anal. Chem.* 2002, **21**, 439.
13. A. Badia, S. Arnold, V. Scheumann, M. Zizlsperger, J. Mack, G. Jung, W. Knoll, *Sens. Actuators B*, 1999, **54**, 145.
14. S. Imabayashi, D. Hobara, T. Kakiuchi, W. Knoll, *Langmuir* 1997, **13**, 4502.
15. T. Kakiuchi, H. Usui, D. Hobara, M. Yamamoto, *Langmuir* 2002, **18**, 5231.
16. A. L. Simonian, A. Revzin, J. R. Wild, J. Elkind, M. V. Pishko, *Anal. Chim. Acta.* 2002, **466**, 201.
17. B. L. Frey, C. E. Jordan, S. Kornguth, R. M. Corn, *Anal. Chem.* 1995, **67**, 4452.
18. J. Voros, *Biophys. J.* 2004, **87**, 553.
19. L. S. Jung, C. T. Campbell, T. M. Chinowsky, M. N. Mar, S. S. Yee, *Langmuir* 1998, **14**, 5636.
20. C. E. D. Chidsey, D. N. Loiacono, *Langmuir* 1990, **6**, 682.
21. E. L. Smith, C. A. Alves, J. W. Anderegg, M. D. Porter, L. M. Siperko, *Langmuir* 1992, **8**, 2707.

22. M. D. Porter, T. B. Bright, D. L. Allara, C. E. D. Chidsey, *J. Am. Chem. Soc.* 1987, **109**, 3559.
23. C. A. Widrig, C. A. Alves, M. D. Porter, *J. Am. Chem. Soc.* 1991, **113**, 2805.
24. C. A. Widrig, C. Chung, M. D. Porter, *J. Electroanal. Chem.* 1991, **310**, 335.
25. C. E. Jordan, R. M. Corn, *Anal. Chem.* 1997, **69**, 1449.
26. V. Silin, H. Weetall, D. J. Vanderah, *J. Colloid Interface Sci.* 1997, **185**, 94.
27. J. Lahiri, L. Isaacs, B. Grzybowski, J. D. Carbeck, G. M. Whitesides, *Langmuir* 1999, **15**, 7186.
28. D. C. Carter, J. X. Ho, *Adv. Protein Chem.* 1994, **45**, 153.
29. E. W. Silverton, M. A. Navia, D. R. Davies, *Proc. Natl. Acad. Sci.* 1977, **74**, 5140.
30. H. Angerstein-Kozłowska, B. E. Conway, A. Hamelin, L. Stoicoviciu, *Electrochim. Acta*, 1986, **31**, 1051.
31. H. Angerstein-Kozłowska, B. E. Conway, A. Hamelin, L. Stoicoviciu, *J. Electroanal. Chem.* 1987, **228**, 429.
32. S. Ye, C. Ishibashi, K. Shimazu, K. Uosaki, *J. Electrochem. Soc.* 1998, **145**, 1614.
33. Y. Iwasaki, T. Horiuchi, M. Morita, O. Niwa, *Electroanalysis*, 1997, **9**, 1239.
34. M. Tian, W. G. Pell, B. E. Conway, *J. Electroanal. Chem.* 2003, **552**, 279.
35. M. R. Anderson, R. Baltzersen, *J. Colloid Interface Sci.* 2003, **263**, 516.

7. MECHANICALLY STRONG ANTIBACTERIAL COATING: SINGLE-WALLED CARBON NANOTUBES ARMORED WITH BIOPOLYMERS

7.1. Introduction

Concern about the spread of infections through contact with contaminated surfaces was once limited to specific groups of people such as astronauts who are subject to confined living spaces and the virulence-enhancing effects of space flight [1] and people requiring surgery or implantable devices [2]. More recently, there has been growing concern about the role of contaminated surfaces in the spread of infections such as severe acute respiratory syndrome (SARS) [3, 4] and staphylococcus aureus particularly methicillin-resistant staphylococcus aureus (MSRA) [5]. Therefore, antimicrobial surfaces are needed not only for the aerospace, defense and medical industries, but also for the consumer product and public transportation industries. We have used layer-by-layer assembly to produce coatings that combine the strength of single-walled carbon nanotubes (SWNT's) with the antimicrobial activity of lysozyme (LSZ).

7.2. Materials and Methods

HiPco SWNT (Rice University) were purified by a thermal oxidation-acid extraction cycle [6]. Lysozyme (LSZ) (Hen egg white) and DNA (Calf thymus) were obtained from Sigma and used as received. Microscopy glass slides (Fisher), silicon wafers (Nova electronic material) and freshly cleaved mica were used as substrate

materials. Dispersion of SWNT in LSZ and DNA were achieved by the previously published method [7]. Zeta potential of the prepared dispersions were analyzed using a ZetaPlus instrument (Brookhaven Instrument Corporation) based on the electrophoretic light scattering (ELS) technique.

7.2.1. Coating Formation

To prepare LBL multilayer's, cationic LSZ-SWNT was alternately assembled with anionic DNA-SWNT. First, glass or silicon slides were cleaned in concentrated $\text{H}_2\text{SO}_4/30\% \text{H}_2\text{O}_2$ (3:1) ("Piranha" solution). Then, the slides were immersed alternately in aqueous dispersion of LSZ-SWNT (15 min immersion times) and DNA-SWNT. Doubling of the SWNT deposition time did not affect the results. Therefore, the adsorption time of 15 min was considered sufficient for the formation of a SWNT monolayer. After each layer deposition, the substrate was blown with 50 psi air from a nozzle. Coatings were also prepared on evaporated gold surfaces. The in-situ assembly of DNA-SWNT & LSZ-SWNT was characterized in real time by surface plasmon resonance using SPREETA™ sensors (Texas Instruments) with two analysis channels. Experimental setup and cleaning steps were performed as previously described [8]. SPR gold surface was initially modified with diluted alkanethiol solution (11-mercaptoundecanoic acid, 1mM in absolute ethanol) for 18-24 h followed by electrostatic adsorption of polyethyleneimine (1% in water). Coating assembly was carried *in-situ* by introducing DNA-SWNT & LSZ-SWNT sequentially to the gold surface. To check the effect of salt, NaCl was added to the dispersion to make 10mM concentration. Real-time assembly steps were monitored by measuring the change in refractive index (RI) as a function of time followed by integration using SPREETA software. The signal is

generally displayed in response unit (RU) (1 Response Unit = 10^{-6} Refractive index unit). Typically a response of 1000RU corresponds to change in surface concentration of $1\text{ng}/\text{mm}^2$.

7.2.2. Coating Characterization

UV-Vis-NIR spectra were measured with a Varian Cary 5E spectrophotometer. Ellipsometric measurements were made with Autoelles Rudolph research ellipsometer. The samples were analyzed with 632 nm laser at 70° the incident angle and the polarizer was set at 45° . Au and Si refractive indices were determined from blank samples. The refractive index of SWNT LBL films was approximated as $N_f = 1.540$. The surface morphology was monitored by JEOL 7000F FE-SEM with EDX detector after sputter coating the samples with gold. The morphology was also tested using non-contact tapping mode atomic force microscopy (AFM) using a Pacific Nanotechnologies AFM (Santa Clara) apparatus. Raman scattering studies were carried out with Renishaw-inVia Reflex (50x objective) with a 514 nm laser. To determine the orientation of the SWNTs, measurements were conducted with a well centered 50x objective configured in the vertical direction geometry where the polarizer and the analyzer were parallel to each other and at discrete angles between 0 and 90° . When air is applied randomly there is no appreciable orientation (Figure 1).

A NanoIndenter XP (MTSnano Oakridge, TN) was used to characterize the mechanical properties using a three-sided pyramid indenter tip. Hardness and Young's modulus have been derived from the measured load-contact depth curves following the procedure in the literature [9]. To minimize the influence from the substrates, the

indentation depth limits on the SWNT thin films were set to less than 20% of the coating thickness. A series of ten indentations was performed for each sample.

7.2.3. Antimicrobial Activity - Turbidimetric assay

The antimicrobial activity of LSZ–SWNT in solution was characterized using *Micrococcus lysodeikticus*, a well-studied substrate organism for LSZ. The assay was performed according to the recommended procedure (Sigma L6876, Enzymatic assay for LSZ). A 0.015% (w/v) of substrate ($A_{450\text{nm}}$ of this suspension = 0.6 to 0.7) was prepared in 66mM potassium phosphate buffer, pH 6.24. Mixing 100 μl of LSZ-SWNT with 2.5ml of freshly prepared cell suspension resulted in a decrease in turbidity of the suspension, allowing us to continuously monitor the LSZ activity in real time. The activity of the LSZ-SWNT in solution is reported relative to the activity of unmodified lysozyme.

The activity of LSZ-SWNT incorporated in layer-by-layer assembly prepared on a pre-cleaned glass slide (0.5cm x 0.5cm) was analyzed similarly. All active films (10, 11, 20 & 21 layers) on the glass slide were introduced in to 200 μl cell suspension with brief mixing and activity was monitored over the time. Unmodified glass slide and glass slide modified with LSZ acts as negative and positive control respectively and activity efficiency is reported relative to the positive control. The durability of the LBL coating was evaluated after storing the slide at room temperature. The data from the turbidimetric assay were fitted using first-order reaction kinetics described by the equation,

$$A_t = A_0 e^{-kt},$$

where A_t = Absorbance at time (t),

A_0 = initial absorbance at zero time,

-k = rate of exponential death when $\ln A_t$ is plotted against time

The lysozyme retentive nature of the film was tested by measuring the activity of the liquid medium surrounding the LBL coating (21 layers). For this, LBL coated glass slide was immersed in 5ml phosphate buffer for 1 hr (with and without shaking) and 100 μ l of this solution was used in turbidimetric assay.

For staphylococcus aureus studies, the bacteria were cultivated in a NZY nutrient broth by shaking at 37°C for 18 h at 200rpm. The overnight culture was washed and centrifuged to remove medium and reconstituted in sterile phosphate buffer solution (PBS) in order to obtain a final concentration of 1.5–3 x 10⁵ colony forming units (CFU) per ml. Two pieces of each test specimen (Si, DNA-SWNT as the top layer, LSZ-SWNT as the top layer) with a fixed surface area (cut into small pieces of about 0.5 cm²) were transferred into pre cleaned glass vials containing 5ml of bacteria in PBS. The samples were incubated at 37°C for 24 hr before examining under electron microscope.

7.3. Results and Discussions

LSZ, a key member of ova-antimicrobials, is a powerful natural antibacterial protein [10]. It is in the class of enzymes which lyse the cell walls of gram-positive bacteria by hydrolyzing the β -1,4 linkage between N-acetylmuramic acid (NAM) and N-acetylglucosamine (NAG) of gigantic polymers in the peptidoglycan (murein) [11, 12]. Unlike many antimicrobials, LSZ has both enzymatic and non-enzymatic microbiocidal activity in both its native and denatured state which makes it useful even in processes which require heat treatment. The potential use of LSZ as an antimicrobial agent in pharmaceuticals, food preservatives and packaging is an active area of research [13, 14]. However, effective use of LSZ requires incorporating it with a more mechanically robust

material. SWNTs are well known for exceptional combination of mechanical, electrical, thermal and optical properties [15-17]. However, the efficient transfer of SWNTs' inherent nanoscale properties to macroscopic structures and devices has been an ongoing research challenge comprised of three main issues: SWNT dispersion, controlled assembly, and efficient load transfer. Favorable intermolecular interactions enable dispersion of individual and small bundles of SWNTs in DNA and proteins such as LSZ [7, 17-20]. In this research, the strong columbic interactions between DNA and LSZ were exploited in the layer-by-layer (LBL) assembly [21-23] of DNA-SWNT and LSZ-SWNT dispersions.

The enzymatic activity of LSZ in the SWNT dispersions was determined by measuring the rate of lysis of gram-positive micrococcus lysodeikticus intact cells (Fig. 7-1). The responses from the turbidimetric assay were modeled with first-order kinetics typically used to quantify exponential death of microorganisms (Fig.7-1b). The analysis shows that LSZ-SWNT dispersions clear approximately 55% of turbidity (optical density at 450 nm) within five minutes compared to 60% for the LSZ dispersion. The decrease in optical density due to cellular lysis confirms that secondary structure of LSZ in LSZ-SWNT conjugate is well preserved [7] as required for enzyme activity.

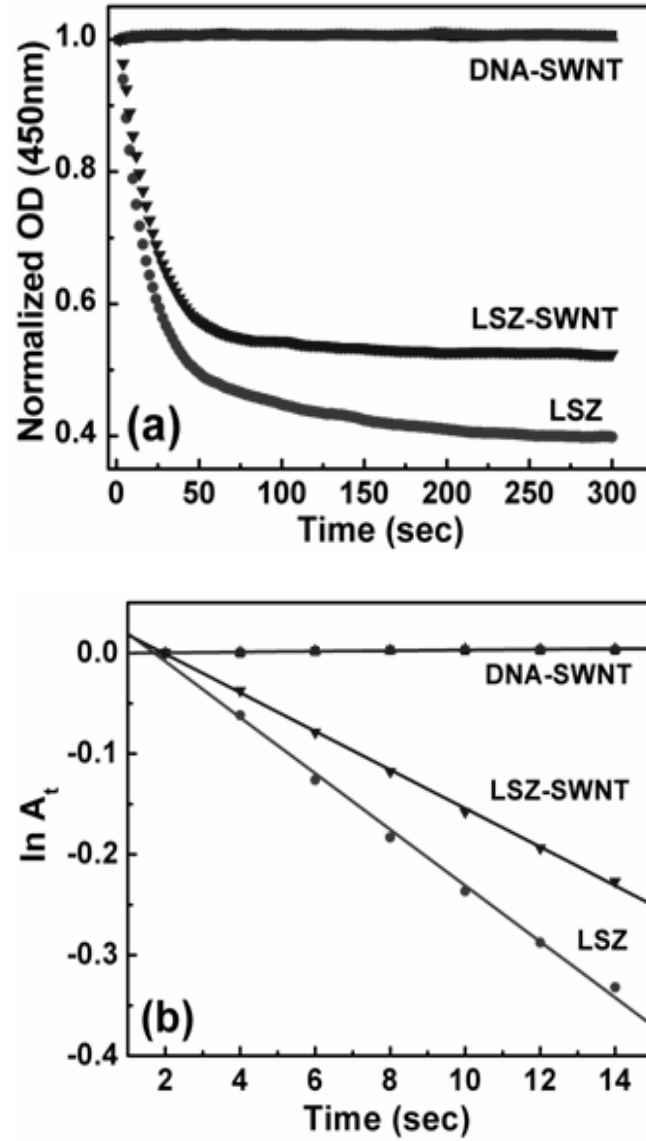


Fig. 7- 1 (a) Turbidimetric assay of LSZ and LSZ-SWNT conjugate in solution against *M. lysodeikticus*. (b) Rate of *M. lysodeikticus* lysis reaction (Regression line is fit to the linear portion of experimental data points in (a) using first-order kinetics).

Table 7-1. Comparison of enzymatic activity of lysozyme in solution and in LBL coating.

In solution		On surface of glass slide	
	Activity ^a	Layers	Activity ^a
LSZ	27.8	LSZ	3.35
LSZ-SWNT	19.2	21 layers	2.8
DNA-SWNT	-0.34	20 layers	0.0852
Control ^b	-0.28	11 layers	2.16
		10 layers	0.128
		Control ^b	-0.12

^a Activity = -k/0.001, ^b For solution, phosphate buffer is used as control and for the surface, uncoated glass slide is used as control

Zeta potential measurements confirmed that the cationic and anionic nature of LSZ-SWNT (+22mV) and DNA-SWNT dispersions (-30mV) provided an excellent platform for strong electrostatic interaction between LSZ-SWNT and DNA-SWNT multilayer's [(LSZ-SWNT)-(DNA-SWNT)]_n. Secondary forces vital in DNA-protein interactions in biological systems, including van der Waals and π - π attractions, were also likely to have played a significant role in inter-layer adhesion. UV-vis-NIR absorption spectroscopy, ellipsometry and surface plasmon resonance (SPR) were used in concert to monitor the growth of the LBL coatings on variety substrates including silicon, gold, glass and mica.

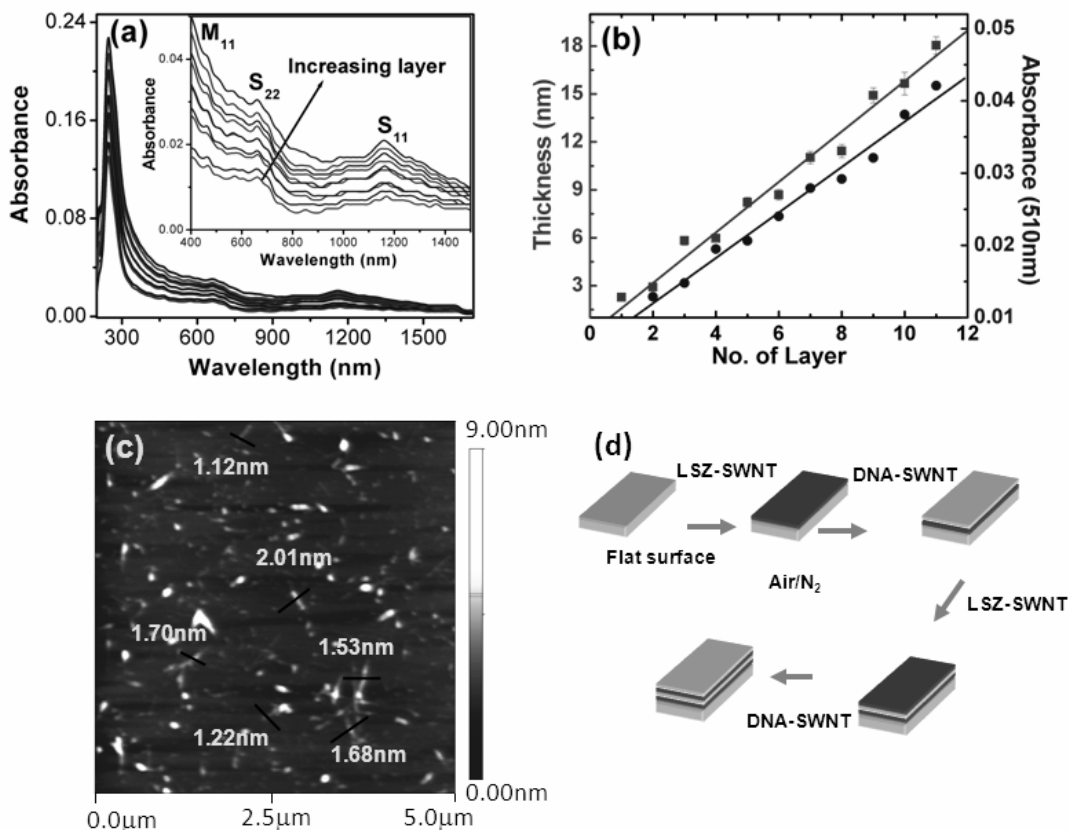


Fig. 7-2 (a) UV-vis-Near IR absorbance spectra of LBL assembly of LSZ-SWNT/DNA-SWNT (concentration of SWNT in dispersion $\sim 25\text{mg/L}$). The inset magnifies the van Hove transitions of metallic and semiconducting SWNT. (b) Comparison of UV-vis accumulation curves for absorbance at 510nm and ellipsometry thickness measurement of the LBL assembly. (c) AFM image of DNA-SWNT dried dispersion. (d) Schematic diagram of LBL assembly of LSZ-SWNT and DNA-SWNT.

Absorbance spectroscopy (Fig.7- 2a) showed well-resolved van Hove transitions of metallic (M_{11}) and semiconducting SWNT (S_{11} and S_{22}), indicating that the SWNTs retained their electronic structure in the matrix and were predominantly dispersed as individual SWNTs [16]. The uniform increase of UV-Vis-NIR absorbance from each

deposition cycle revealed that film growth was linear and uniform. Moreover, ellipsometry showed a 1.6 nm (± 0.03 nm) increase in thickness per layer; a value consistent with the previously reported diameter of individual SWNT/DNA hybrids (Fig.7- 2b) [19]. Atomic force microscopy (AFM) provided further verification of deposition of individual SWNTs; the average diameter of the DNA-SWNT (Fig. 7- 2c) was 1.6 nm. This extremely fine control of assembly process is the direct result of the quality of the initial dispersion.

SWNT orientation within each layer was achieved by applying a directed air stream between each deposition step. This step decreased the time required for assembly by eliminating the need for the rinsing step inherent in most LBL processes. Furthermore, the air stream enabled shear alignment of SWNTs within each individual layer generating the possibility to create coatings where each layer has a distinct orientation. Fig.7-3a and 3b shows the SEM image of the aligned 8th and 68th layer respectively. Uniform deposition and alignment were further confirmed by Raman spectroscopy. It is well established that Raman intensity of SWNTs is maximal when exciting light polarization is along the nanotubes axis [24-26]. It can be clearly seen in Fig.7-3c that the intensity of the G-band Raman signal changed significantly ($I_{0^\circ}^G/I_{90^\circ}^G = 7$) when rotating the film sample, while no intensity change was observed for a randomly oriented SWNTs composite film (Fig. 7-4). Raman mapping was conducted to evaluate the spatial distribution of SWNT on the surface; G band intensities across a wide area ($10 \mu\text{m}^2$) are almost uniform showing that the SWNTs were not only highly aligned but uniformly spaced (Fig. 7-3 d).

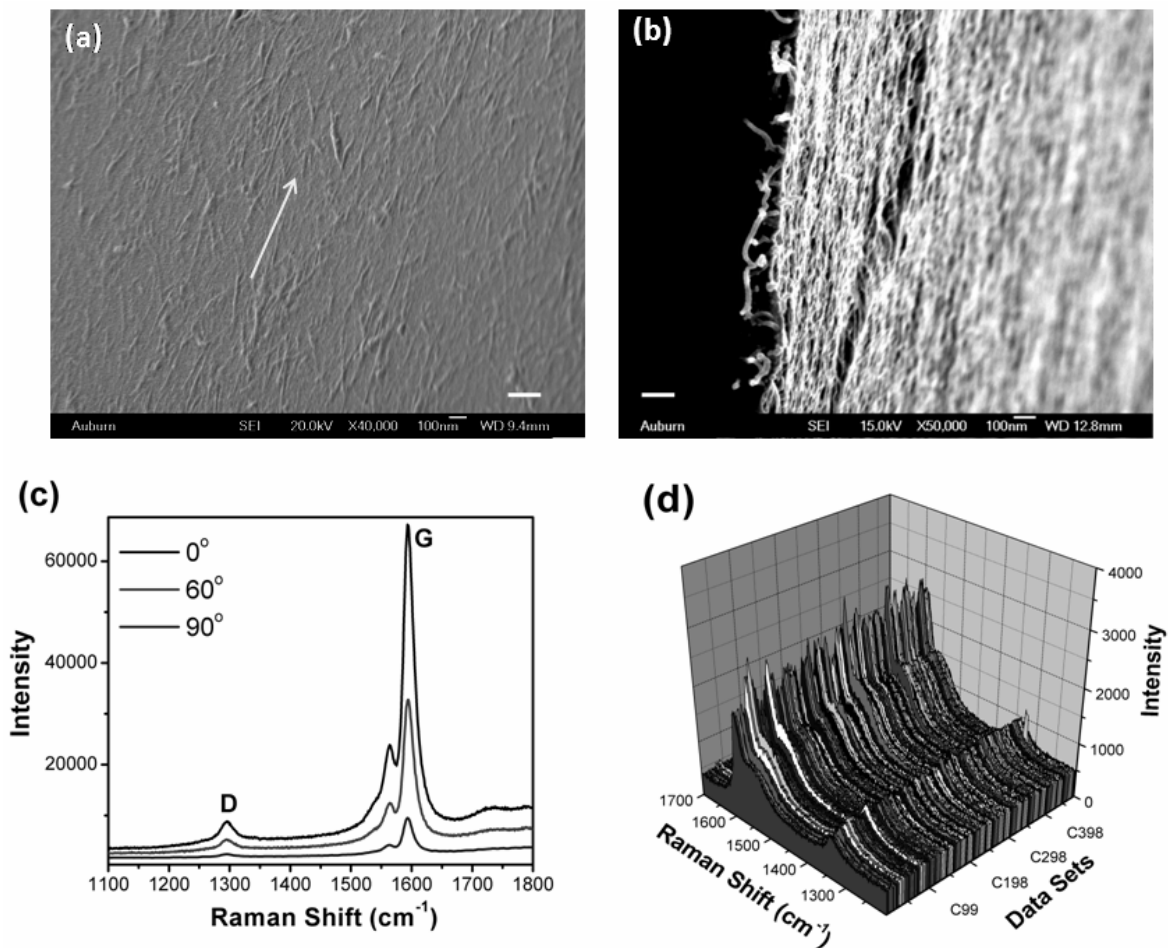


Fig. 7-3 SEM images of LBL assembly of LSZ-SWNT/DNA-SWNT of the (a) 8th layer and (b) 68th layer. (c) Raman spectra of the assembly (8th layer) showing D-band to G-band recorded at various angles between the polarization of laser excitation and SWNT alignment direction using 514nm laser d) Raman mapping collected at 10 x10 μm area (8th layer) showing D-band and G-band. The scale bars in (a) and (b) represent 200 nm.

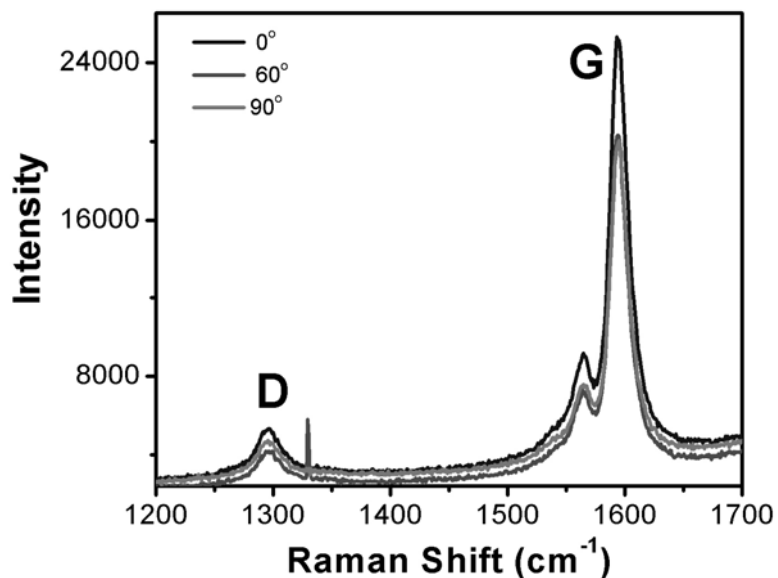


Fig. 7-4 Raman spectra of LSZ-SWNT/DNA-SWNT (at 8th layer) (prepared by random air directions) showing D-band to G-band recorded at various angles between the polarization of laser excitation and SWNT alignment direction using 514nm laser.

In order to better understand the LBL process, dispersions with different SWNT concentrations were produced with and without added electrolyte. SWNT concentration was found to strongly influence coating thickness. For example, ellipsometry showed (Fig.7-6a) that increasing SWNT concentration from 25mg/L to 45mg/L increased the average layer thickness from 1.6 nm to 3.28 nm. Fig.7-5a shows the UV-Vis-NIR absorbance of in-situ growth of LBL assembly from the 45mg/L SWNT dispersion. The increasing intensity corresponds to increased SWNT concentration after the deposition of each layer. The presence of clear van Hove peaks suggests that the SWNTs were predominantly individuals, but SEM revealed some small aggregates non-parallel overlapping SWNTs. Thus, the increased layer thickness at higher concentrations is

believed to be largely due to SWNTs overlapping during the deposition process, and perhaps an increase in the number of small bundles in the dispersion.

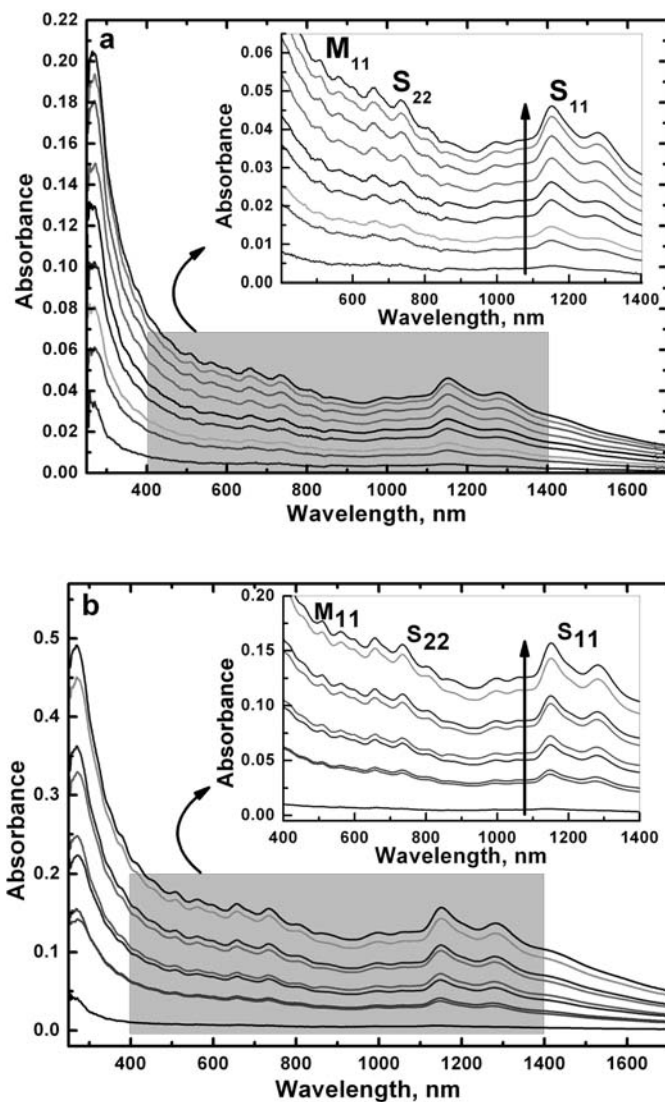


Fig. 7-5 UV-Vis-Near IR absorbance spectra of LBL assembly of LSZ-SWNT/DNA-SWNT obtained from dispersion of SWNT at higher concentration (~ 45 mg/L). (a) without NaCl, (b) with addition of NaCl (10 mM). The insets in (a) and (b) magnifies the van Hove transitions of metallic and semiconducting SWNTs.

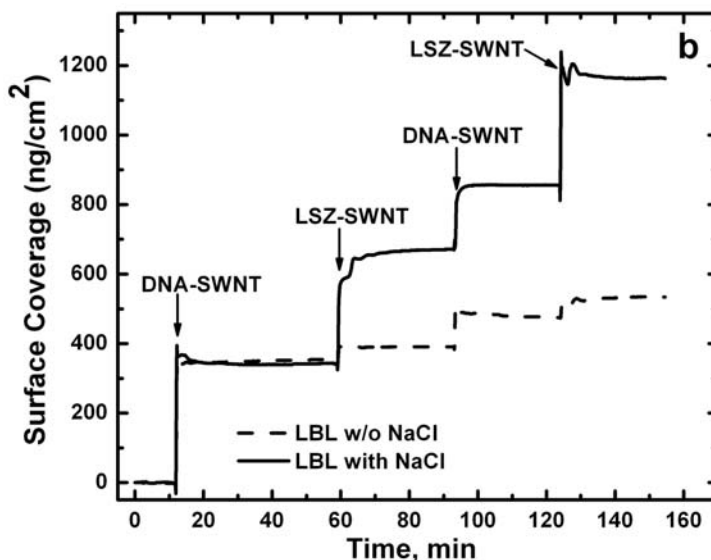
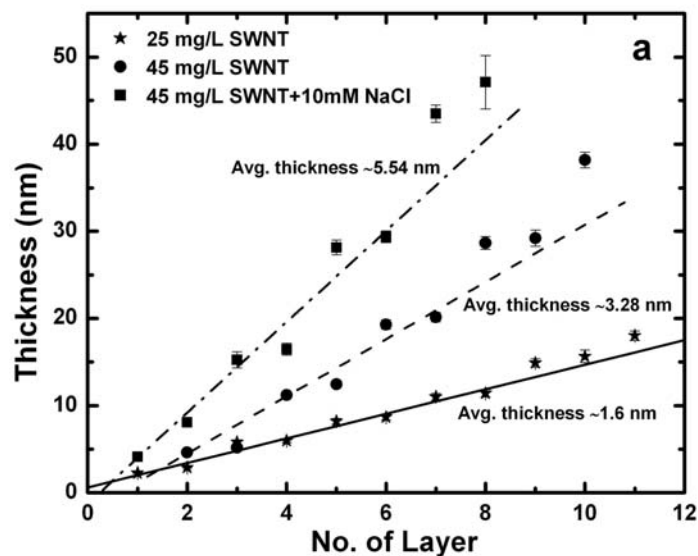


Fig. 7-6 a). Comparison of ellipsometry thickness measurement of the LBL assembly b). Surface plasmon resonance of in-situ thin film deposition showing the surface coverage.

The addition of electrolyte also had an effect on the assembly process. Fig.7-5b shows the absorbance spectroscopy of LBL growth prepared from ~45mg/L concentration of SWNT in LSZ-SWNT and DNA-SWNT dispersions containing 10mM NaCl. On each LSZ-SWNT layer the rate of growth of absorbance is faster than that with

DNA-SWNT. This corroborates with ellipsometry results (Fig.7-6a) and is further confirmed by surface plasmon resonance (SPR) spectroscopy, a surface sensitive technique which unambiguously demonstrates the effect of salt in LBL film assembly (Fig.7-6b). The rapid increase in SPR response provides strong evidence for electrostatic interactions between oppositely charged SWNT-bioadducts. SPR response increases smoothly over each layer indicating progressive assembly; surface coverage calculations indicate that more nanotubes were deposited in the presence of 10mM NaCl. The influence of added salt [27] agrees well with reported values for similar SWNT-polyelectrolyte multilayer's [28-30]. The presence of salt did not result in any obvious morphological differences in the coating after multiple deposition cycles.

Nanoindentation was used to assess the mechanical properties of coatings 205 nm (68 layers) thick. Fig.7-7 shows the hardness and Young's modulus as a function of penetration depth. The coatings had a hardness of 1 GPa (Fig. 7-7c) and a Young's Modulus of 22GPa (Fig. 7-7b). These results are similar to those measured by Mamedov *et al.* [31] and Xue *et al.* [32] and confirm effective load transfer between the SWNTs and the biomacromolecular matrix.

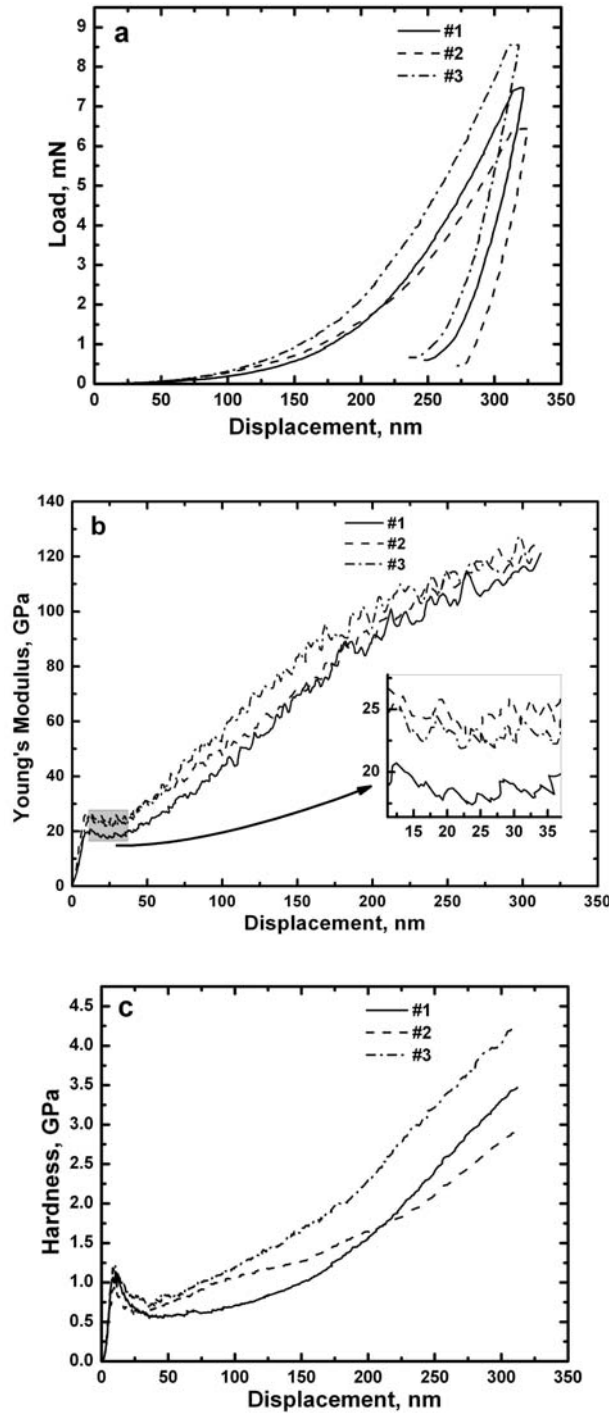


Fig. 7-7 Nanoindentation tests on a 68 layer coating (LSZ-SWNT/DNA-SWNT)₆₈ (a) Load-displacement curve from which b). Young's modulus and c). Hardness were obtained

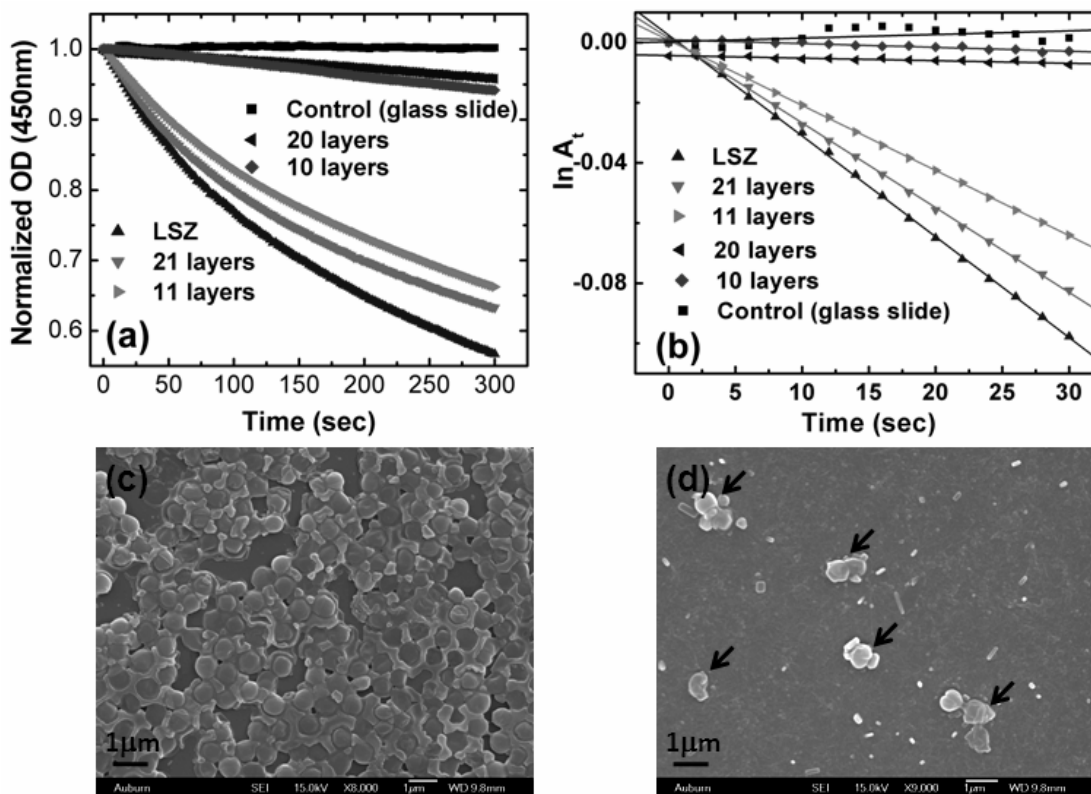


Fig. 7-8 (a) Effect of different layers of LBL coating against *M. lysodeikticus* in turbidimetric assay. (b) Rate of *M. lysodeikticus* lysis reaction (Regression line is fit to the linear portion of experimental data in (a) using first-order rate kinetics). SEM image of samples incubated with *Staphylococcus aureus* at 37°C for 24hrs of (c) a clean silicon wafer (control) and (d) LBL assembly at 11th layer (top surface LSZ-SWNT) arrows indicating damaged cells). The scale bars in (c) and (d) represent 1 μm .

The enzymatic activities of the LBL coatings were evaluated as described in the experimental section. Remarkably, coatings terminating in a LSZ-SWNT layer exhibited a relative antimicrobial activity of 84% compared to 69% in the initial dispersion (Fig.7-8 a). The clearing of the turbid micrococcus lysodeikticus solution by the coatings is due to the enzyme activity of the exposed LSZ-SWNT layer suggesting a dynamic interaction

between the coating surface and the surrounding solution. It is important to note that no lytic activity was observed for surface layers ending with DNA-SWNT or unmodified surfaces (Student's t-test, $P < 0.05$). This confirms that the antimicrobial activity was specifically due to the LSZ enzyme reaction. Of particular interest, is that the number of layers has an influence on the antimicrobial activity of the coating (Fig.7-8 b). This behavior suggests that a zone-model behavior is observed as outlined by Ladam *et al* [33] where the substrate affects the growth of initial layers forming Zone I followed by growth of Zone II and Zone III as the number of layers increased. On the other hand, this may also arise from interplay of charges during film growth as the underlying layers are overcompensated compared to terminal layers [34]. This unequal distribution of charges on different layers may influence the activity of LSZ since it must have an optimal balance of charges in order to express lytic activity [14]. The coatings exhibited impressive long term stability. No leaching of enzyme was observed in the supernatant when the coatings were stored in buffer and the antimicrobial activity is retained for at least 60 days (fig.7-9). This confirms that dynamic interaction occurs between LBL coating and surrounding solutions.

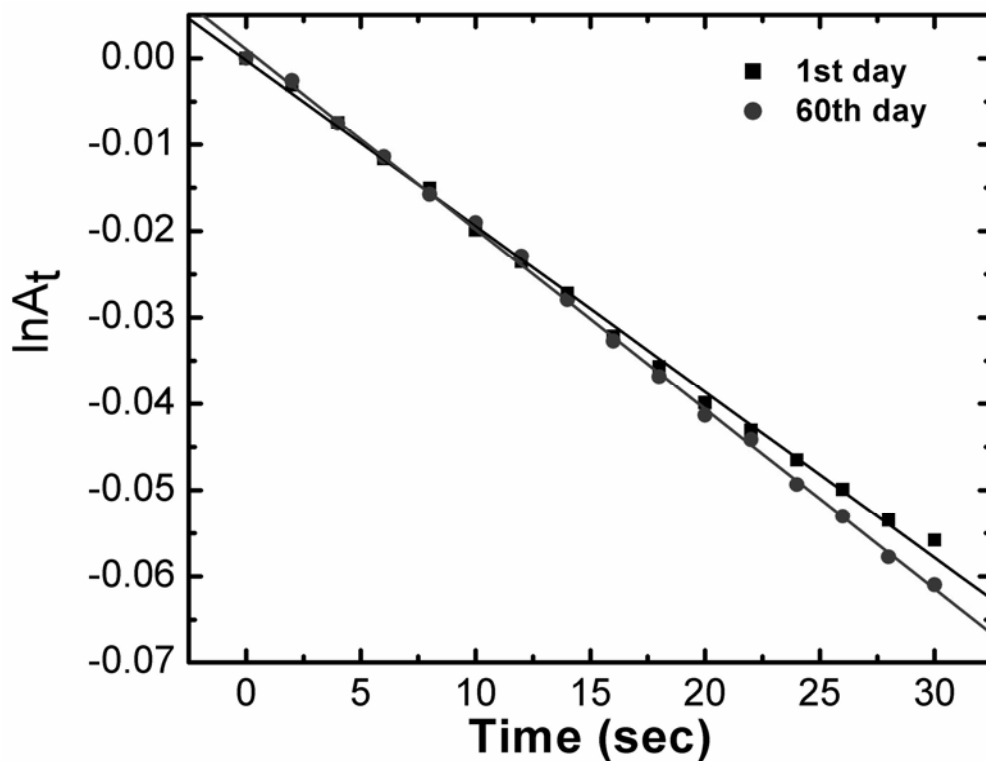


Fig. 7-9. The activity of 21 layer LBL coating on the first and sixtieth day by turbidimetric assay

Exposing surfaces to freshly prepared staphylococcus aureus provided further evidence of the antimicrobial activity of LSZ-SWNT terminated coatings. When a silicon substrate with and without the LBL coating was incubated with staphylococcus aureus for 24 h at 37°C and imaged under SEM, significantly more bacteria adhered to the uncoated (Fig. 7-8c) surface than the coated surface (Fig. 7-8d). In addition, the few adhered bacteria on LBL coated substrate underwent severe morphological changes compared to the uncoated silicon surface where the cells remained intact and maintained their cocci structure. These morphological changes in staphylococcus aureus cells are speculated to be the result of lysozyme triggered autolysis of bacteria which is the

generally accepted mechanism of lysozyme action on staphylococcus aureus cells [35, 36].

7.4. Conclusion

In conclusion, we have developed a unique multifunctional biomimetic material comprised of SWNT, DNA and LSZ using LBL assembly. Precise control of both layer thickness and SWNT alignment within each layer was achieved and the final coatings had robust mechanical properties. Coatings ending in an exposed LSZ-SWNT layer exhibit excellent long-term antimicrobial activity. This has several distinct advantages over coatings which release antimicrobials over time; controlled release coatings lose their antimicrobial efficiency once the concentration of the antimicrobial agent drops below the minimum inhibitory concentration (MIC). On the other hand, our non-leaching coatings exhibit robust mechanical properties and long term protection against bacterial colonization. Furthermore, the spectrum of disinfection of LSZ-SWNT layers can be extended to gram-negative bacteria by simply including chelators such as EDTA [14]. The results of this research demonstrate the significant possibilities for the molecular design of layered hybrid structural materials from SWNTs and natural biopolymers. Such robust, antimicrobial materials have significant promise in applications including medicine, aerospace engineering, public transportation, home appliances and sporting goods.

7.5. References

1. Wilson, J.W., et al., *Space flight alters bacterial gene expression and virulence and reveals a role for global regulator Hfq*. Proceedings of the National Academy of Sciences, 2007. **104**(41): p. 16299-16304.
2. Darouiche, R.O., *Treatment of Infections Associated with Surgical Implants*. The New England Journal of Internal Medicine, 2004. **350**(14): p. 1422-1429.
3. Cheng, V.C.C., et al., *Severe Acute Respiratory Syndrome Coronavirus as an Agent of Emerging and Reemerging Infection*. Proceedings of the National Academy of Sciences, 2007. **20**(4): p. 660-694.
4. Chu, C.-M., et al., *Viral Load Distribution in SARS Outbreak*. Emerging Infectious Diseases, 2005. **11**(12): p. 1882-1886.
5. Klevens, R.M., et al., *Invasive Methicillin-Resistant Staphylococcus aureus Infections in the United States*. The Journal of the American Medical Association, 2007. **298**(15): p. 1763-1771.
6. Xu, Y.Q., et al., *Controlled multistep purification of single-walled carbon nanotubes*. Nano Letters, 2005. **5**(1): p. 163-168.
7. Nepal, D. and K.E. Geckeler, *pH-sensitive dispersion and debundling of single-walled carbon nanotubes: Lysozyme as a tool*. Small, 2006. **2**(3): p. 406-412.
8. Balasubramanian, S., et al., *Lytic phage as a specific and selective probe for detection of Staphylococcus aureus--A surface plasmon resonance spectroscopic study*. Biosensors and Bioelectronics, 2007. **22**(6): p. 948-955.
9. Bhushan, B. and X. Li, *Nanomechanical characterisation of solid surfaces and thin films*. International Materials Reviews, 2003. **48**(3): p. 125-164.

10. Jolles, J. and P. Jolles, *What's new in lysozyme research? Always a model system, today and yesterday*. Mol. Cell. Biochem., 1984. **63**: p. 165-189.
11. Nepal, D. and K.E. Geckeler, *Functionalization of Carbon Nanotubes*, ed. K.E. Geckeler and E. Rosenberg. 2006, Valencia, CA: American Scientific Publishers. 57-79.
12. Nepal, D., et al., *Supramolecular conjugates of carbon nanotubes and DNA by a solid-state reaction*. Biomacromolecules, 2005. **6**(6): p. 2919-2922.
13. Proctor, V.A. and F.E. Cunningham, *The chemistry of lysozyme and its use as a food preservative and a pharmaceutical*. Critical Reviews in Food Science and Nutrition, 1988. **26**(4): p. 359-395.
14. Losso, J., S. Nakai, and E. Charter, *Lysozyme*, in *Natural Food Antimicrobial Systems*, A.S. Naidu, Editor. 2000, CRS Press. p. 185–210.
15. Huang, J.Y., et al., *Superplastic carbon nanotubes*. Nature, 2006. **439**(7074): p. 281-281.
16. O'Connell, M.J., et al., *Band Gap Fluorescence from Individual Single-Walled Carbon Nanotubes*. Science, 2002. **297**(5581): p. 593-596.
17. Nepal, D. and K.E. Geckeler, *Functional Nanomaterials in Functionalization of Carbon Nanotubes* K.E. Geckeler and E. Rosenberg, Editors. 2006, American Scientific Publishers: Valencia. p. 57-79.
18. Tan, Y. and D.E. Resasco, *Dispersion of Single-Walled Carbon Nanotubes of Narrow Diameter Distribution*. J. Phys. Chem. B, 2005. **109**(30): p. 14454-14460.
19. Zheng, M., et al., *DNA-assisted dispersion and separation of carbon nanotubes*. Nature Materials, 2003. **2**: p. 338-342

20. Nepal, D. and K.E. Geckeler, *Proteins and Carbon Nanotubes: Close Encounter in Water*. *Small*, 2007. **3**(7): p. 1259-1265.
21. Hammond, P.T., *Recent explorations in electrostatic multilayer thin film assembly*. *Current Opinion in Colloid & Interface Science*, 1999. **4**(6): p. 430-442.
22. Tang, Z., et al., *Biomedical Applications of Layer-by-Layer Assembly: From Biomimetics to Tissue Engineering*. *Advanced Materials*, 2006. **18**: p. 3203-3224.
23. Jiang, C. and V.V. Tsukruk, *Freestanding Nanostructures via Layer-by-Layer Assembly*. *Advanced Materials*, 2006. **18**(7): p. 829-840.
24. Jorio, A., et al., *Polarized Raman Study of Single-Wall Semiconducting Carbon Nanotubes*. *Physical Review Letters*, 2000. **85**(12): p. 2617.
25. Ericson, L.M., et al., *Macroscopic, Neat, Single-Walled Carbon Nanotube Fibers*. *Science*, 2004. **305**(5689): p. 1447-1450.
26. Chae, H.G., M.L. Minus, and S. Kumar, *Oriented and exfoliated single wall carbon nanotubes in polyacrylonitrile*. *Polymer*, 2006. **47**(10): p. 3494-3504.
27. Hofmeister, F., *Zur Lehre von der Wirkung der Salze. II*. *Arch. Exp. Pathol. Pharmacol.*, 1888. **24**: p. 247-260.
28. Paloniemi, H., et al., *Layer-by-Layer Electrostatic Self-Assembly of Single-Wall Carbon Nanotube Polyelectrolytes*. *Langmuir*, 2006. **22**(1): p. 74-83.
29. Kovtyukhova, N.I. and T.E. Mallouk, *Ultrathin Anisotropic Films Assembled from Individual Single-Walled Carbon Nanotubes and Amine Polymers*. *Journal of Physical Chemistry B*, 2005. **109** (7): p. 2540 -2545.

30. Rouse, J.H., et al., *Polymer/Single-Walled Carbon Nanotube Films Assembled via Donor-Acceptor Interactions and Their Use as Scaffolds for Silica Deposition*. Langmuir, 2004. **16**(20): p. 3904-3910.
31. Mamedov, A.A., et al., *Molecular design of strong single-wall carbon nanotube/polyelectrolyte multilayer composites*. Nature Materials, 2002. **1**(3): p. 190–194
32. Xue, W. and T. Cui, *Characterization of layer-by-layer self-assembled carbon nanotube multilayer thin films*. Nanotechnology, 2007. **18**(14): p. 145709.
33. Ladam, G., et al., *In Situ Determination of the Structural Properties of Initially Deposited Polyelectrolyte Multilayers*. Langmuir, 2000. **16**(3): p. 1249-1255.
34. Schwarz, B. and M. Schonhoff, *A 1H NMR relaxation study of hydration water in polyelectrolyte mono and multilayers adsorbed to colloidal particles*. Colloids and Surfaces A: Physicochemical and Engineering Aspects, 2002. **198-200**: p. 293-304.
35. Virgilio, R., et al., *Electron Microscopy of Staphylococcus Aureus Cell Wall Lysis*. Journal Of Bacteriology, 1966. **91**(5): p. 2018.
36. Wecke, J., et al., *Cell-Wall Degradation of Staphylococcus-Aureus By Lysozyme*. Archives of Microbiology, 1982. **131**(2): p. 116-123.

8. Overall Conclusion

The research presented in this thesis has investigated several areas of biosensor design in order to develop a portable system for infectious pathogen detection with high sensitivity and specificity. In addition, a special study has been made on multifunctional antimicrobial coatings based on SWNT-biocomposites to combat the threat of surface assisted disease spread.

Rapid and reliable detection of harmful pathogens at low levels are vital due to the related environmental and economical impact. While antibodies (monoclonal or polyclonal) are successfully employed in many immunoanalysis procedures as a biorecognition element, many of them remain costly with a comparatively short shelf-life and uncertain manufacturability. Additionally, they suffer from several limitations, such as susceptibility to hostile environmental stresses such as temperature, pH, ionic strength, and cross-reactivity. Several attempts have been made to utilize fluorescent tagged bacteriophages and phage-displayed peptides for bacterial detection. However, involvement of complex labeling and detecting procedures make these approaches time-consuming and complicated. Here, for the first time, the label-free detection of *S.aureus* using lytic phage as highly specific and selective biorecognition element on a biosensor platform was reported. Lytic phage was immobilized on the gold surface of SPREETA™ sensor through direct physical adsorption. The detection limit was found to be between

10^3 and 10^4 cfu/ml. The competitive inhibition assay demonstrates that detection was specific while selectivity was confirmed with *Salmonella typhimurium*.

Poly-L-lysine-grafted-polyethylene glycol (PLL-g-PEG) copolymer was synthesized to overcome problems of surface fouling associated with traditional protein blocking agents. Protein blockers are typically contaminated with serum proteins during purification processes and hence cross-interact with the target of interest thereby decreasing detection sensitivity. The synthesized polymer reduced *S.aureus* fouling on gold by ~97% compared to unblocked surface. When used as blocking buffer in the detection of enzyme β -galactosidase by specific filamentous bacteriophage, this polymer improved the sensitivity dramatically by 2 to 3-orders of magnitude compared to BSA and Casein blockers. Several factors were speculated to affect the sensitivity of biosensor; a) hydrophilicity of PEG and b) protein-protein hydrophobic interactions between BSA, Casein and β -gal. Hence, PLL-g-PEG shows large potential application in the field of biosensor by improving the sensitivity of “guest-host” interactions in addition to resisting non-specific adsorption.

Because of the high affinity interaction between antibody and antigen, immunosensors for environmental diagnostics are single-use devices with little control over reusability. Typically, harsh chemicals such as strong acids and detergents are used to disrupt antigen-antibody interactions which results in decreased sensitivity in subsequent applications. This will be appropriate if the sensor is used for one type of antigen-antibody study. Here, a facile way to immobilize and remove antibody completely from sensor surface with the flexibility of introducing different antibodies was developed using electro-reductive nature of alkanethiols. Coupled, SPR -

electrochemistry setup was developed to monitor molecular assembly events on gold electrodes and to correlate these events with changes in electrochemical properties of the substrate. Model proteins like bovine serum albumin (BSA) and immunoglobulin G (IgG) were conjugated via carbodiimide (EDAC) chemistry to a layer of mercaptoundecanoic acid (MUA) assembled on SPR sensor surfaces. The surface-bound proteins were completely removed by applying a reductive potential of -1200 mV vs. Pt electrode in a physiological saline buffer. Importantly, the sequence of protein immobilization followed by desorption could be repeated multiple times, thus demonstrating ability to reuse the sensing surface for different antibody immobilization. Controlled removal of protein molecules from electrode surfaces is envisioned to have important applications in affinity or cell-based biosensing, cellular micropatterning and cell sorting.

Finally, large scale biomimetic carbon nanotube coatings with significant antimicrobial activity, high Young's Modulus and controlled morphology were fabricated using layer-by-layer assembly. The favorable intermolecular interactions enabled dispersal of individual SWNTs in both DNA and lysozyme. As a result, it was possible to control layer thickness within 1.6 nm. Drying the layers with a directed air stream accelerated the assembly process and enabled control over SWNT alignment within each layer. The unique blend of multifunctionality and vertical and lateral control of a bottom-up assembly process is a significant advancement in developing macroscale assemblies with the combined attributes of SWNTs and natural materials.

9. FUTURE RECOMMENDATIONS

9.1. Long-range Surface Plasmon Resonance (LRSPR) Biosensors

Surface plasmon resonance (SPR) based biosensors are a unique biophysical tool used for studying protein-protein, antigen-antibody, DNA/RNA and enzyme-substrate interactions in real-time without the use of labels. Due to its high sensitivity to the refractive index changes produced during biomolecular interactions, the recent SPR based biosensors have achieved sensitivity up to femto molar concentrations of target species. However, the reported detection sensitivity for larger analytes such as bacteria using SPR is typically in the range from 10^5 to 10^7 cfu/ml with few exceptions [1]. This is less than satisfactory given the infectious doses for several pathogens is very low, usually from 10 to 10^4 cfu/ml [2, 3]. As pointed out in the discussion section of chapter 4 of this work, the application of SPR for bacterial detection is severely limited by the penetration depth, L_p of the probing evanescent wave. Depending on the wavelength of the incident light, commercially available sensors have a typical penetration distance from 150 to 300 nm. However, typical bacterial pathogens have a size ranging from 500 nm to several microns and hence the large proportion of the bacterial cell lies outside the sensitive part of the evanescent wave thereby diminishing the sensitivity of the detection.

The limited penetration depth observed in conventional SPR design arises from the loss associated during the optical excitation of surface plasmons at the metal-dielectric interface [4]. This can be circumvented by sandwiching a thin metal strip

between two dielectrics; a design reduces the loss associated with propagation by forming a symmetric mode called long-range surface plasmon polaritons (LRSPPs) [5-8]. By varying the thicknesses of the metal and dielectrics, the evanescent wave can penetrate as long as several micrometers into the dielectrics. Such designs are very popular in the fabrication of optical communication devices like optical switches and light routers [9].

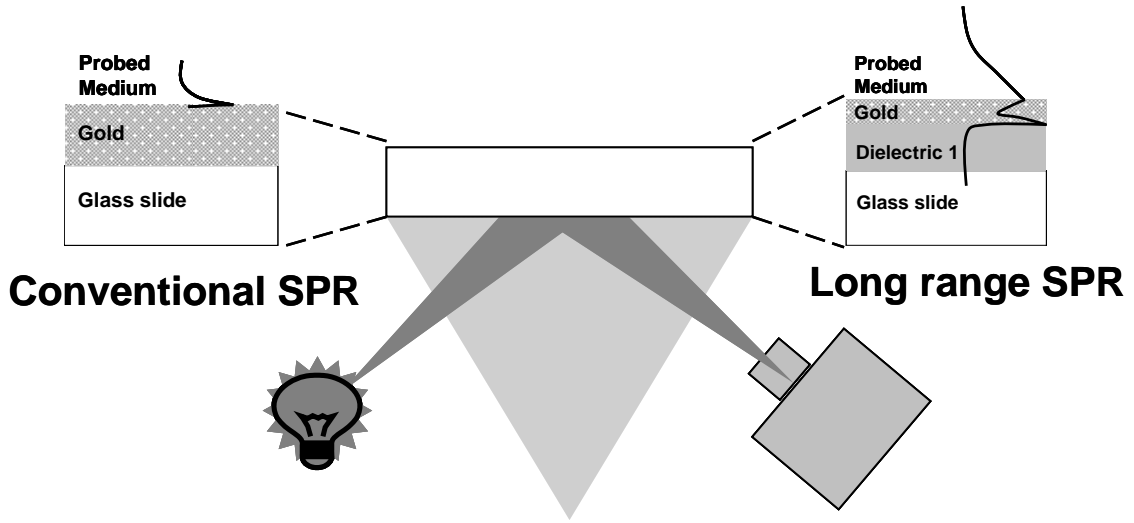


Fig. 9-1 Proposed design of long range SPR (LRSPR) system for bacterial detection in comparison with conventional SPR [10]

In addition to enhanced penetration depth, these LRSPPs have narrow resonance curves with longer propagation length and hence recently exploited for DNA biosensor development [11]. Even though these designs are transferable, one has to realize the matching of optical properties between dielectric 1 and the medium under study (fig.9-1) in order to extend the surface plasmons to probe greater distance. Since, most of the detection is carried in aqueous condition ($RI \sim 1.33$), finding materials with optical properties close to water in the visible region will be challenging. Fig 9-1 shows the schematic of the proposed design of long range SPR sensor for enhanced detection of

larger analytes such as bacteria. For e.g. Slavik *et al* demonstrated an eight fold increase in penetration distance ($L_p \sim 1400\text{nm}$) when Teflon AF (RI ~ 1.31) was used as dielectric layer compared to conventional SPR ($L_p \sim 180\text{nm}$) [10].

9.2. Devising a Surface That Destroy Bacteria on Contact

As outlined in chapter 2, spread of pathogenic diseases is a complex interplay between the host, pathogen and environment. As the saying goes, “*prevention is better than cure*”, hence designing surfaces that resist bacterial contamination thereby preventing disease transmission would be the ideal way to fight the war against pathogenic bacteria. Even though many kinds of antibiotics were developed, bacterial species have evolved with a knack to overcome the antibiotic susceptibility through mutations. On the other hand, bacteriophages are specifically developed to prey on bacteria with high specificity. As bacteria, phage is also changing constantly demonstrating an evolutionary arms race between the tiny microbial communities. Due to their ability to destroy the bacteria *in vivo* without eliciting immune response in humans, they have been recognized as “next-generation” therapeutic agents to treat diseases caused by deadly pathogens such as MRSA.

Aided by bacteriophage extreme specificity, in this work we were able to demonstrate a highly sensitive and specific biosensor for the detection of *S.aureus*. Encouraged by these results, a preliminary study was undertaken to investigate the lytic property of immobilized bacteriophage on gold surface against *S.aureus* growth and the results are shown below. Fig 9-2 a shows the *S.aureus* growth curve studied in the presence of gold surface coated with and without the selected lytic bacteriophage. It is

evident that phage covered gold surface certainly discourages *S.aureus* growth after 3hr which is similar to the lytic activity observed in solution for this phage-bacteria interaction (fig. 9-2 b).

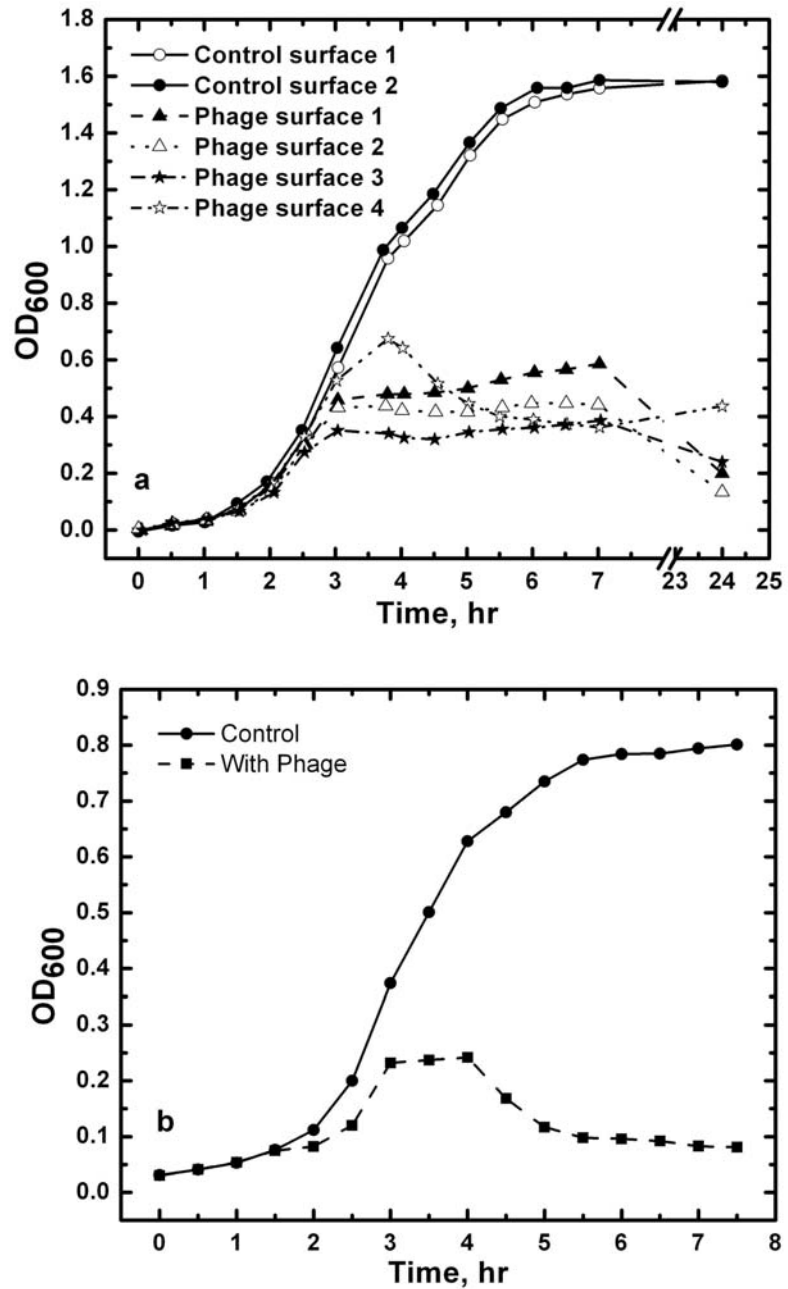


Fig. 9-2 Phage induced lysis of *S.aureus* a). on gold coated sensor surface and b). in solution

The bacteria stopped to grow after 3 hrs on phage coated gold surface compared to uncoated control surfaces followed by significant declined in bacterial population after 24 hrs. These results unambiguously demonstrate that the immobilized lytic phage not only has the ability to capture the bacteria but also retains its lytic property. This is very encouraging in light of the multifunctional antimicrobial coating developed during this study. Given that the bacteriophages can be engineered using phage display technique, a library of phages each having lytic activity specific to a pathogenic bacterium can be developed. These phages can then be coupled with mechanically robust materials such as carbon nanotubes or flexible polymer material to eventually develop into a surface or coatings that resist bacterial contamination and hence prevent disease transmission.

9.3. References:

1. Homola, J., *Surface Plasmon Resonance Sensors for Detection of Chemical and Biological Species*. Chem. Rev., 2008. **108**(2): p. 462-493.
2. Schaad, U.B., *Which number of infecting bacteria is of clinical relevance?* Infection, 1983. **11**: p. S87-S89.
3. Schmid-Hempel, P. and S.A. Frank, *Pathogenesis, virulence, and infective dose*. Plos Pathogens, 2007. **3**(10): p. 1372-1373.
4. Raether, H., *Surface Plasmons on Smooth and Rough Surfaces and on Gratings*. Springer Tracts in Modern Physics; 111. 1988, Berlin: Springer-Verlag.
5. Craig, A.E., G.A. Olson, and D. Sarid, *Experimental-Observation Of The Long-Range Surface-Plasmon Polariton*. Optics Letters, 1983. **8**(7): p. 380-382.

6. Quail, J.C., J.G. Rako, and H.J. Simon, *Long-Range Surface-Plasmon Modes In Silver And Aluminum Films*. Optics Letters, 1983. **8**(7): p. 377-379.
7. Stegeman, G.I. and J.J. Burke, *Effects Of Gaps On Long-Range Surface-Plasmon Polaritons*. Journal of Applied Physics, 1983. **54**(9): p. 4841-4843.
8. Wendler, L. and R. Haupt, *Long-Range Surface Plasmon-Polaritons In Asymmetric Layer Structures*. Journal of Applied Physics, 1986. **59**(9): p. 3289-3291.
9. Bozhevolnyi, S.I., *Dynamic components utilizing long-range surface plasmon polaritons*, in *Nanophotonics with Surface Plasmons*, V.M. Shalaev and S. Kawata, Editors. 2007, Elsevier: Amsterdam.
10. Slavík, R. and J. Homola, *Ultra-high resolution long range surface plasmon-based sensor*. Sensors and Actuators B: Chemical, 2007. **123**(1): p. 10-12.
11. Wark, A.W., H.J. Lee, and R.M. Corn, *Long-range surface plasmon resonance imaging for bioaffinity sensors*. Analytical Chemistry, 2005. **77**(13): p. 3904-3907.